MOSSBAUER STUDIES OF IRON MINERALS AND COMPOUNDS

Thesis

Submitted to the University of Roorkee
for the award of the degree
of
DOCTOR OF PHILOSOPHY
in
PHYSICS

By

AJAY KUMAR SINGH

DEPARTMENT OF PHYSICS
UNIVERSITY OF ROORKEE
ROORKEE (INDIA)
NOVEMBER, 1977

C E R T I F I C A T E

This is to certify that the thesis entitled ' MOSSBAUER STUDIES OF IRON MINERALS AND COMPOUNDS'which is being submitted by Sri Ajay Kumar Singh in fulfilment for the award of the degree of Doctor of Philosophy in Physics of the University of Roorkee, Roorkee is a record of his own work carried out by him under my supervision and guidance. The matter embodied in this thesis has not been submitted for the award of any other degree.

It is further certified that he has worked from January 1975 to July 1977 for preparing his thesis for the Ph.D. Degree at the University.

Dated: 29 November,1977

K Chandra

(K.Chandra)
Department of Physics
University of Roorkee
ROORKEE-247672 (INDIA)

ACKNOWLEDGEMENT

It is quite gratifying to acknowledge my thesis supervisor, Dr. K.Chandra, for his thorough understanding of the subject, unfailing guidance, distinct suggestions and constant encouragement which helped me in reaching at this stage of my academic career. His ambitious approach towards dealing with the problems, skilfulness and carefulness are some of the qualities worth appreciating.

I am highly grateful to Prof. S.K.Joshi, Head, Department of Physics for rendering all the help and facilities, within his reach, at my disposal.

Research work today is, to the highest degree, a question of teamwork. Here I was lucky enough to have a nice and cooperative company of my group colleque Mr. B.K.Jain. Dr. Vishwamittar and Mr. R.K.Gupta, incorporated in our Mossbauer group during last one year, deserve equal acknowledgement for showing fine collaboration and friendship.

Thanks are also due to Dr. N.G.K.Nair of the sister Geology Department and Dr. G.C.S. Gaur, Wadia Institute of Himalayan Geology, Dehradun for helpful and fruit-bearing discussions at various stages of this work, to Dr. S.K.Date, TIFR, Bombay, India and Dr. Tore Ericsson, Uppsala University, Sweden for helping in computer fitting of the Mossbauer data.

The homely atmosphere which I enjoyed in the midst of so many friends and staff members is highly appreciable.

Lastly, the financial support received from C.S.I.R. and U.G.C.,India is no less acknowledgeable.

(AJAY K. SINGH)

'' The world is a poor affair if it does not contain matter for investigation for the whole world in every age. Nature does not reveal all her secrets at once. We imagine we are initiated in her mysteries: We are as yet, but hanging around her outer courts ''.

-- Seneca

RÉSUMÉ

The present thesis reports some investigations carried on natural samples namely Ochres, goethite and bog iron ore; Iron Ores; and chromites. Main tool of the study was Mossbauer spectroscopy in which the probe was 14.4 KeV gamma-rays of Fe^{57} radioactive source. Chemical, differential thermal and infrared absorption analyses were also done in some cases to support the results. Thin and polished section studies were done to identify the minerals in case of iron ore and chromite samples. Its subject matter has been divided in following chapters:

Chapter 1 - After comparing the advent of Mossbauer effect with those of others, the former has been defined and its suitability has been discussed. A brief review of the previous work and its applications have been given. Lastly, the motivation behind the problem, pursued, has been elaborated.

Chapter 2 - Theoretical background and hyperfine parameters connected with Mossbauer Spectroscopy have been discussed in this chapter. In the next step introduction about superparamagnetism and the applications of Mossbauer spectroscopy in mineralogy have been given. At later stage preliminary idea about Differential thermal and Infrared absorption analyses and their application in the study of natural samples have been given.

Chapter 3 - Details regarding the instruments involved in the work form the matter of this chapter. Kankeleit type constant acceleration drive, binary frequency divider, cryostat and furnace, all fabricated in the lab. where this work has been performed, have been discussed. Details about the whole spectroscopic set-up and a brief account of the temperature controller, which was used and is capable of keeping the temperature controlled to within $\pm 0.05^{\circ}K$ from $77^{\circ}K$ to $800^{\circ}K$, have also been given.

Chapter 4 - Mossbauer studies on naturally occurring ochres namely red and yellow ochre form the subject matter of this chapter. Ochres are considered to be those iron bearing earths that contain between 15 to 40% Fe_2O_3. The samples were annealed at various temperatures ranging from 200 to $1000^{\circ}C$ and their Mossbauer spectra were taken at room temperature. It has been concluded that red ochre contains iron mainly as α-Fe_2O_3 with small particles exhibiting superparamagnetic (SPM) effects while yellow ochre is mainly α-FeOOH. The studies throw some light about the genetic conditions which have been observed to be different for both the samples. DTA, IR and chemical analyses were also done to support the results.

Chapter 5- This chapter deals with the studies done on natural goethite and bog iron ore. The studies were carried out by annealing the samples at various temperatures and then taking their spectra at room temperature. DTA, IR and chemical analyses were also performed on these samples. Goethite showed SPM effects and inclusion of impurities, while bog iron ore exhibits pure α-FeOOH phase with larger grain size. The studies led to conclude that crystallization in case of goethite was incomplete while bog iron ore was of the hard type of the lake ore deposits.

Chapter 6- The content of this chapter is about the investigations performed on three iron ore samples taken from an ore band which was found in carbonate suite of Chamoli, Garhwal Himalayas. The ore band has acted as plane of movement and hence differential stresses were developed across this band. Apart from Mossbauer spectroscopy, thin and polished section studies were also performed. Sample taken from the central part of the band was found magnetite rich whereas that from the top was hematite rich. Sample from bottom part of the band was found to be having more of hematite and less magnetite. This variation in the amount and in the structure of minerals have been correlated with the stresses generated across the band. The genesis of the ore band has also been discussed.

Chapter 7 - Here the investigations performed on natural chromites taken from three Indian localities namely Byrapur, Ladakh and Sukinda have been elaborated. Chromites show a wide compositional range and hence must be relatively sensitive to physico-chemical and thermal conditions that accompanied their formation. Apart from Mossbauer, polished section studies, and chemical analyses were also performed. One of the samples from Byrapur, and those from Ladakh and Sukinda showed normal while another from Byrapur showed inverse spinel structure. The last one also exhibits SPM effects. All these samples have been found to form under high oxygen pressure. Further conclusions have been drawn about their genesis.

Chapter 8 - In this final chapter, some remarks have been given regarding the suitability of this technique in the field of mineralogy. Mossbauer spectroscopy can be very helpful in studying such minerals as chromites, pyrites etc., their composition being very sensitive to physico-chemical and thermal conditions, from the view point of rock- and paleo-magnetism. A very potential application of this technique lies in studying ancient pottery which leads to prediction about their dating, an important problem from archaeological point of view.

LIST OF PUBLICATIONS

I. Included in the thesis*

1. Mossbauer studies of naturally occurring red ochre and yellow ochre. To appear in J.Phys. D-Appl. Phys. 11 (1978).
(with B.K.Jain and K.Chandra)

2. Mossbauer studies of natural goethite and bog iron ore. To appear in Phys.Stat. Solidi (a) 44 (1977).
(with B.K.Jain and K.Chandra)

3. Mossbauer studies of Iron Ore.
Proc. NP and SSP Symposium 19C, 420 (1976).
(with B.K.Jain and K.Chandra)

4. Mineralogy and genesis of iron ore band associated with the meta-acidic intrusive of carbonate suit in Chamoli, Garhwal Himalayas. Can. J. Earth Sci. (Communicated).
(with G.C.S.Gaur and K.Chandra)

5. Structural and compositional studies of natural chromites of Indian origin. J. Phys. D-Appl. Phys. (accep. for publication)
(with B.K.Jain, S.K.Date and K.Chandra)

* The contribution of other authors in these papers is limited to marginal extent.

II. Not included in the thesis.

1. X-ray K-abs. edge study of chemical shift in cobalt complexes. J. Phys. F -Metal Phys. 5, 822 (1975).

(with B.M.S.Kashyap)

2. Shift in X-ray K-abs. edge of Co and As in cobalt arsenate. Ind.J. Pure and Appl. Phys. 14, 498 (1976).

3. Effect of alloying elements in plain carbon steels. To appear in Phys.Stat. Sol.(a) 43 (1977).
(with B.K.Jain and K.Chandra)

4. Mossbauer studies of Corroded steels. To appear in Japanese J. of Applied Physics 16 (1977).
(with B.K.Jain,K.Chandra and I.P.Saraswat)

5. An investigation of binary system FeSe. J. Phys. F-Metal Phys. (Communicated).
(with B.K.Jain and K.Chandra)

6. Observation of antiferromagnetism in ϵ iron antimonide. Appl. Phys. Lett. (Communicated).
(with B.K.Jain and K.Chandra)

CONTENTS

CHAPTER 1

INTRODUCTION

In the last couple of decades a large number of new methods in Physics have been developed which have become of immense use in many fields of sciences, e.g.

NMR (Nuclear magnetic resonance)

PAC (Perturbed angular correlation)

EPR (Electron paramagnetic resonance)

ENDOR (Electron nuclear double resonance)

LEED (Low energy electron diffraction)

ESCA (Electron spectroscopy for chemical analysis)

FIM (Field ion microscopy), and

NGR (Nuclear gamma resonance) or Mossbauer Effect.

Usually a new method emerges by advancing, refining and combining certain aspects in theory and experimental sophistication. Sometimes theoreticians have made predictions which could experimentally be verified only after few years of hard work. In contrast to the usual development of new methods, Mossbauer effect has all the attributes of a wonderful discovery by a young German experimentalist.

Nuclear gamma resonance, popularly known as 'Mossbauer effect', was observed by R.L. Mossbauer during 1957-58 at Max Planck Institute in Heidelberg, West Germany. This effect is concerned with the resonance absorption phenomenon in nuclear case accompained with recoil free transitions. As there is no recoilling of the nucleus, the lines observed have width comparable to natural line width and hence this effect is a very useful tool in studying hyperfine parameters|1|.

It has got certain advantages over methods hitherto used for hyperfine measurement work. These are:

(a) This effect can determine isomer shift which is a measure of total electronic charge density. NMR and other methods are insensitive to this quantity.

(b) It can study hyperfine interactions involving both ground and excited state splittings. Of the other methods PAC does not give information about ground state splitting, whereas NMR is not suitable for magnetically concentrated systems and for metals. EPR and ENDOR work only with paramagnetic centres and also generally with diluted systems only.

(c) This technique always shows the spectrum of a specific isotope and is rather insensitive to impurities below a certain extent. This is one of the advantages over NMR which measures the total spectrum of bulk sample.

(d) Spin-spin interactions has negligibly small effect on ME spectrum because of their resolution poorer than NMR.

(e) There is no limitation existing for very high internal fields in this technique unlike the case of PAC.

Mossbauer effect spectroscopy, however, has the following disadvantages:

(a) ME works only for solids or solid-like environments e.g. liquid crystals. Whereas NMR and PAC find wide applications in liquids and sometimes in gases also.

(b) The exponential dependence of recoilless fraction over

square of gamma-ray energy places a practical upper limit of about 150 KeV for observing this effect.

(c) The above limit also restricts the upper boundation of life time (useful τ's are usually less than 10^{-6} sec. for this effect) and hence very high resolution can not be obtained.

(d) This effect is strongly dependent upon temperature and transition energies larger than 30 KeV require temperature lower than $300^{\circ}K$ to observe reasonable effect.

These demerits, however, do not outweigh its merits and in a life span of seventeen years it has come out as a very useful technique covering different branches of science. Recent application of this spectroscopy has emerged in archaeology |2,3|, soil science |4|, studying texture problems |5|, plant and animal fossils |6| , in mining |7| and in studying moon-rock samples |8|.

Its vast utilization in various branches is reflected from huge number of research papers |9,10|, ME methodologies |11|, and text books |12-22| dealing with its principle and applications.

Although the observation of Mossbauer effect has been reported in about eighty isotopes, a major portion ($\sim$70 %) of the work is pertaining to Fe^{57} and Sn^{119} isotopes. The reasons may be the ease of observation of this effect in these isotopes and the abundance of compounds and alloys of iron and tin.

Application of Mossbauer technique in the field of earth sciences has taken a rather encouraging trend. First of the

studies reported in the present dissertation is about naturally occurring pigments yellow and red ochre. The two samples were studied, before and after giving heat treatment, through Mossbauer technique, Infrared absorption and Differential thermal analysis. These studies were done in order to find out the mineralogical character of these ochres. The heat treatment were given,to the samples, to understand the behaviour of constituent minerals and impurities lying in their structure at different temperature. Development of particle size with gradually increasing temperature of annealing was also observed. As these ochres have been frequently used by ancient potters and painters as painting material, possible application of these studies lie in investigating the artifacts.

Next part of the dissertation concerns with the studies done on natural goethite and bog iron ore through Mossbauer, Infrared absorption and Differential thermal techniques. Effect of annealing on these samples was studied by taking the Mossbauer spectra of annealed samples. The observations were performed in order to find out the form of iron and its grain size present in these natural samples and to study the heat treatment effects. The aim was finally to obtain information on the genetic conditions and type of these deposits.

The third phase of this study pertains to the investigations done on three samples obtained from top, middle and bottom part of an iron ore band. This ore band was 1 meter thick and was found associated with meta-acidic intrusive. This ore band

has suffered remobilization. The purpose of the study was to identify the different mineral phases present in these samples and to study variations in their amount and structure caused by differential stresses produced as a result of remobilization and available impurity ions. Lastly attempt has been made to suggest about the genesis of this ore band on the basis of the results obtained through Mossbauer spectroscopy, thin and polished section studies and chemical analysis.

Closing part of the present programme deals with naturally occurring chromites of Indian origin. Chromites exhibit wide variation in their composition and hence may be useful indicator of the physico-chemical and thermal conditions under which its host rocks have formed. The investigations were carried out through chemical, polished section and Mossbauer spectroscopic analyses, with the purpose of finding out chemical composition, cation distribution and associated gangue minerals. On the basis of these findings suggestions have been proposed about their classification and genetic conditions.

CHAPTER 2

PRELIMINARY THEORETICAL BACKGROUND

2.1 RESONANCE FLUORESCENCE

Resonance fluorescence, predicted first by Lord Rayleigh in atomic systems [23] at the end of last century, could be demonstrated only in 1904 by Wood [24]. Since atomic resonance depends essentially on the existence of quantized levels which also occur in a nucleus, the possibility of observing nuclear resonance absorption was obvious and the search was started in 1929 by Kuhn [25]. However, all the attempts in this direction remained fruitless for nearly two decades. One of the reasons for such failure was recoil of the nucleus. Consider a nucleus of mass M with transition levels A and B separated by energy E_γ. Whenever a gamma quantum is emitted, the nucleus is recoiled with energy E_R (recoil energy) given by

$$E_R = E_\gamma^2/2Mc^2 \qquad .. (2.1)$$

In conformity with the law of conservation of momentum, the direction of recoiling nucleus is opposite to that of the emitted gamma quantum. The result is that the emission line, instead of being centered at E_γ(in energy scale), shifts to lower energy by E_R (Fig. 2.1a). The absorption line, on the contrary, is displaced towards higher energy side by the same amount (Fig. 2.1b). Typical values of E_R lie in the region 10^{-2} to 10^2 eV.

One more feature enters in the discussion namely 'natural line width' , Γ , which, from Heisenberg's uncertainity relation, is given by

$$\Gamma = \hbar/\tau \qquad .. (2.2)$$

where τ is mean life time of the excited state. Usual values of Γ for low lying excited states vary from 10^{-8} to 10^{-4} eV.

To observe resonance the emission and absorption lines should overlap each other which is possible only if $\Gamma \sim E_R$. In nuclear case, however, this overlapping does not occur as $\Gamma << E_R$ and that is why resonance absorption was not observable. However, sharp lines exhibiting natural line width are normally not observable and they are broadened due to a variety of mechanisms. One of them is thermal motion of nuclei in source and absorber, which leads to Doppler broadening of emission and absorption lines, given by

$$\Delta = 2\sqrt{E_R kT} \qquad .. (2.3)$$

At room temperature, Dopplar broadening is of the order of recoil energy and hence a small probability exists for nuclear resonance absorption (Fig. 2.1c) but its smallness precludes the detection process.

2.2 ATTEMPTS TO OBSERVE NUCLEAR RESONANCE ABSORPTION

P.B. Moon [26] was first to observe this effect in 1950 only. The fundamental idea in his experiment was to compensate for the recoil energy losses of the gamma quanta by moving the source at suitable high velocity towards the absorber. The resulting displacement of emission line, towards higher energy, produced measurable nuclear resonance absorption. The total recoil energy loss is $2E_R$, hence the source should be moved with

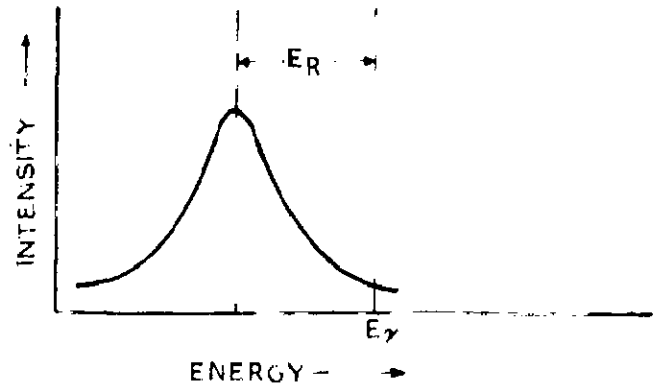

(a)

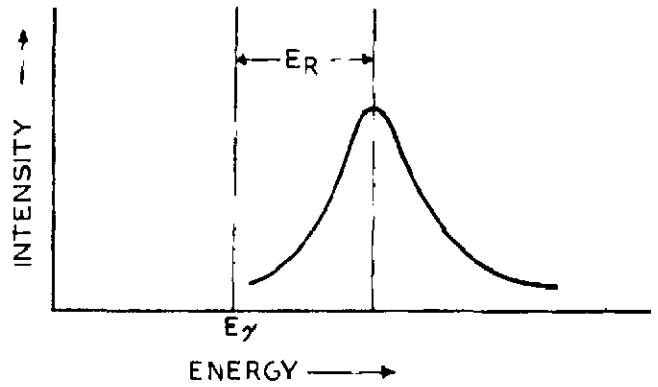

(b)

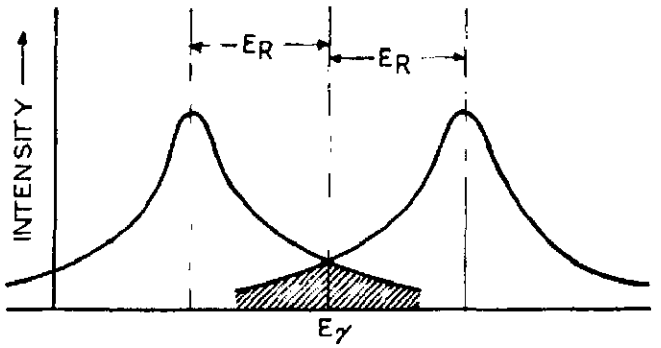

(Shaded zone shows the area of resonance absorption)

(c)

FIG.2.1 – (a) EMISSION LINE WITH RECOIL, (b) ABSORPTION LINE WITH RECOIL AND (c) EFFECT OF RECOILLING PHENOMENON ON RESONANCE ABSORPTION.

twice the recoil velocity, given by

$$v_R = E\gamma/Mc \qquad .. (2.4)$$

These velocities are of the order of 10^4 mm/sec.

Later on other experiments were also performed in this direction | 27-29|, but in all these the principle involved was to compensate for the recoil energy losses in someway or the other.

2.3 EXPERIMENT OF MOSSBAUER AND BIRTH OF MOSSBAUER EFFECT

During 1956 - 57, R.L. Mossbauer was doing experiments in order to find out the life time of 129 keV state of Ir^{191} by utilizing nuclear resonance absorption method. The simultaneous cooling of source and absorber led to striking result in that a strong increase in absorption was observed instead of the decrease. The result was in quite contradiction to the then available theoretical expectations.

To explain this anomalous resonance effect, he assumed nuclei in source and absorber to be bound, instead of free, as both were taken in crystalline form. Thus the recoil energy is transferred to the crystal as a whole which is taken up partly in the form of translation and rest in the form of internal energy.

The resultant increase in translational energy of crystal is negligible because of its enormous mass in comparison to that of a single nucleus. An increase in the internal energy leads

to changes in the occupation number of individual crystal oscillators. A gamma quantum can, therefore, be emitted and simultaneously crystal oscillators may undergo transition to a neighbouring or next energy state. Since crystal oscillators are having quantized energy states, there exists, in principle, the possibility of gamma emission without any change in the state of crystal oscillators. With the help of Lamb's theory [30], Mossbauer showed the existence of high probability of nuclear transitions without simultaneous change of lattice state under his experimental conditions. Since these transitions are not associated with energy loss caused by recoil phenomenon, these are known as 'recoilless transitions'. In these, momentum is still transferred but it is always taken up by the crystal as a whole and, therefore, the corresponding translational velocity is negligibly small. Fairly large number of papers have discussed its classical and quantum mechanical aspects [1, 12, 31-34].

In an Einstein solid, the vibration state of the crystal is defined by frequency, ω, the Einstein frequency. In the case $E_R >> h\omega$, nuclear processes will be associated with the simultaneous transitions of crystal oscillators and hence the probability of recoilless process is quite small. On the other hand for the case $E_R << h\omega$ the situation is reverse i.e. the probability of recoilless transition is high. However, real crystals exhibit a continuous frequency spectrum with higher oscillator densities at high frequencies. Einstein frequency can, therefore, be replaced by upper frequency of vibration spectrum of real

crystal. This upper frequency 'ω_D' is related to Debye temperature θ_D of solid by

$$\hbar\omega_D = k\,\theta_D$$

The condition for recoilless process can, hence, be written as

$$E_R << k\,\theta_D \qquad .. (2.5)$$

Thisis, thus, alsothe condition of recoilless resonance absorption i.e. ' Mossbauer Effect'. Further hecalculated the probability of this effect in a general form known as 'recoilless fraction' (described in a later section).

2.4 PECULARITIES OF MOSSBAUER SPECTRUM

Mossbauer spectrum is a plot between transmitted (or scattered) gamma-ray intensity and relative velocity between source and sample. Various characteristics of the lines appearing in a spectrum are as follows:

2.4.I LINE SHAPE

A Mossbauer gamma-ray emitting nucleus may be considered as a damped harmonic oscillator |13|. Under the condition that reaction forces, responsible for damping, are small, one can write its equation of motion as

$$x = x_0\, e^{-\gamma t/2}\, e^{-i\nu_0 t} \qquad .. (2.6)$$

where

$$\gamma = \frac{2}{3}\,\frac{e^2}{Mc^3}\nu_0^2 << \nu_0 \;|35|$$

The radiation emitted by such an oscillator will vary in amplitude similar to that of the oscillator. So, for $t > 0$, vector $\bar{E}$ (of radiation) is given by

$$\bar{E} = \bar{E}_0 \, e^{-\gamma t/2} \, e^{i\nu_0 t} \qquad ..(2.7)$$

The intensity distribution from its Fourier transform, can be written as

$$I(\nu) = I_0 \, \gamma/2\pi \quad \frac{1}{(\nu-\nu_0)^2 + \gamma^2/4} \qquad .. (2.8)$$

Above equation represents ' Lorentzian ' or' Breit Wigner' line, with breadth at half maximum as ' γ '.

The breadth at half maximum is equal to total transition probability per unit time. Hence mean life time can be given as

$\tau = 1/\gamma$, and

natural line width

$$\Gamma = \hbar\gamma \qquad ..(2.9)$$

Hence, equation (2.8) can be written as

$$I(E) = \text{Const.} \frac{\Gamma}{2\pi} \quad \frac{1}{|(E-E_0)^2 + \Gamma^2/4|} \qquad ..(2.10)$$

Thus recoil free gamma rays have lorentzian line shape. having natural line width at half maximum.

2.4.II LINE WIDTH

It was observed in the preceding section that line shape of emission and absorption lines are Lorentzian with natural line width. Since line shape in the Mossbauer spectrum is superposition of emission and absorption lines, width of line in it is a sum of the two i.e. $(\Gamma_a+\Gamma_s)$ where subscripts 'a' and 's' refer to absorber and source respectively. However, this line width is never attained and is broadened because of the following effects.

Thickness of the absorber is one of the causes responsible for broadening |20|. The experimental line width is

$$\Gamma_{ex} = \Gamma_a + \Gamma_s + 0.27\,\Gamma_H\, n\, f_a\, \sigma_o \qquad .. (2.11)$$

where n is number of atoms of Mossbauer isotope per cm^2 in the absorber. Thus with increase in n, caused by increase in thickness of absorber, Γ_{ex} increases. 'Solid angle effects' also broaden Mossbauer line |36|. The broadening is proportional to the diameter of detector and varies inversly as the source-detector distance.

Certain solid state properties of samples also cause line broadening. Thus partially relaxed hyperfine structure (Superparamagnetism, paramagnetic relaxation etc.) broaden the line because here spin relaxation time is of the order of Larmor precession time of nucleus. Motional narrowing is yet another reason for this effect |37|.

2.4.III LINE INTENSITY

One of the most important reasons for difference in the intensity of lines is different values of transition probabilities. In single crystals, the line intensity is dependent on angle between directions of gamma-ray and crystal axis. This angular dependence averages out in polycrystals due to their random orientation resulting into lines of equal intensity. Yet another reason, even in polycrystals, is anisotropic f-factors|38|. This is known as 'Goldanskii-Karyagin effect'.

2.5 SIGNIFICANCE OF MOSSBAUER EFFECT

The most significant aspect in Mossbauer spectrum was the observance of Lorentzian lines with line width $\sim 10^{-9}$ eV (comparable to natural line width) which is many orders of magnitude smaller than width of thermally broadened lines ($\sim 10^{-2}$eV). This extraordinary sharpness of the lines helped the workers to observe nuclear hyperfine structure which remains hidden in gamma lines (observed with recoil) because their thermal width is always larger than the spacing of nuclear hyperfine levels.

Another aspect is measurement of energies with higher resolution. The energy resolving power is given by

$$\frac{\delta E}{E} \sim \frac{10^{-9}}{10^{3}} = 10^{-12}$$

Thus energy of gamma-rays is defined here to 1 part in 10^{12} and hence extraordinarily small energy differences can be measured.

Total cross-section for resonant absorption of gamma-rays, in case of Fe^{57}, is about 200 times as great as that of next important process, photoelectric effect. The resonant process is, therefore, dominant even if the presence of radioactive nuclei is in minority.

2.6 RECOILLESS FRACTION

With the help of Lamb's theory, Mossbauer could calculate a finite probability for recoil free process. This is known as 'recoilless fraction'. Its value is zero for a free atom and increases with lattice regidity. The classical and quantum mechanical theory |39| yield following expression for recoilless fraction.

$$f = \exp\left[- \frac{4\pi^2 \langle x^2 \rangle}{\lambda^2} \right] \qquad .. (2.12)$$

where $\langle x^2 \rangle$ is mean square displacement of Mossbauer nuclide in the direction of gamma-rays, and λ represents wavelength of gamma-ray photon.

Thus to have fairly large probability of recoilless process $\langle x^2 \rangle / \lambda^2 \ll 1$ i.e. the mean square displacement should be very small in comparison to wavelength of gamma-ray.

2.7 DETAILS OF MOSSBAUER ISOTOPE

Co^{57} isotope (parent nucleus of Mossbauer isotope Fe^{57}) has been used in present investigations. Preference for this lies in the following reasons. It has got low lying gamma-ray level, which causes low recoil energy and hence high recoilless

fraction even atroom temperature (f$\sim$0.80), with suitable line width. Its half life is 270 days. It has got low internal conversion coefficient and high value of resonant absorption cross-section. The natural abundance of Fe^{57} is about 2%. Above all, iron is a transition metal most common in day-to-day life having familiar compounds and alloys. The decay scheme of Co^{57} isotope, responsible for emitting 14.4 keV Mossbauer gamma-ray, has been shown in Fig. 2.2 and important physical parameters |10| are given in Table 2.1.

2.8 CHOICE OF A SUITABLE 'HOST MATRIX' FOR GAMMA-RAY SOURCE

To observe recoil-free gamma-rays, the source is placed in a lattice known as 'host matrix'. Number of criteria determine the selection of a suitable host matrix |15| which are as follows. Firstly the lattice should have high Debye temperature to ensure high probability of recoil-free gamma-rays. Secondly the lattice should be metallic or ionic which gives largest 'f' factors. To obtain narrowest possible Lorentzian line, each source atom should be placed in precisely equivalent lattice sites having cubic symmetry. The host matrix should also not produce interfering X-rays, compton scattering etc. so that it gives maximum signal to noise ratio. Above all the source should be chemically inactive and it should not react with the atoms of host matrix.

For Co^{57} isotope, the common matrices used are Cr, Cu, Pd

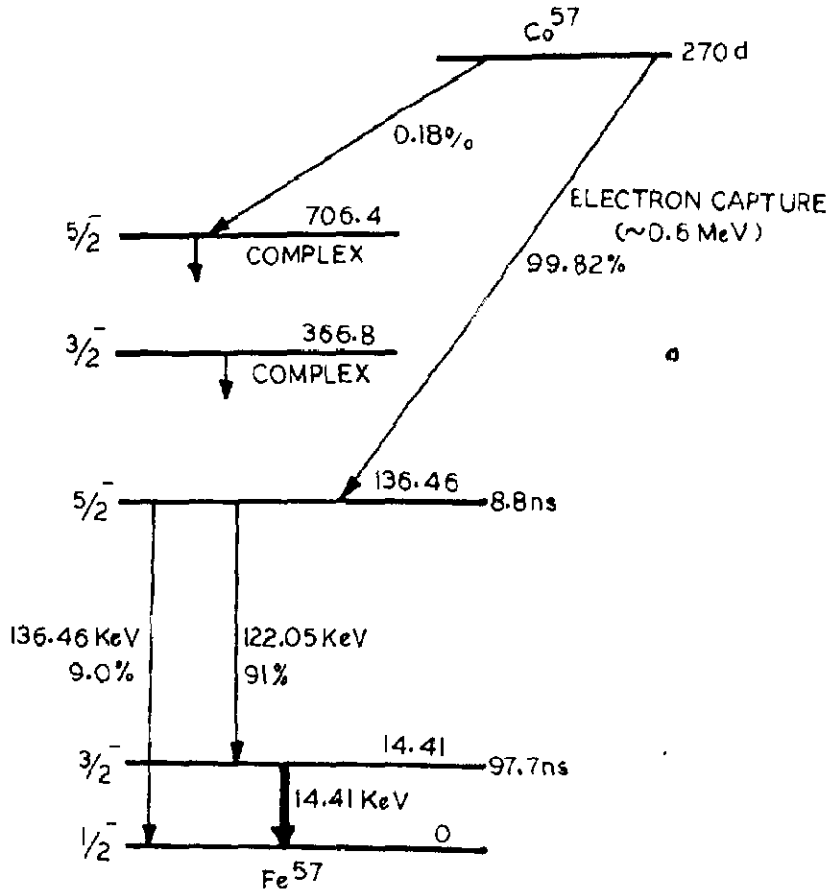

(Thick line is indicating Mössbauer transition)

FIG.2.2 _ DECAY SCHEME OF Co^{57} ISOTOPE.

TABLE 2.1-IMPORTANT PHYSICAL PARAMETERS OF 14.4 KeV MOSSBAUER GAMMA-RAY TRANSITION

(i) Measured Properties

Energy of gamma radiation, E_γ	14.41303 ± 0.00008 KeV
Half life of excited state, $T_{1/2}$	97.81 ± 0.14 ns
Total internal conversion Coefficient, α_T	8.21 ± 0.12
Natural abundance of isotope, IA	2.14 %
Spin and parity of ground state, I_g	$1/2^-$
Spin and parity of excited state, I_e	$3/2^-$
Magnetic moment of ground state, μ_g	+0.090604 nm
Magnetic moment of excited state, μ_e	-0.15491 nm
Quadrupole moment of excited state, Q_e	+0.21 ± 0.01 barns

(ii) Derived parameters

Maximum resonance cross-section, σ_o	2.566×10^{-18} cm^2
Natural line width, Γ	4.665×10^{-9} eV (0.096 mm/s)
Observable width, W_o	0.1940 mm/s
Recoil energy, E_R	1.956275×10^{-3} eV
Debye temperature, θ_D	420°K
Recoilless fraction, f, with θ_D=420°K	f(300°K)=0.79, f(90°K)=0.92

and stainless steel. Of these Pd is considered to be most suitable matrix.

2.9 HYPERFINE INTERACT

A major portion of research papers on Mossbauer spectroscopy deals with the study of interactions of nucleus with surrounding electrons. These are known as 'hyperfine interactions' and are of two types.

2.9.I ELECTROSTATIC INTERACTION

It is an interaction between nuclear charge density $\rho(\bar{x})$ and electrostatic potential $V(x)$ arising from all extra nuclear charges and is given as

$$H_e = \int d^3x\, \rho(\bar{x}) \left[V_0 + \sum_j \left(\frac{\delta V}{\delta x_j}\right)_0 x_j + \frac{1}{2} \sum_{jk} \sum \left(\frac{\delta^2 V}{\delta x_j \delta x_k}\right)_0 x_j x_k + \ldots\right] \quad .. (2.13)$$

where integration has been taken over entire nuclear volume. In the above expression the second and fourth terms are zero as the integrand is an odd function. Magnitudes of further terms are negligibly small. Hence only first and third terms of (2.13) will be discussed.

2.9.Ia. MONOPOLE INTERACTION OR ISOMER SHIFT

The first term considers two approximations (i) nucleus is spherical in shape and (ii) charge density is uniform.

The correction term δE (in interaction energy) which accounts for nuclear size |13|, is given by

$$\delta E = \frac{2\pi}{5} Ze^2 |\psi(o)|^2 R^2 \qquad .. (2.14)$$

where $e|\psi(o)|^2$ represents electronic charge density in the viccinity of nucleus (since contribution of only s electrons is dominating, this quantity will be referred to as s-electron density hereafter) and 'R' denotes radius of nucleus. As 'R' for excited and ground state is different, δE for these will be different. The situation has been depicted in Fig. 2.3a for source and absorber both. The energy difference between excited and ground state is given by E_s and E_a in source and absorber respectively. Isomer shift 'δ' is defined as

$$\delta = (E_a - E_s) = \frac{4\pi}{5} Ze^2 \left(\frac{\delta R}{R}\right) R^2 \left[|\psi_a(o)|^2 - |\psi_s(o)|^2\right] .. (2.15)$$

where $\delta R = R_{ex} - R_{gd}$. The Mossbauer spectrum will show a resonance line shifted from zero velocity (Fig. 2.3b) by an amount equivalent to 'δ'.

'δR' for Fe^{57} is negative |39|, hence isomer shift is smaller for absorber having larger s-electron density and vice-versa. The shift also depends upon number of 'd' electrons because they spend part of their time nearer to nucleus than s-electrons and hence produce screening effects. Thus $Fe^{2+}(d^6)$ ions have larger isomer shift than $Fe^{3+}(d^5)$ ions. The variation of isomer shift has been found to be in the

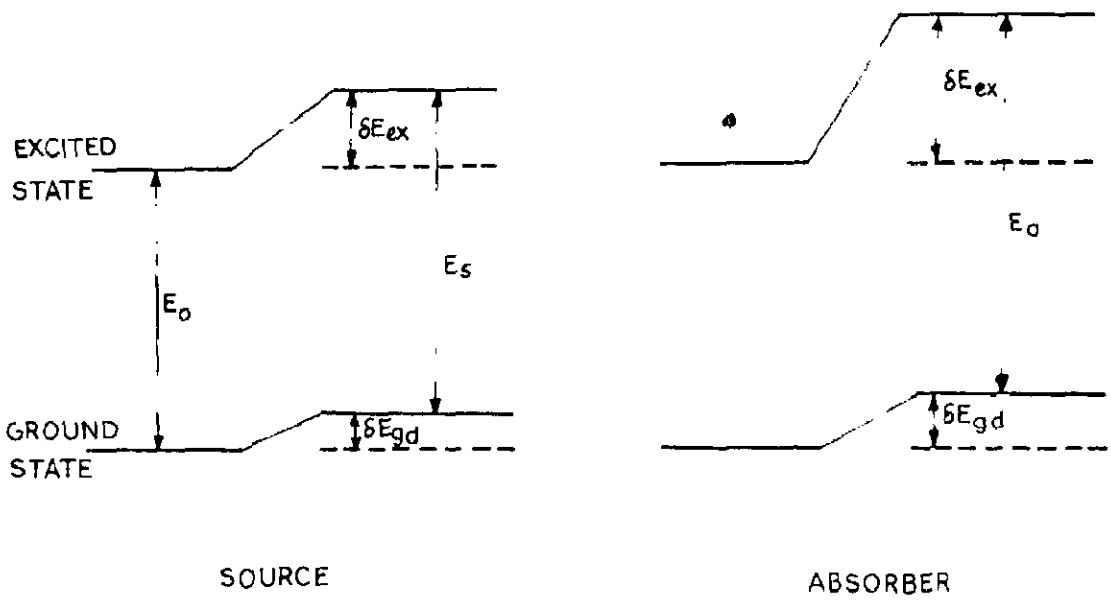

ISOMER SHIFT = $(E_a - E_s)$

(a)

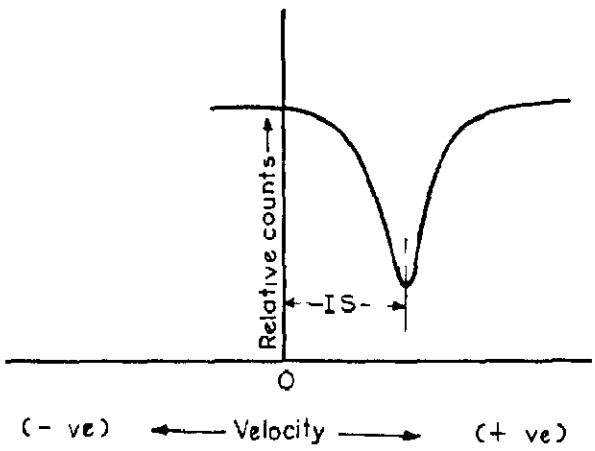

(b)

FIG. 2.3 - (a) SHIFT IN ENERGY LEVELS IN SOURCE AND ABSORBER DUE TO MONOPOLE INTERACTION.
(b) MÖSSBAUER SPECTRUM SHOWING ISOMER SHIFT.

following order:

$$Fe^{2+}(\text{ionic}) > Fe^{3+}(\text{ionic}) > Fe^{2+}(\text{covalent}) > Fe^{3+}(\text{Covalent})$$

2.9.Ib. QUADRUPOLE INTERACTION OR QUADRUPOLE SPLITTING

The second non zero and effective term in eqn. 2.13 is quadrupole term arising out of the interaction between quadrupole moment and gradient of electric field.

By appropriate choice of coordinate system, the components of electric field gradient (EFG) tensor are reduced to three: V_{xx}, V_{yy}, V_{zz}, such that

$$V_{xx} + V_{yy} + V_{zz} = 0 \text{ and } |V_{zz}| > |V_{yy}| > |V_{xx}|$$

Two new parameters are introduced. These are

$$q = V_{zz}/e \quad \text{and} \quad \eta = \frac{V_{xx} - V_{yy}}{V_{zz}} \qquad .. (2.16)$$

'η' is known as 'asymmetry' parameter.

The quantum mechanical analogue of quadrupole interaction is given by [13],

$$H_Q = \frac{e^2qQ}{4I(2I-1)} \left[3I_z^2 - I(I+1) + \eta/2 \, (I_+^2 + I_-^2) \right] \qquad .. (2.17)$$

where I_z is z component of spin I and I_+ and I_- are raising and lowering operators. The eigenvalues of eqn. 2.17,

in axially symmetric system, are given by

$$E_Q = \frac{e^2qQ}{4I(2I-1)} \left[3m_I^2 - I\,(I+1)\right] \qquad .. (2.18)$$

For Fe^{57}, only I=3/2 level splits into two sublevels corresponding to $m_I = \pm 3/2$ and $\pm 1/2$. The energy separation between these two levels is

$$\Delta E_Q = \frac{1}{2} e^2qQ \qquad .. (2.19)$$

'ΔE_Q' is called quadrupole splitting (Q.S.). The Mossbauer spectrum in this case is a doublet with energy separation of 'ΔE_Q'. The level scheme and Mossbauer spectrum have been depicted in Fig. 2.4.

The intensity of doublet has following angular dependence |20|,

Transition	Angular dependence
$\pm 3/2 \rightarrow \pm 1/2$	$(1+ \mathrm{Cos}^2\theta)$
$\pm 1/2 \rightarrow \pm 1/2$	$(5/3 - \mathrm{Cos}^2\theta)$

where 'θ' is angle between crystal axis and gamma-ray direction. This dependence will be only in case of single crystals. In powder samples doublet components are of equal intensity due to random orientation of crystals.

Q.S. values are characteristics of Fe^{2+} and Fe^{3+}

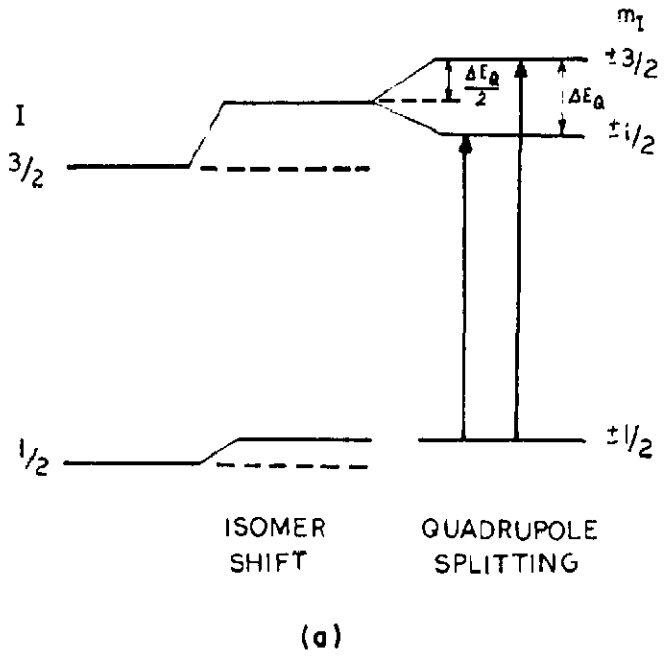

(a)

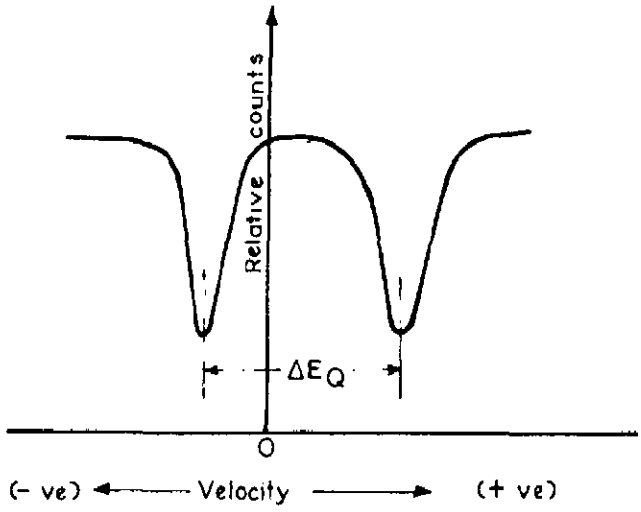

(b)

FIG.2.4 - (a) LEVEL SCHEME WITH QUADRUPOLE INTERACTION IN CASE OF Fe^{57}.
(b) MÖSSBAUER SPECTRUM SHOWING QUADRUPOLE SPLITTING.

compounds with further differentiation of low and high spin state |20|. The largest quadrupole interaction has been found in the case of Fe^{2+} high spin compounds followed by Fe^{3+} low spin. Q.S. is also indicative of site distortion. Thus Fe^{2+} low spin and Fe^{3+} high spin compounds having near octahedral surrounding show less Q.S. than those having tetrahedral or any other symmetry less than cubic.

2.9.II MAGNETIC DIPOLE INTERACTION OR NUCLEAR ZEEMAN EFFECT

This effect is a result of interaction between nuclear dipole moment μ and the magnetic field H. This field may be an externally applied or due to the atom's own electrons. The hamiltonian of this interaction is given by

$$H_M = -\bar{\mu} \cdot \bar{H} = - g\mu_n \bar{I} \cdot \bar{H} \qquad .. (2.20)$$

The energy eigen values are given by

$$E_m = - g\mu_n H\, m_I \qquad .. (2.21)$$

Thus in case of Fe^{57}, I = 3/2 splits into four and I = 1/2 into two levels due to this interaction. The transitions are restricted to six in number because of selection rule $\Delta m_I = 1, 0$. The resulting Mossbauer spectrum will, therefore, consist of six lines. The value of intensity of allowed transitions alongwith their angular dependence and energy position of splitted levels has been shown in Table 2.2. The spectrum

TABLE 2.2- VARIOUS QUANTITIES CONNECTED WITH MAGNETIC HYPERFINE TRANSITIONS

S.No.	Transitions	m_I	Energy Position	Total relative Intensity	Angular Dependence
1	$-3/2 \rightarrow -1/2$	-1	$E_o-(\frac{3}{2} g_e\mu_n H+ \frac{1}{2} g_g\mu_n H)$	3	$\frac{9}{4}(1+\cos^2\theta)$
2	$-1/2 \rightarrow -1/2$	0	$E_o-(\frac{1}{2} g_e\mu_n H+ \frac{1}{2} g_g\mu_n H)$	2	$3\sin^2\theta$
3	$+1/2 \rightarrow -1/2$	+1	$E_o+(\frac{1}{2} g_e\mu_n H- \frac{1}{2} g_g\mu_n H)$	1	$\frac{3}{4}(1+\cos^2\theta)$
4	$-1/2 \rightarrow +1/2$	-1	$E_o+(-\frac{1}{2} g_e\mu_n H+ \frac{1}{2} g_g\mu_n H)$	1	$\frac{3}{4}(1+\cos^2\theta)$
5	$+1/2 \rightarrow +1/2$	0	$E_o+(\frac{1}{2} g_e\mu_n H+ \frac{1}{2} g_g\mu_n H)$	2	$3\sin^2\theta)$
6	$+3/2 \rightarrow +1/2$	+1	$E_o+(\frac{3}{2} g_e\mu_n H+ \frac{1}{2} g_g\mu_n H)$	3	$\frac{9}{4}(1+\cos^2\theta)$

g_e and g_g are nuclear 'g' factor for excited and ground state respectively.

and energy level scheme are projected in Fig. 2.5.

The angular dependence of intensities of sextet components is as follows: (i) For a random orientation of H with respect to gamma-ray, the intensities are in the ratio 3:2:1::1:2:3, (ii) when H is perpendicular to the direction of gamma-ray, intensity ratio of lines is 3:4:1::1:4:3; and (iii) In case of axial magnetic field, the intensity ratio is 3:0:1::1:0:3.

The effective magnetic field is a sum of three quantities as follows:

$$H = H_C + H_L + H_D \qquad .. (2.22)$$

The term 'H_C' is called Fermi contact interaction and arises as a result of direct coupling between nucleus and s-electrons. It may be written as

$$H_C = - \frac{16\pi}{3} \mu_B \langle \Sigma \left(|\Psi(o)|^2_{s\uparrow} - |\Psi(o)|^2_{s\downarrow} \right) \rangle \qquad ..(2.23)$$

where $|\Psi(o)|^2_{s\uparrow}$ and $|\Psi(o)|^2_{s\downarrow}$ represent s-electron density, at nucleus, of electrons with spin up and down respectively. The difference between these two remains non zero even in the presence of filled s-shells. This happens because of the difference in interaction between spin up-3d and spin down-3d electrons.

Another term, H_L, in 2.22 arises due to unquenched

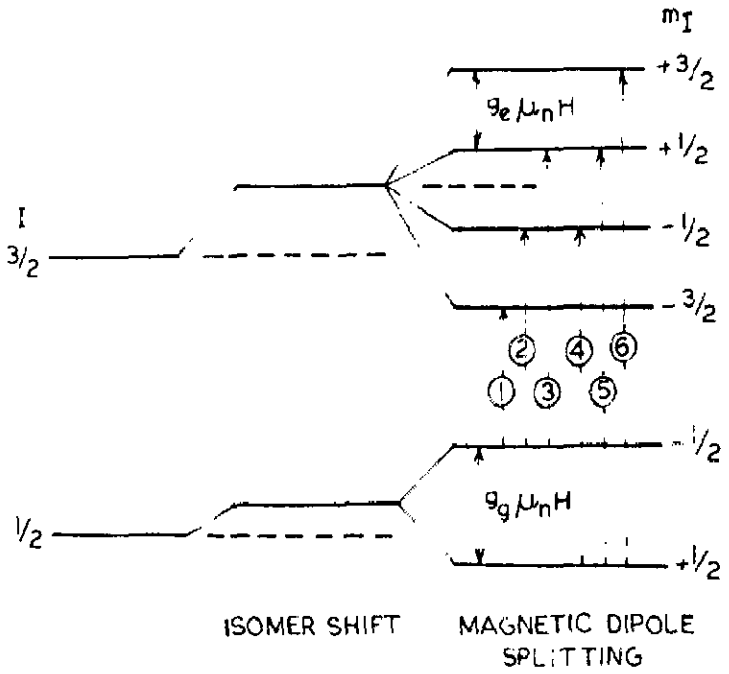

(g_e and g_g represents neclear 'g' factor for excited and ground states respectively)

(a)

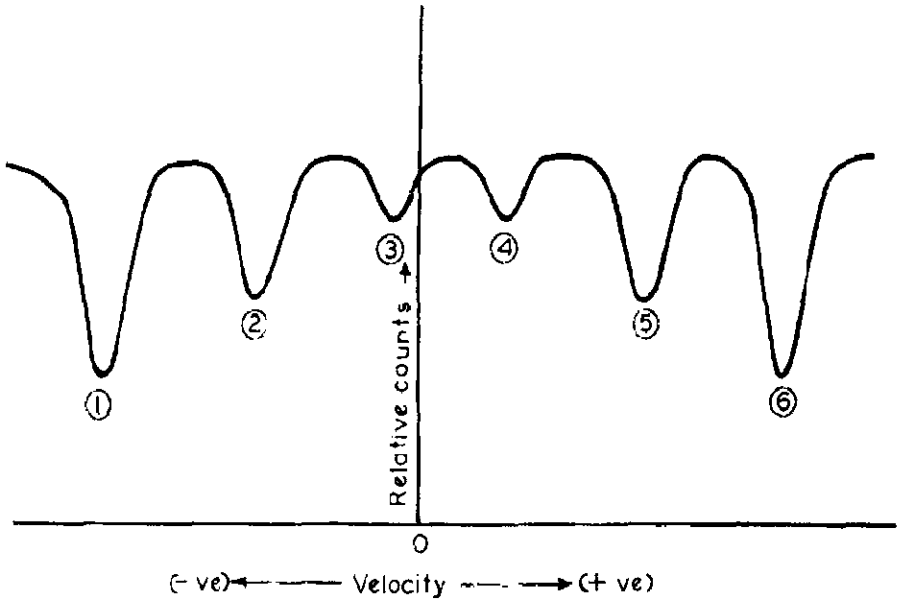

(b)

FIG. 2.5 _ (a) LEVEL SPLITTING IN Fe^{57} DUE TO MAGNETIC DIPOLE INTERACTION.

(b) MÖSSBAUER SPECTRUM SHOWING MAGNETIC HYPERFINE SPLITTING.

orbital moment of the atom and is

$$H_L = -2\mu_B \langle r^{-3} \rangle \langle \bar{L} \rangle \qquad .. (2.24)$$

where $\bar{L}$ is orbital angular momentum. In metallic iron this term is estimated to be +70 KOe. This is zero in the cases where 'd' level is partially (d^5) or fully filled (d^{10}).

H_D in 2.22 originates from the interaction between the nuclear and electronic dipole and is given by

$$H_D = -2\mu_B \langle 3\bar{r}(\bar{S}.\bar{r})/r^5 - \bar{S}/r^3 \rangle \qquad ..(2.25)$$

Its magnitude in the case of iron is many orders of magnitude smaller than H_C. In cubic materials where spin-orbit coupling is absent, this term is zero. Of the three interactions described above, the most dominant one is Fermi contact interaction and its direction is opposite to those of the other two.

2.9.III COMBINED ELECTRIC AND MAGNETIC INTERACTION

In certain cases e.g. α-Fe_2O_3 both the electric quadrupole and magnetic dipole interactions are present simultaneously. Here the energy values are given by |40|,

$$E = -g\mu_n H\, m_I + (-1)^{|m_I|+1/2} \frac{e^2qQ}{4} \frac{(3\cos^2\theta - 1)}{2} \qquad ..(2.26)$$

where 'θ' is angle between directions of EFG and mangetic axis.

When $\theta = 0^{o}$, i.e., the EFG axis is along the magnetic axis, the energy is given by

$$E = -g\mu_n H\, m_I + (-1)^{|m_I|+1/2}\ \frac{e^2qQ}{4} \qquad .. (2.27)$$

The splitting of levels is shown in Fig. 2.6a.

When $\theta = 90^{o}$, the energy values modify to

$$E = -g\mu_n H\, m_I + (-1)^{|m_I|+1/2}\ \frac{e^2qQ}{4}\,(-1/2) \qquad .. (2.28)$$

The energy levels have been depicted in Fig. 2.6b.

When $\theta = 0^{o}$, the magnitude of quadrupole splitting is given by , from Mossbauer spectrum, $(\Delta_{56}-\Delta_{12})/2$ (where Δ_{56} is energy difference between 5th and 6th line and Δ_{12} is that between 1st and 2nd line). In the case $\theta = 90^{o}$, the same is defined as $(\Delta_{56} - \Delta_{12})$.

2.10 SUPERPARAMAGNETISM

Within recent years, a relatively new field, superparamagnetism (spm) has made tremendous use of Mossbauer spectroscopy. The concept of spm was originally advanced by Neel [41] and is concerned with the particles, of magnetically ordered systems, having size so small that thermal energy starts playing a significant role in its magnetic behaviour. The problem has been reviewed [42,43] showing that thermal energy kT,

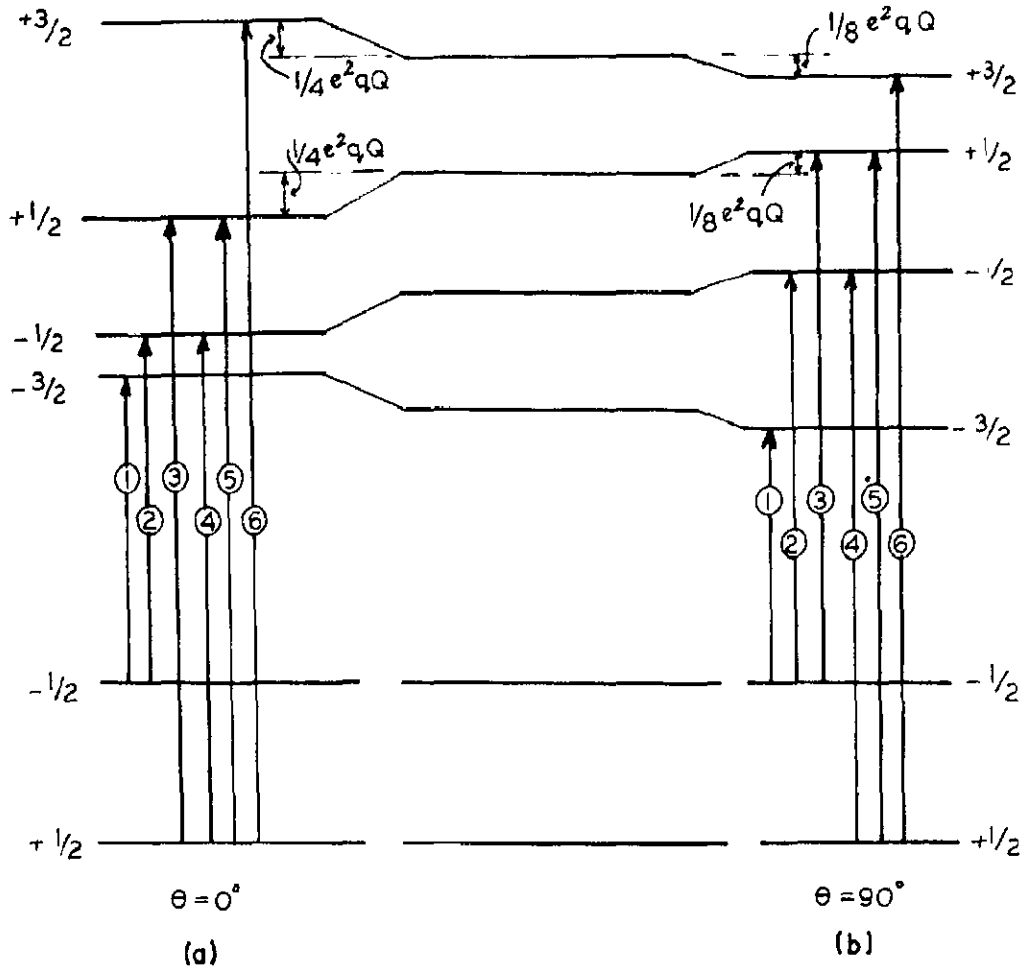

FIG.2.6 - LEVEL SPLITTING IN Fe^{57} IN PRESENCE OF ELECTRIC QUADRUPOLE AND MAGNETIC DIPOLE INTERACTIONS WHEN (a) $\theta = 0°$ AND (b) $\theta = 90°$.

at temperature of experiment, is sufficient to randomise the magnetisation of cluster in a time short compared to that of experiment. An assembly of such clusters is analogous to paramagnetic particles and is called as 'superparamagnetic'. The system has got much larger magnetic moment, μ, than that of paramagnetic system. Indeed, it may describe a cluster containing upto 10^5 atoms coupled magnetically. However, the cluster-cluster interactions are absent. That is why hysteresis effect remains absent which are normally shown by magnetically ordered materials. Spm has been observed in systems having ferro |44|, antiferro |45| and ferrimagnetic |46| ordering.

The application of Mossbauer spectroscopy in analysing the magnetic properties of individual species in a superparamagnetic cluster arises from the fact that the effect sees the behaviour of individual particle. However, the presence of spm will have to be confirmed from an independent experiment (magnetic susceptibility etc.).

Mossbauer spectra of spm systems are similar to those of paramagnetic systems at room temperature due to relaxation effects. The spin relaxation time, according to Neel |47|, is expressed by

$$\tau_s = (1/f_o) \exp (KV/kT) \qquad .. (2.29)$$

where f_o is a temperature insensitive constant of the order of 10^{10} c/s, K is effective anisotropy constant, V represents

particle volume and kT represents thermal energy. In the case of fine particles(spm) KV<kT |48|. With decreasing particle size and increasing temperature, τ_s decreases. At certain point this is just possible that spin relaxation time is smaller than the nuclear Larmor precession time ($\sim 10^{-8}$ sec. in usual iron compounds and alloys). Nucleus, thus,does not see any effective mangetic field and hence six line Mossbauer pattern collapses to either a doublet or a single broad line. The effects of spm,on the Mossbauer spectra, have been studied widely by varying particle size and temperature of measurements | 45,46,49-53|. The calculation of intensity ratio of magnetic pattern and doublet due to spm and its variation with temperature has led workers to conclude about the distribution of anisotropy energy and particle size |4,54-56|. Krop et.al. |54| have recently discussed the calculation of relaxation time of spm particles with the help of Mossbauer spectra.

The observation of spm in soils, clays and many natural samples has been established by taking Mossbauer spectra at room temperature and liquid nitrogen or liquid helium temperature and by comparing the ratio of magnetic to paramagnetic part of the spectrum which increases at lower temperature |56-58|.

2.11 APPLICATION OF MOSSBAUER SPECTROSCOPY IN STUDYING NATURAL SAMPLES

The mineralogical and geochemical applications of

Mossbauer spectroscopy have developed rapidly over the last few years. Although some studies have been done with tin and tungsten isotopes but a vast majority of the work has been performed with Fe^{57} gamma ray source. One of the reasons is the wide and varied distribution of iron inside the earth's crust. It is among the most abundant elements in nature and constitutes about 5% by weight of continental crust and 7% by weight of the entire crust. Accordingly, the natural solid inorganic materials of lithosphere e.g. rocks, soils, sediments, muds etc. typically contain iron in amount sufficient for investigations by Mossbauer spectroscopy.

With the help of Mossbauer spectroscopy one can get information about (i) oxidation state of iron, (ii) electronic configuration (e.g. low or high spin), (iii) coordination symmetry about iron atom and distortion from these symmetries, (iv) structurally distinct cation positions, (v) quantitative estimation of Fe^{2+} and Fe^{3+} both in different phases, (vi) Semi-quantitative estimation of iron containing minerals in bulk samples such as lunar rock or a meteorite and (vii) estimation of particle size of mineral grains which indicates whether a mineral is well crystallized or not.

In the pre-Mossbauer era, the determination of oxidation state of iron, was a problem. The commonly available methods e.g. X-ray analysis and electron probe were unable to distinguish between Fe^{2+} and Fe^{3+}. Whereas chemical analysis gave

unreliable results especially when the mineral dissolves with difficultyor when other transition metals are also present. Mossbauer spectroscopy has got the capability of distinguishing ferrous and ferric iron qualitatively as well as quantitatively.

Iron exists commonly in two valence forms and passes relatively easily from one to other as a result of oxidation or reduction. The determination of Fe^{2+}/Fe^{3+} in a rock or sediment sample can, therefore, provide information on its geochemical history. This ratio is also of considerable geological importance in explaining such phenomena as colour, pleochroism, oxidation and weathering of minerals. The expansion of paleomagnetism during last several years has focussed attention on solid state physics and chemistry of rocks particularly those which are chiefly responsible for magnetic properties. The minerals showing magnetic properties are essentially all iron-bearing. An understanding of rock magnetism requires identification of magnetic mineral phases and their respective grain size, which can be done by this technique successfully. This technique has also led to superior petrographic information, particularly on fine grained rocks or poorly crystallised sediments, even in case of specimens which have already been studied through other methods.

The first studies on minerals were started shortly after the discovery of Mossbauer effect. Magnetite was studied by Bauminger et.al|58| while hematite was investigated by

Kistner and Sunyar |59|. Later on Decoster et.al. studied natural silicates |60|. Sprenkel-Segel and Hanna |61| have done studies on the distribution of iron in stone meteorites. A large number of investigations have been performed since then with a considerable divergence of interests to collect data of geological significance. Some review articles |62-64| have been published which tell about the growth of application of this technique in tackling problems of geological and mineralogical importance. Recently it has been applied in studying lunar samples brought by Surveyor, Apollo and Luna missions. A review of these studies has been given by Hafner |65|.

2.12 INFRARED ABSORPTION SPECTROSCOPY

2.12.I INTRODUCTION

Infrared (IR) absorption spectroscopy concerns with studying the absorption spectrum of a sample with the help of infrared radiations. Wavenumber range of these radiations lies from 250 to 4000 cm^{-1}. Thus infrared radiation is a moving electric field oscillating at frequencies of $10^{12} - 10^{14}$ Hz. The internal movements of the atoms in a molecule with respect to its centre of mass occur within same frequency range. Hence whenever IR radiation, of the same frequency as those of vibrating atoms in a molecule, falls on it the same is absorbed provided the atomic vibration is coupled with a changing dipole moment. The energy thus absorbed is rapidly dissipated

in less than 10^{-6} sec. through either transforming into kinetic energy or releasing again as photon. As the direction of liberated photon is random in space and the absorption can be repeated for such a photon on its way through medium, the reemergence of once absorbed photon is least probable.

There are several modes of vibration for each atomic group which are dependent on inter-atomic distances, bond angles and bond forces, and the relative masses of constituent atoms. Each of these modes has a characteristic frequency and is normally independent of other modes. The IR absorption spectrum, a plot between percent absorption of radiation and incident wavelengths, will, therefore, be characteristic of a particular material. Thus in addition to giving data on structure and bonding characteristics within the molecules, IR analysis can also be used in identifying different constituents in an unknown mixture. In contrast to X-ray diffraction, IR analytical method is extremely sensitive to short range ordering and hence is an excellent tool for studying glasses and amorphous materials.

2.12.II APPLICATION IN MINERALOGY

Infrared absorption analysis has been used extensively and successfully in the study of organic compounds, however, literature on inorganic compounds is comparatively less. Its application in the field of mineralogy is possible due to the fact that most metal-oxygen bonds have fundamental vibrations

in the region 850 to 2000 cm^{-1}. All silicates, whose occurrence is quite common in nature, show marked absorption near 1000 cm^{-1} caused by Si-O stretching vibration, with Si-O bending vibrations at 'short' wavenumbers 665 to 400 cm^{-1}. The 330-1000 cm^{-1} region is also the region of fundamental vibrations for most of the inorganic salts e.g. carbonates, nitrates, sulphates, phosphates etc. that occur in the terrestrial rocks, and thus it is the region of paramount interest to the mineralogists.

Infrared analytical techniques are capable of distinguishing four major groups (a) minerals of relatively constant composition (e.g. quartz) (b) mineral that exhibits ranges of composition (e.g. between two end members as in the plagioclase feldspars and olivines), (c) minerals of constant chemical composition but with different crystal structures (e.g. SiO_2 as quartz, tridymite, cristobalite etc.) and (d) minerals that vary both in chemical composition as well as crystal structure. The ability of IR technique to distinguish between two types of water- one that is lost at or below 110°C (generally called adsorbed water on surfaces) and other that is evaporated well above 110°C (called '' constitutional water'') is an additional attraction to mineralogists. This is possible due to appearance of different absorption peaks of water because of differing degrees of freedom of hydrogen bonding in various forms |66,67|. White and Burns |68| have predicted the presence of 'hydronium', $(H_3O)^+$, ions in micaceous minerals. Some of the useful articles regarding IR analysis of minerals

have been written by Adler |69|, Hunt et.al.|70|. Grim |71| has reviewed IR studies on different clay minerals.

Thus IR studies are quite helpful in identifying minerals in a rock sample, in studying the structure of various minerals, the type of water present in a mineral etc.

2.13 DIFFERENTIAL THERMAL ANALYSIS

2.13.I INTRODUCTION

The study of thermal reactions, taking place at higher temperatures in a sample, dates back its history to about 1887 when Le Châtelier |72| tried to determine the constitution of different clays by heating them and finding the rate of change of temperature at different temperatures. The drawback with this method was that the difference in rate of heating due to changes in the substance itself could not be distinguished from those due to external causes. To overcome this defect, Roberts-Austen |73| devised the differential thermocouple method for measuring temperature differences between sample and a reference body which does not undergo any physicochemical transformation upto the maximum temperature to be attained.

Thus in differential thermal analysis (DTA),one heats two separately contained samples simultaneously (one that is to be analysed and the other which is reference). The temperature difference between them remains zero, shown by a base

line, till there is no reaction taking place in the analysing sample. As soon as reaction starts, the difference between the temperatures of the two is indicated by a dip if reaction is endothermic (because now the temperature of sample will be less than that of reference) and by a peak if reaction is exothermic, indicating that temperature of sample is more than that of reference material. No sooner than reaction is over, the pen of recording system returns to base line indicating that the two samples have returned to zero temperature difference again. The reference material normally used is alumina.

There are a number of changes which take place on heating and give rise to evolution or absorption of heat. Reactions involving crystallization, oxidation etc. are exothermic whereas phase changes, dehydration, decomposition and crystalline inversions are generally endothermic. The more energetic the reaction, the greater the amount of heat evolved or absorbed and the large will be the area covered by peak or dip on differential thermal curve. There are some reactions which begin slowly and gain impetus as temperature rises. These show a broadening of peak or dip at low temperature side and a rapid fall on the high temperature side. Crystalline inversion is a quite rapid raction and hence is shown by a sharp dip. Broader peaks are shown by sluggish reactions. The position and shape of peak or dip is dependent on the presence of impurity, grain size, degree of crystallinity of

sample and also on heating rate.

2.13.II APPLICATION IN MINERALOGY

Although differential thermal analysis was devised in 1899 and was widely used by metallurgists since then, it was only in 1913 that Fenner |74| applied this technique in the field of mineralogy. Since that time DTA has become a common method in mineralogy and geology. The DTA technique, as an analytical tool, can not distinguish a completely unknown material on its own. It is more effective when used in conjunction with other analytical methods e.g. X-ray analysis.

Silica minerals have been studied in considerable detail by this technique |71|. Keith and Tuttle |75| demonstrated that the $\alpha \rightleftharpoons \beta$ inversion of quartz was in fact quite variable, an important result with applications to geothermometry. Grimshaw and Roberts |76| have shown that DTA of rocks e.g. fine grained quartzite,gives lower results for silica contents than X-ray and chemical methods which has been suggested to be due to occurrence of chalcedonic silica which does not give a reliable thermal effect at inversion. This technique has also been applied for the study of minerals of iron oxide |77-78|, aluminium oxide |79|, carbonates, sulphates, nitrates etc. A large body of data on DTA studies of minerals may be obtained from the index of Mackenzie |80|.

CHAPTER 3

INSTRUMENTATION AND EXPERIMENTAL TECHNIQUE

3.1 INTRODUCTION

In a Mossbauer spectroscopy experiment one observes a resonance absorption of recoil free gamma-rays being emitted by an isotope Fe^{57m} (in present case). Resonant absorption is possible only if the nuclear levels involved in transition, of absorber (obviously a compound or alloy of iron) are having the same transition energy as that of incoming recoil free gamma-rays. This is, however, a rare case and the abovesaid levels have been found to shift or split due to hyperfine interactions, as has been discussed in chapter 2. The resonance absorption is achieved, in Mossbauer experiment, by modifying the energy of recoil free gamma-ray (14.4 KeV in case of Fe^{57m}) through producing a relative motion between the source and the absorber within a suitable velocity range. The modification in energy is governed by Doppler effect and is given by

$$E_\gamma \pm \Delta E = E_\gamma \pm \frac{v}{c} E_\gamma \qquad .. (3.1)$$

where positive velocity refer to the direction when source is approaching towards the abosrber and negative velocity to the opposite motion. Since the shift or splitting in the nuclear levels is of the order of 10^{-7} eV to 10^{-8} eV, velocity of the order of mm/s are sufficient to modify the energy of recoil free gamma ray so as to observe resonant absorption. As has been discussed in chapter 2, the width of recoil free gamma line is of the order of 10^{-8} eV. (in case

of 14.4 KeV of Fe^{57m}), hence a very precise and vibration and distortion free drive system is required for the motion of source so that the gamma-line is not broadened. Thus a very precise way of measuring quite small energy differences is at hand. This precision is,however, in the relative sense and not in the absolute measurement of energy. Review articles by Benczer-Koller |81| and Kalvius |82| have recently appeared on instrumentation in concern with Mossbauer spectroscopic experiments.

3.2 MOSSBAUER SPECTROMETER

In comparison to many other spectroscopic experiments the basic Mossbauer equipment is rather simple and inexpensive. The block diagram of the Mossbauer spectrometer used in the present investigation is shown in Fig.3.1. It consists basically of Mossbauer isotope (Co^{57} in present case) fixed upon a drive mechanism which imparts a known and controllable velocity, an absorber (sample to study), a gamma-ray detector with associated amplifying and sorting equipment and some sort of data storing device e.g. a multichannel analyzer. Each of these will now be discussed briefly.

3.2.I MOSSBAUER SOURCE

The isotope which is used as gamma-ray source in Mossbauer experiments is diffused in a suitable lattice usually referred to as'host matrix' so as to obtain maximum possible recoil free

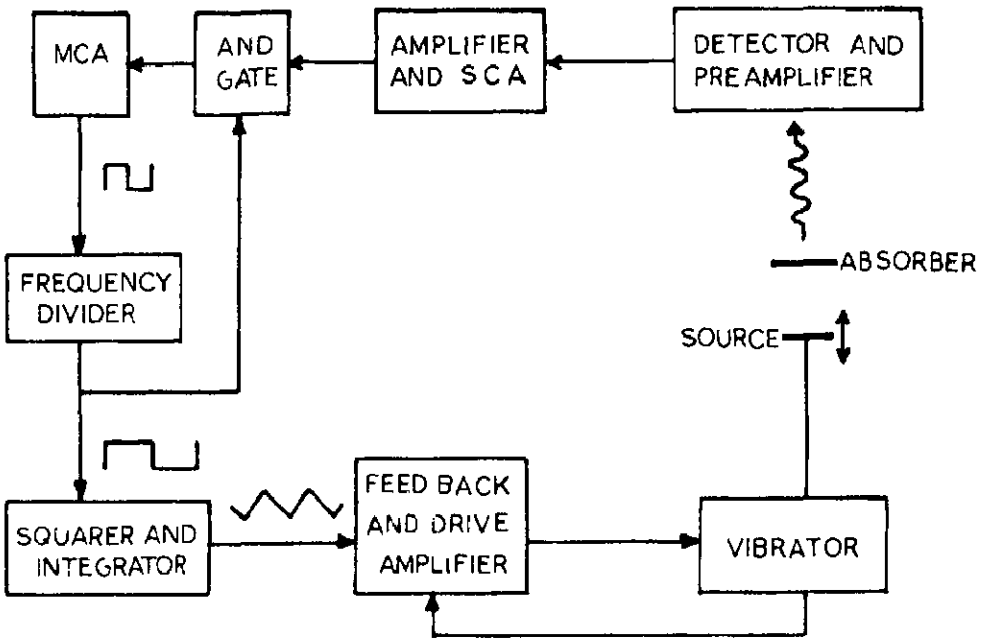

FIG. 3.1- BLOCK DIAGRAM OF MÖSSBAUER SPECTROMETER FOR RECORDING THE SPECTRUM IN TRANSMISSION GEOMETRY.

gamma radiations with least intefering radiations which increases signal to noise ratio. The criteria for chosing a suitable host matrix has already been discussed in section 2.8. One of them is that the Debye temperature of the lattice after putting the source in'host', should be much larger than recoil energy. The effective Debye temperature,when Mossbauer nuclei is introduced as an impurity in a host lattice, is given by |83|

$$\theta_{eff} = \theta_D \left[\frac{m_{host}}{m_{Imp}} \right]^{1/2} \qquad .. (3.2)$$

where m_{host} and m_{Imp} are masses of host and impurity atoms respectively while θ_D is Debye temperature of lattice. Thus to increase θ_{eff}, $m_{host} > m_{Imp}$ or the host matrix should have larger atomic mass than that of Mossbauer atom. After considering all the factors Pt, Pd, Cu have been found to be suitable host matrices.Of these Pd matrix has been found to be a reasonable compromise while considering recoil free factors, chemical inertness, line width, interfering radiations.

There is no fixed procedure to prepare a good source and the literature |84,85| indicates it to be trial and error method. The methods of inserting the radioactive isotope in suitable host are generally of three types (i) diffusion of isotope in host |19|, (ii) ordinary synthesis of a compound having parent nuclei |86|,(iii) by electroplating the activity on host lattice |87|.

The sources used in the present study were (a) Co^{57} in Cu matrix with initial activity of 3 mCi and (b) Co^{57} in Pd matrix with initial activity of 5.5 mCi . These were commercially certified and were purchased readymade from Bhabha Atomic Research Centre,Bombay, India. These were mounted on Mossbauer drive so as to obtain their motion within required velocity range.

3.2.II MOSSBAUER DRIVES

A Mossbauer spectrum is a plot between count rate and relative velocity between source and absorber. Thus a system which is capable of giving desired velocity to source or absorberforms an essential part of a Mossbauer spectrometer. This system is called 'Mossbauer drive'. Spectra can be recorded in two modes. In 'constant velocity' mode the source is moved by giving a particular constant velocity for a preset time during which the transmitted gamma counts are recorded. Similarly different constant velocities are given for the same preset time and transmitted gamma counts are recorded corresponding to respective velocities. In this way the spectrum builts up point by point. The drive used here should be able to provide constant velocity and hence is known as 'constant velocity drive'. In 'constant accelaration mode', the source is given a known range of velocities (say from -v to +v mm/s) in one cycle. The motion of the drive is such that rate of change of velocity remains constant. The transmitted gamma counts corresponding to each velocity are recorded

simultaneously in a data storing device e.g. multichannel analyzer. The cycles are repeated twice, thrice and so on upto a definite time and the whole spectrum is recorded simultaneously. The data is stored till a measurable absorption is observed. The drive used in this mode is known as ' constant accelaration drive'.

Mossbauer drives are mainly of two types. The mechanical drives which give motion to source mechanically with the help of motor while electromechanical drives use a predecided electrical signal and convert it to mechanical motion. Both of these types will now be discussed.

3.2.II a. MECHANICAL DRIVES

The mechanical drives make use of rotating discs |88|, cams |89|, lathe |90|, lead screws |91| etc. Of these the most applicable is cam driven type. The full assembly consists of motor, a reduction gear system, and a cam. In order to have a constant velocity, the cam is cut with great precision and have three regions, defined by polar equation, (Fig.3.12 of Ref. 19),

$r = a + b\theta$ Region A

$r = a - b\theta$ Region B

$r = a$ Region C

where 'r' is radius vector. A follower capable of carrying source or absorber is pressed on to the cam with spring. The

cam is driven by a motor at a fixed rpm, the angular velocity of cam converts to linear velocity in the follower system. The velocity is changed by changing speed of motor (or rpm) with the help of a gear system. During the rotation of cam, the follower moves forward during region'A',backward during region'B' and remains stationary during region 'C'. Region 'C' of cam helps in chekcing stability of electronic system. In this manner different constant velocities are given to source. Mechanical drives are very simple, less expensive, and their associated electronics is also simple. Extraneous vibrations, mechanical wear and tear and limitation of its use in constant velocity motion only, where the drift in the counting equipment becomes important, are certain disadvantages which make them less popular Further the range of velocities, in these drives, is restricted to about one or two cm/sec. because of vibrations. The study of complicated spectrum,therefore,can not be made with these drives.

3.2.II b. ELECTROMECHANICAL DRIVES

Electromechanical drives are much more widely used than the mechanical drives because of the ease of their operation, large coverable range of velocities, and practically little problem of drifts in counting system. Another point in its favour is its applicability in both constant velocity as well as constant accelaration mode with equally good accuracy. The essentials of an electromechanical drive include electrodynamic transducer, function generator and amplifier and feedback

system for stabilization of the mechanical motion. The electromechanical drive fabricated and used for the present investigations is of Kankeleit type |92,93|. Only a brief account of it will be given, the details are given elsewhere |94|.

The electromechanical transducer used in present investigations have been shown in Fig. 3.2. It consists of two permanent magnets rigidly connected back to back with brass bolts and an aluminium disc as spacer. The permanent magnets produce a field of about 5000 Gauss in the radial air gap of 0.18 cm. The field is kept constant to less than 0.3% over a length of 8 mm in axial direction. Pick-up coil and drive coil are wound on separate latheroid paper (5 mil) which are in turn mounted on aluminium holder and each is screwed near the opposite ends of a stainless steel rod passing through the axis of magnets. One end of the coil holder, of length 10 mm, passes through air gap between magnetic poles. Winding of coil has been done in 5 mm of the length passing through air gap between magnetic poles. The number of turns in drive coil are 64 (in two layers) of the enamelled copper wire of gauge number 32. The construction of other holder is similar at which pick-up coil is wound. In this case the enamelled copper wire is of 46 gauge and number of turns are 800 (in 4 layers). Two phosphor bronze springs (Fig. 3.3), each attached at the opposite ends of stainless steel rod passing through the axis of magnets, are shaped in such a way that the radial displacement is minimum and moving system is held up friction free on the

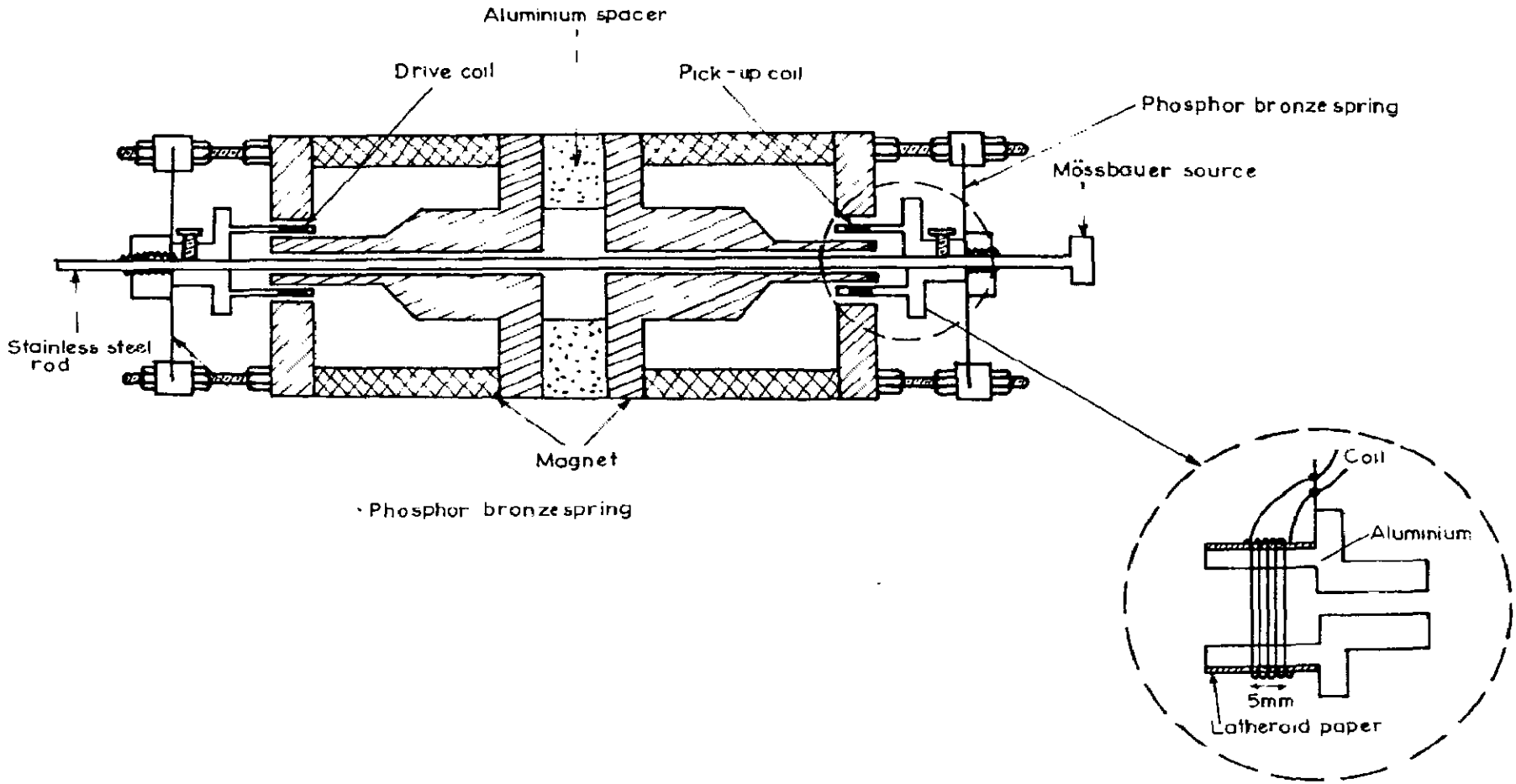

FIG.3.2 _ ELECTROMECHANICAL TRANSDUCER.

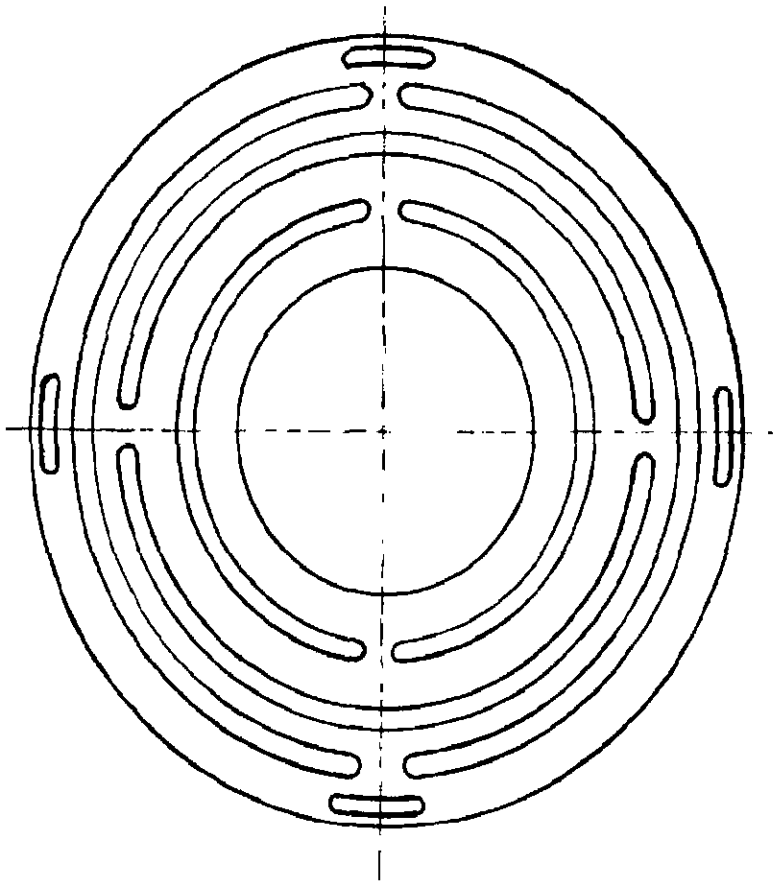

FIG.3.3 - PHOSPHOR BRONZE SPRING.

axis. These springs are better than those used previously by Kankeleit |93| in that the former show less tendency to resonate and are more sturdy.

The next important part of the drive system consists of function generator and amplifier and reverse feed-back system. In present set up the signal was generated from multichannel analyser, a data storing device. This is done by placing two bistables into their different stable states according to the quarter which is chosen, or by one bistable for the two halves. If, in the time mode, the signal generator is closing the last channel of first half, for instance, and opening the first channel of second half, one bistable will flip from one stable position into the other and vice-versa when first channel of first half is opened after the last channel of second half is closed. The output of the bistable will generate a square wave signal. Thus obtained square wave signal is then given to squarer unit, consisting of one operational amplifier with two pairs of zener diodes, so as to obtain pure square wave signal. This square wave signal is then integrated to obtain triangle signal. The triangle waveform is then diverted to two paths. At one path it acts as reference signal and sent to drive circuit for comparison with pick-up coil signal. In the other circuit the waveform is further integrated to obtain parabolic signal which is sent to drive coil to give the source constant accelaration motion. Circuit diagram of reference signal generator has been shown in Fig.3.4.

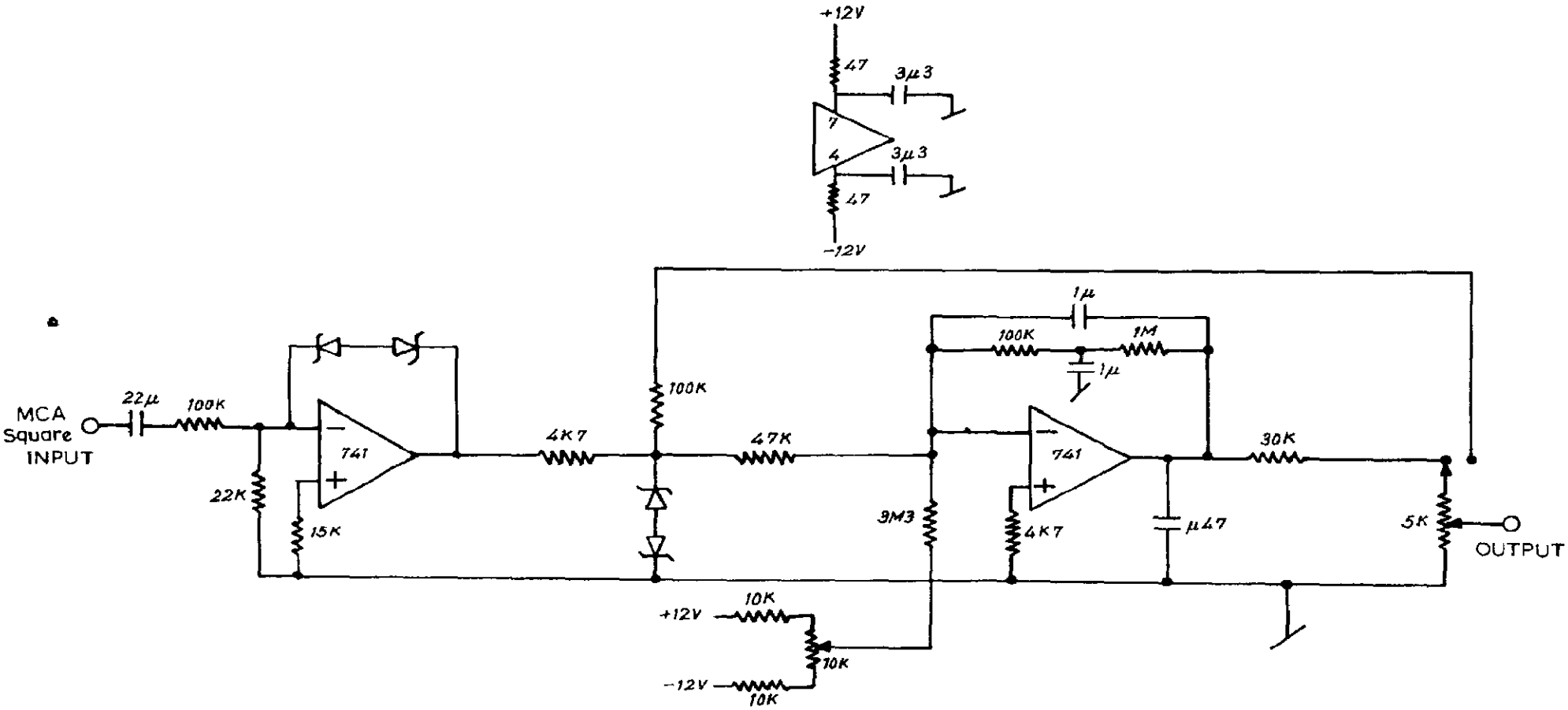

FIG. 3.4 - REFERENCE SIGNAL GENERATOR .

After generating reference signal and drive coil signal, the feed-back circuit will be discussed. The function of this circuit is to transform the drive signal so as to impart, to source, a velocity that is very accurately proportional to the reference signal. Complete diagram of feed-back circuit used in present investigations, is shown in Fig. 3.5.

The parabolic pulse given to drive coil forces the rod, passing through the axis of magnets and having radioactive isotope fitted on its pick-up coil end, to move along the axis of magnet. The motion is such that accelaration or rate of change of velocity is constant. However, the motion does not represent pure parabolic curve because of air resistance, air vibrations etc. Hence the pulse in the pick-up coil will also not be pure triangle because the pulse in this coil will be an induced one due to motion of the rod in the magnetic field. This triangle wave form is then matched with reference triangle. The error thus obtained is amplified, in present case the gain is 50, and then sent to integrator. A further gain control has been provided for integrated signal which gives total gain achieved through feedback circuit of the order of 3750. Thus obtained parabolic pulse is further amplified in a power amplifier so that it is able to drive the massive transducer armature. The resulting pulse is then sent to drive coil. At this point the error in the parabolic motion is decreased due to negative feedback. Again the pick-up coil sends a triangle wave, but lesser impure, and the same process is repeated.

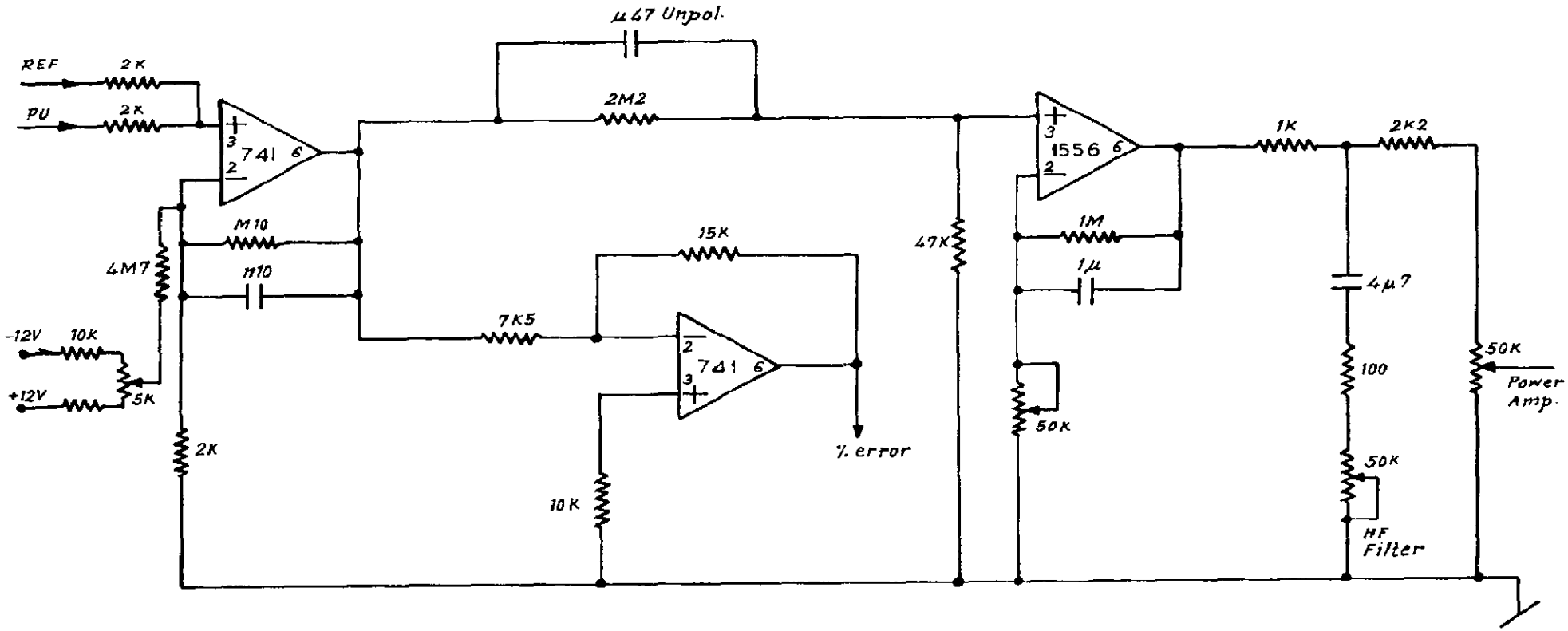

(FEED - BACK CIRCUIT)

CONTD. - - - - - - - - - - -

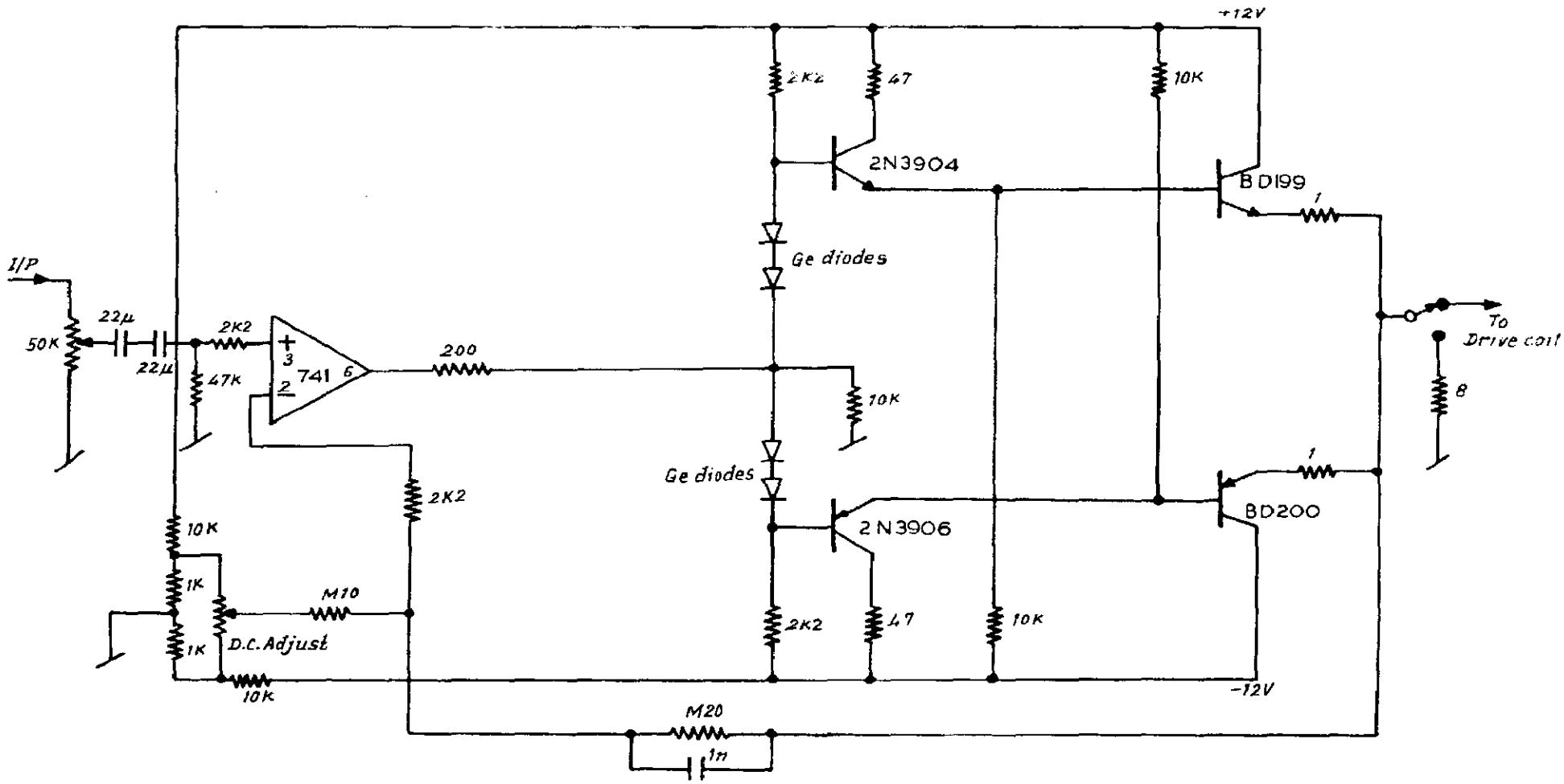

(POWER AMPLIFIER)

FIG.3.5- FEED- BACK CIRCUIT WITH POWER AMPLIFIER UNIT.

In this manner the error is reduced to maximum possible extent. In present case the error has been reduced to 0.2 percent of the reference. Thus a very precise motion of gamma-ray source is achieved.

These drives can be used in both constant velocity as well as constant accelaration mode. To use it in constant velocity mode the pulse to drive will be triangle while reference signal will be square, both of which can be obtained from multichannel analyser.

To use Mossbauer drive in constant accelaration mode, for present investigations, parabolic pulse has been used to give motion to source. Another possible waveform is sinusoidal waveform to operate the drive in this mode. With a scanning repitition rate of 5 KHz, the spectrum is taken essentially at once, and one can see the spectrum statistics improving as counts accumulate in all channels. It is, therefore, possible at all times during a run to judge the quality of collected information. Long term drifts produce, if at all, only an uncertainity in the size of the observed effect but do not affect its shape as is observed in constant velocity mode.

In some special cases, when one is interested in scanning a specific region of the spectrum, alternate waveforms such as saw tooth or trapezoidal can be used. Methods for producing suitable waveform have been illustrated by Cranshaw |95|.

3.2.III BINARY FREQUENCY DIVIDER

Mossbauer spectra of natural samples having two or more iron containing phases are quite complicated and, therefore, are difficult to resolve while using a 256-channel analyser. The difficulty becomes even more when two or more phases are magnetic at room temperature, because then one needs higher velocity range which reduces velocity resolution. The difficulty can be overcome by increasing the velocity resolution by the introduction of frequency divider. This divider allows the frequency division of the square wave form, taken from 2^7 binary unit, by two or four without changing the velocity of source. Thus in a time when MCA sweeps through all of its channel, the source moves half or one fourth of its original cycle according to the divider used and hence the velocity resolution is doubled or quadrupled.

For present investigations, the provision was made for division of square wave frequency by two and four. However, only former mode was found suitable enough for resolution of the spectra of present studied sample. The division of the waveform frequency was guided by the principle illustrated by Michalski et.al.|96|. Two basic circuits needed for recording spectrum with division of frequency are (i) Frequency divider and (ii) Gates, which allow counts to store in MCA only during a particular part of drive cycle.

In the present circuit, IC SN7493 was used as frequency divider (Fig. 3.6a). Point 1 on this IC was given input from

MCA clock (designated by 1A) which is a square pulse with frequency equal to that of MCA sweep. The output is taken from point 8, a square wave with frequency one fourth of the original (denoted by 3A), from point 9, a square wave of frequency half of the original (denoted by 2A).

To store counts in the mode, when frequency of drive has been halved, the output 2A is given to squarer of drive. After proper shaping, the square wave is given to drive circuit at one path and to emitter follower at second path (Fig.3.6b). The output,denoted by S, is given to IC SN74 H21N (Fig.3.6e), which has been used for gating purpose. Output from SCA, denoted by 1B, is given to another emitter follower circuit (Fig.3.6c). The output denoted by Y, is given to IC (Fig.3.6e). Here double coincidence between S and Y is achieved in such manner that whenever S is positive the gate opens otherwise remains closed. The output,denoted by 2B, is then passed through inverter circuit to match with MCA input (Fig. 3.6f). The output Z goes to MCA. Thus the counts are stored in the case when S is positive whereas data does not accumulate when S is negative. Thus counts corresponding to only first half of the drive cycle are stored. The waveforms showing the accumulation of data with drive cycle frequency divided by 2, have been shown in Fig. 3.7. Thus counts corresponding to shaded region only are stored in MCA. In this way velocity resolution of the spectrum is doubled without affecting v_{max} because now only half of the drive cycle has taken time equal to that taken by MCA

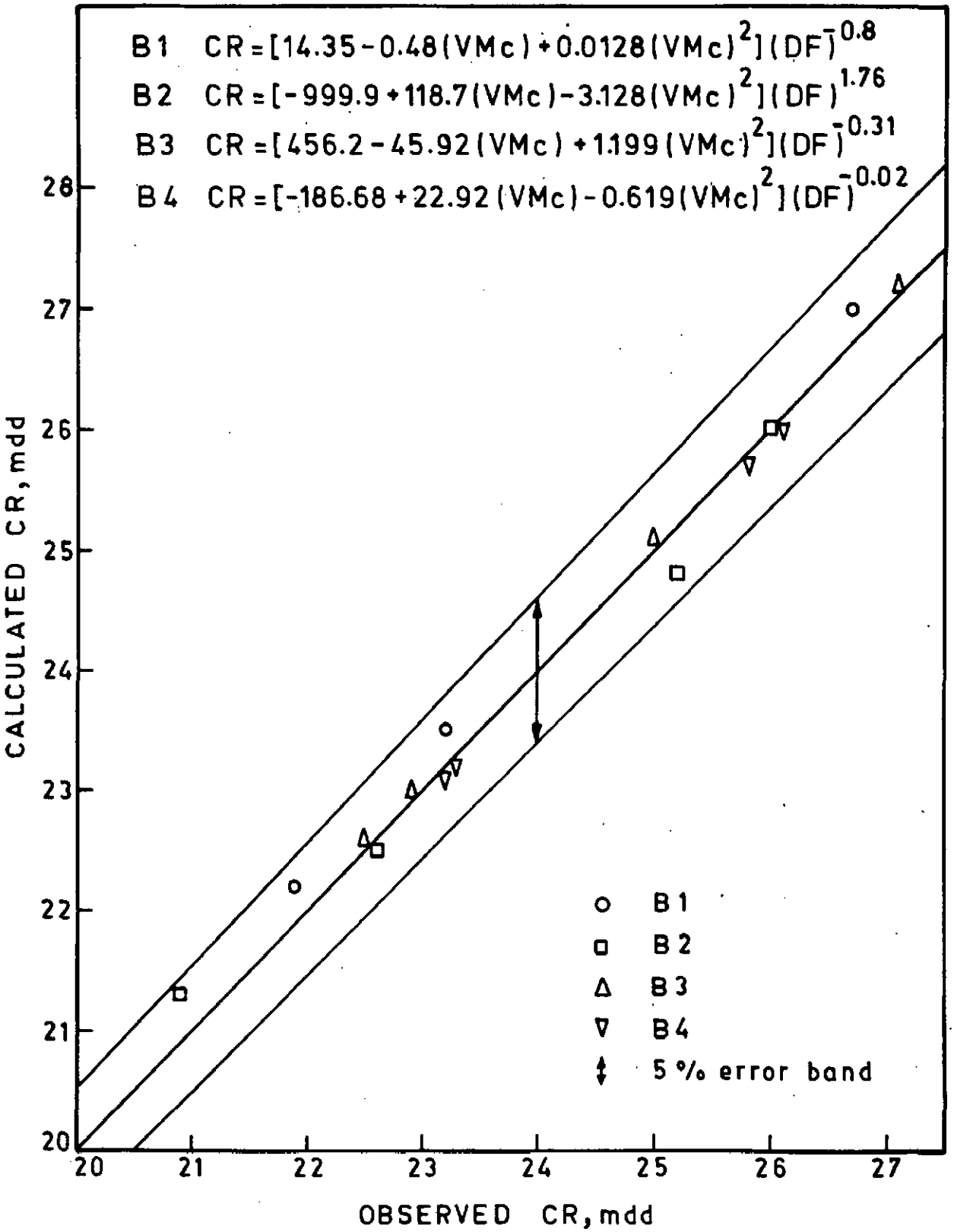

FIG. A-3 CALCULATED Vs. OBSERVED CORROSION RATE VALUES OF EXPERIMENTAL ALLOYS (Appendix-3).

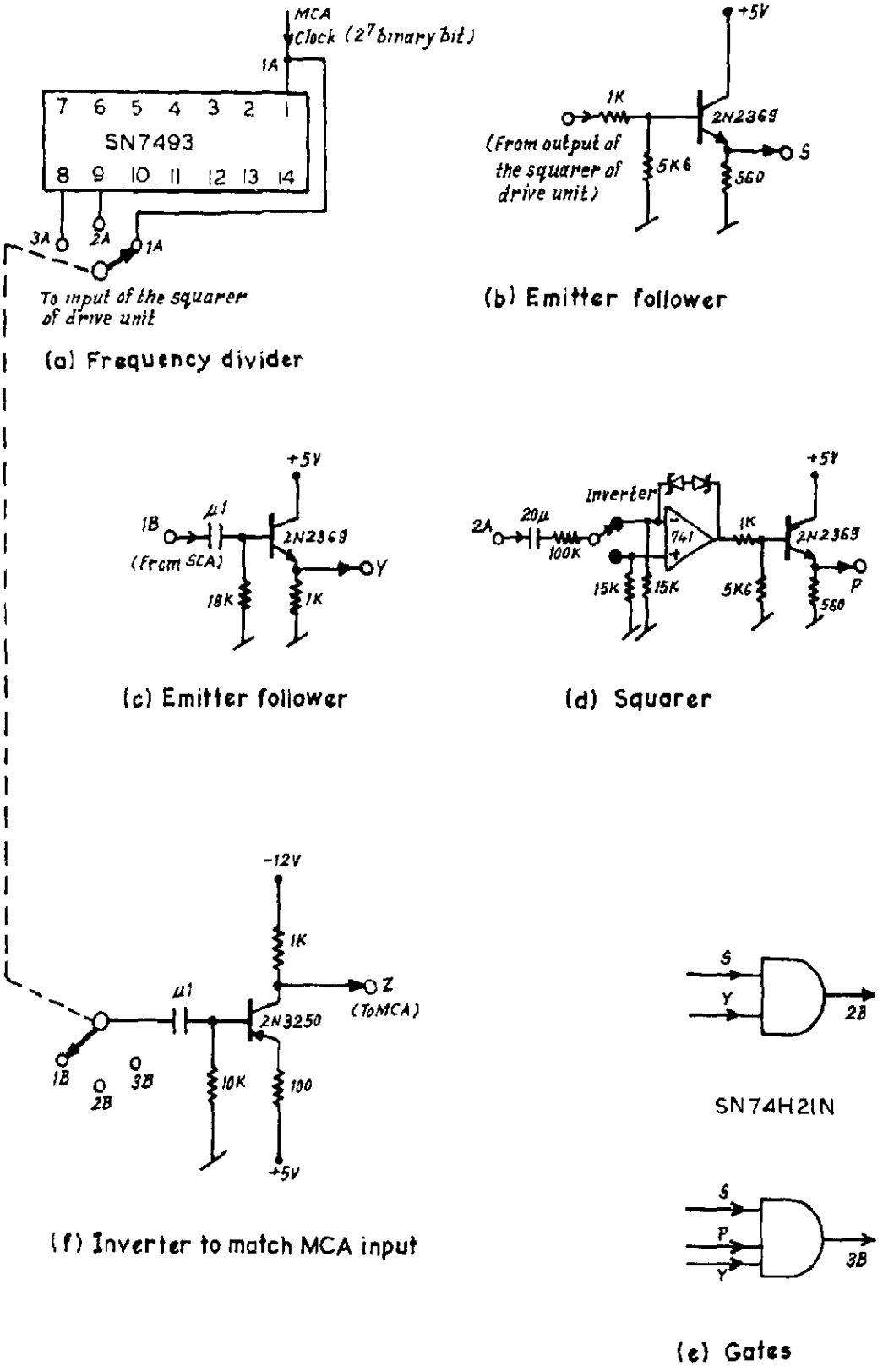

FIG.3.6 - BINARY FREQUENCY DIVIDER UNIT.

(a) SQUARE WAVE

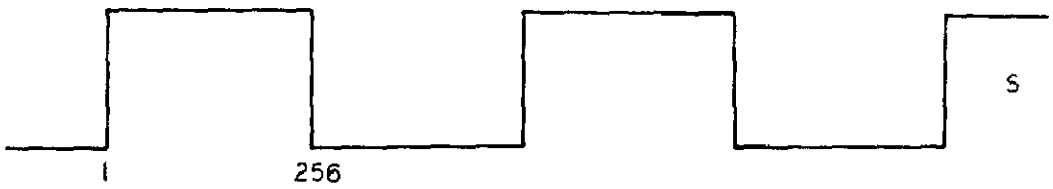

(b) SQUARE WAVE HAVING FREQUENCY HALF OF ORIGINAL

(c) GATED OUTPUT

FIG. 3.7 - WAVEFORMS SHOWING ACCUMULATION OF DATA IN THE FIRST HALF OF DRIVE CYCLE (shown by shaded portion) HAVING FREQUENCY HALF OF THAT OF MCA SWEEP.

in sweeping all the 256 channels.

The data storage is obtained in the following manner when frequency of drive waveform is one fourth of original one. The output 3A (Fig. 3.6a) is given to squarer of drive unit. The pure square waveform is then fed to drive circuit at one path and to emitter follower at other path (Fig.3.6b). The output 'S' is given to IC (Fig. 3.6e) used for gating purpose. The output 2A is given to another squarer unit (Fig. 3.6d) for proper shaping whose output 'P' is given to IC (Fig.3.6e). Output from SCA,through emitter follower circuit (Fig.3.6c), denoted by Y, is given to IC used for gating purpose (Fig.3.6e). Here triple coincidence is obtained between P,S and Y. The gate opens when both P and S are positive and data starts storing through inverter circuit (Fig. 3.6f). If any one of these two becomes negative the gate closes and counts do not store in MCA. The different waveforms have been shown in Fig.3.8. The data accumulates corresponding to only shaded region. This shaded region corresponds to energy of gamma-rays varying from $(E_\gamma + E_\gamma v/c)$ to E_γ where E_γ is energy of recoilless gamma-rays. To obtain energies in range E_γ to $(E_\gamma - E_\gamma v/c)$, the inverter given in circuit of Fig.3.6d is used. Upon inversion the counts during other quarter of Y cycle are stored, while in the first quarter of cycle the storing device remains idle. Thus velocity resolution is increased to four times that of initial.

3.2.IV. ABSORBERS

A Mossbauer spectrum may be recorded in transmission as

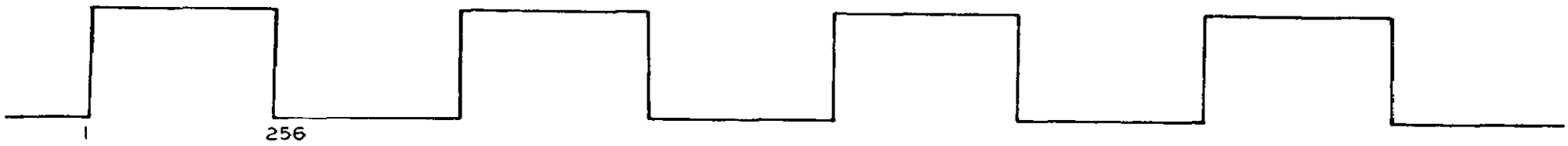

(a) SQUARE WAVE WITH FREQUENCY HALF OF ORIGINAL .

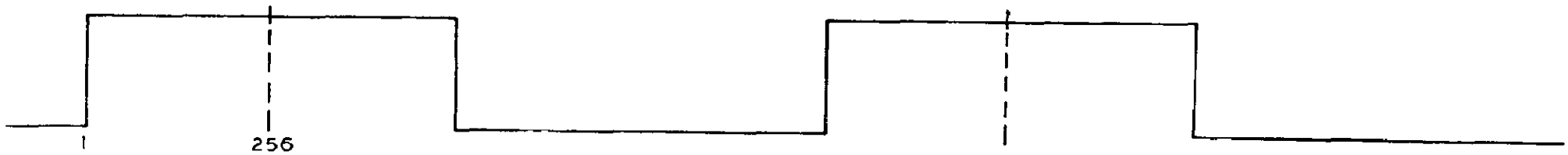

(b) SQUARE WAVE HAVING FREQUENCY ONE FOURTH OF ORIGINAL .

(c) GATED OUTPUT .

FIG.3.8 - WAVE FORMS SHOWING ACCUMULATION OF DATA IN THE FIRST QUARTER OF DRIVE CYCLE (Showing by shaded region) HAVING FREQUENCY ONE FOURTH OF THAT OF MCA SWEEP.

well as scattering geometry. A sample, to be studied, can therefore be used either as an absorber or as a scatterer. In the present study, all the measurements were taken in trans — mission geometry and hence the samples were used as absorbers. To prepare an absorber, the sample was, first of all, ground finely in an agate mortar (because of hardness of sample). Since the width of lines increases with the 'thickness' of sample (section 2.4.II), the amount of iron in the absorber should be very small so as to achieve Lorentzian line shape with line width very near to ($\Gamma_a + \Gamma_s$). This amount is normally very small to make sufficiently strong pellet and, therefore, is mixed with an inert matrix, boron nitride, in the required amount. The pellet is then prepared by pressing the mixture.

3.2.V DETECTION SYSTEM

Most of the Mossbauer sources are not monochromatic and emit radiation of other energies simultaneously with Mossbauer radiation. To have high signal to noise ratio one has to isolate the required Mossbauer transition from the complicated emission spectrum as efficiently as possible. The energy of gamma-rays and X-rays encountered in Mossbauer spectroscopy varies between 3-200 KeV (the highest energy Mossbauer transition, to-date, is 187 KeV). Three different types of detectors are useful in this energy range:

(a) NaI (Tl) Scintillation detector.

(b) Proportional Counter.

(c) Ge(Li) Solid State detector.

For present studies, Argon - Methane gas filled proportional counter was used for the detection of gamma-rays. Methane acts as quenching gas to stop continuous electric discharge by dissipating the energy by dissociation. These have better energy resolution and signal to noise ratio than that in case of scintillation detector below 40 KeV but at the expense of a low efficiency.

Ge(Li) solid state detectors although give extremely good energy resolution (600 eV at 14.4 KeV) but are very expensive. Moreover they must be kept at liquid nitrogen temperatures. In addition, special amplifier cooled to liquid nitrogen temperature are normally essential for best resolution. These are some of the reasons which make them less popular in Mossbauer studies with Fe^{57} isotope.

A high voltage power supply (ECIL make) provided high tension to proportional counter (about 1900 volts) and a preamplifier was used for necessary impedence matching in addition to amplifying. The pulses, in turn, were fed to linear amplifier and then to single channel analyser (both ECIL make). The latter is set for 14.4 KeV peak. The pulses then are fed to gate circuit of binary frequency divider (section 3.2.III) so that counts are recorded only in the desired portion of drive cycle and otherwise not. The output

of gate circuit goes to two decade scalers, joined in series, and to a 256-channel analyser operating in multichannel scaling mode. The analyser is of Northern Scientific make model NS-260 and is acting as data storing device. As the square wave form, used for drive coil after shaping and doubly integrating, has been generated from MCA itself, there is no need of synchronisation of MCA sweep and drive coil sweep as they are already in phase. This is necessary to keep velocity increment per channel constant during every cycle of spectrum recording. The decade scaler tells one the total number of counts stored. Since the limit of each channel of MCA is 10^5 counts, overflow occurs each time when this much counts have been stored in one channel thus 25.6×10^6 total counts must indicate one overflow, however, it has been found to occur at about 37×10^6 total counts during present investigations perhaps due to loss of some counts. Thus total number of counts indicated in decade scalers gives one number of overflows occurred in each channel. When sufficient data has stored, decided by observing suitable absorption in Mossbauer spectrum in CRT's screen, it is taken out with the help of an Adox printer, which give counts stored in each channel. These counts can be atmost in five digits. By knowing number of overflows observed by each channel, one can get total number of counts stored in each channel. Counts are plotted against channel number. Velocity/channel and zero velocity channel are already calculated with the help of calibration Mossbauer spectrum of natural iron. Thus a plot

between counts versus velocity is obtained which is known as Mossbauer spectrum.

3.3 CALIBRATION

The calibration of the Mossbauer spectra was done by taking the spectrum of iron foil (supplied by Radiochemical Centre, Amersham, England) as reference. The source-detector distance was kept at about 10 cm. so as to avoid solid angle effects. The selection of 14.4 KeV gamma-ray (Mossbauer radiation) was good enough to give about 15% absorption in each of the outer most peaks. The intensity ratio obtained was approximately 3:2:1::1:2:3. Value of full width at half maximum (FWHM) = 0.295 mm/s and was about same for all the lines.

3.4 DESIGN OF CRYOSTATE AND FURNACE

The need of taking Mossbauer spectra at low and high temperatures may be due to several reasons. The high temperature spectra may show some change in structure due to increase in mobility of ions. Substances which are magnetically ordered at room temperature show transition to paramagnetic state at higher temperature and thus their spectra at high temperature may help one to know about their Curie or Neel point. The recoilless fraction 'f' of gamma ray increases with decrease in temperature and, in fact, only few transitions show appreciable Mossbauer effect at room temperature. This motivates

one to take the spectra at lower temperatures. Some of the substances which show paramagnetic state at room temperature may transit to magnetically ordered state at lower temperature. Determination of Neel or Curie point of such substances, change of structure at lower temperature etc. are some of the reasons for observing the spectra at lower temperature.

The identification of substances in natural samples by seeing their transformation at low and high temperature and studying the distribution of iron ions at different sites in certain other minerals by taking their Mossbauer spectra at lower temperature motivated the fabrication of cryostat and furnace which have been described in following lines.

3.4.I CRYOSTAT

The cryostat fabricated for present investigations is suitable for cooling down to $77^{o}K$. Hence the coolant in present case was liquid nitrogen. The comparatively large heat of vaporization (38.6 K Cal/litre) of liquid nitrogen does not demand as complicated temperature shielding as in case of liquid helium cryostat. Various types of cryostats have been described in literature [81,97-102]. Some of these have used principle of 'cold finger' while others have cooled the sample by flowing down liquid nitrogen, through cryostat, by gravity. In another method temperature upto $93^{o}K$ was obtained by passing the cold nitrogen gas through cryostat. All of these methods

were defective in the sense that either the shape of cryostat and the way of insulating it was crude or the consumption of liquid nitrogen was much. The cryostat described in following lines is free from both of these defects. It is continuous flow type i.e. the coolant is allowed to flow round the sample holder with the help of a suction pump. While making a cryostat, two points are worth keeping in notice (i) there must be no vibration inside the cryostat. In case of Fe^{57}, vibration amplitudes of a few microns per second causes a perceptible increase in line width, and (ii) there must be a path through the system which is transparent to the gamma-rays under study.

The cryostat has been shown in Fig. 3.9 (top view) and Fig. 3.10 (sectional view). The covering cylindrical chamber is of gun-metal. It has got two lids which can be joined vacuum tight on either side with the help of O-rings. Each of these two lids has got one window for incoming and outgoing gamma radiations. Both windows are of aluminium coated Mylar sheets which do not absorb low energy gamma-rays and at the same time acts as good thermal insulator. The cylindrical surface of covering chamber has four openings (Fig.3.9). Opening A is meant for evacuating the system, where a speedi-valve (Edwards High Vacuum Ltd., Sussex) has been fitted. Another opening 'B' is meant for male-female connector for thermocouple as well as for heating element which has been wound round the sample holder. A copper pipe of diameter 2 mm is soldered round the sample holder so that its large contact

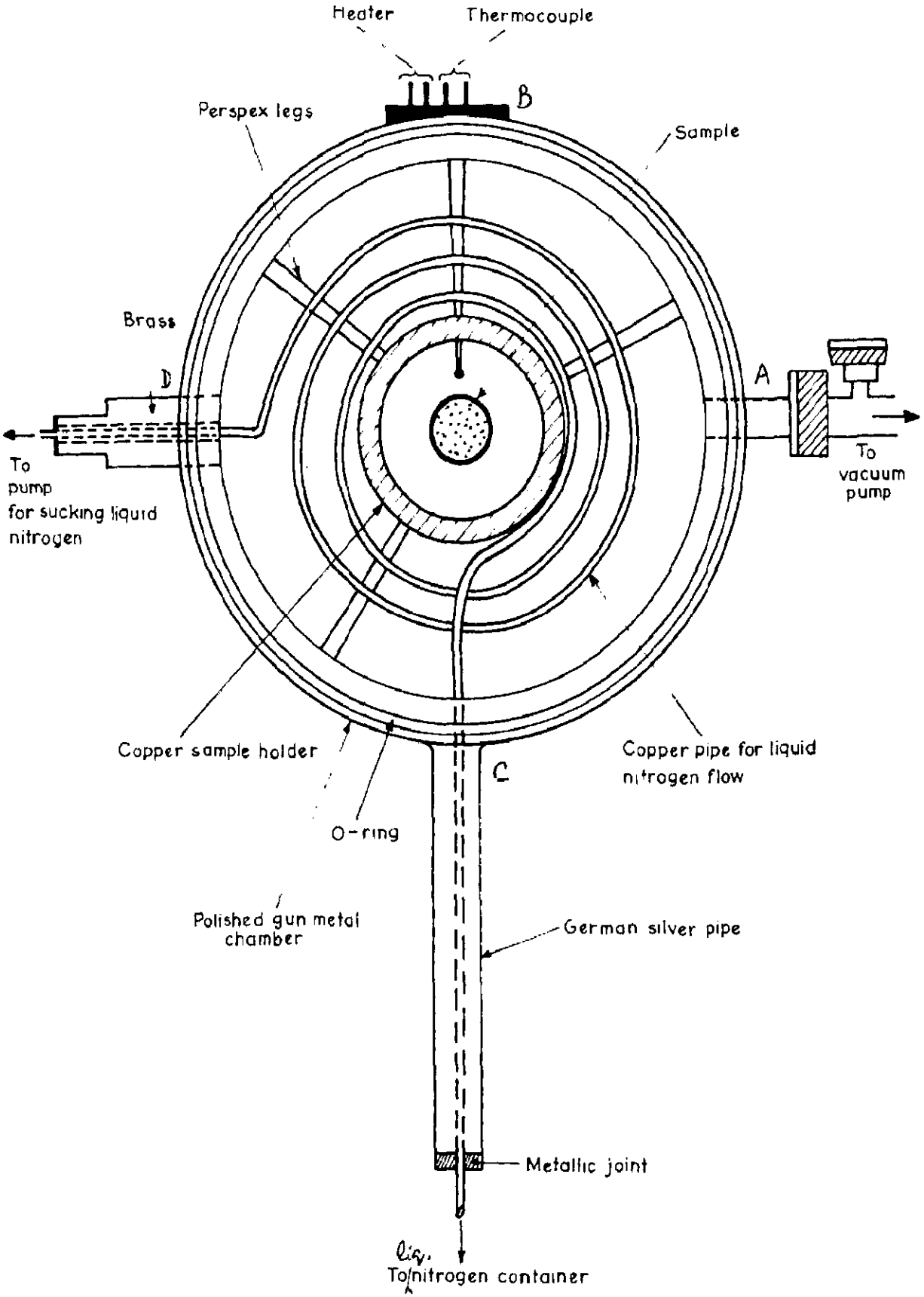

FIG.3.9 _ TOP VIEW OF CRYOSTAT .

area minimizes the thermal gradient within sample holder. One end of this pipe comes out from opening C and goes to liquid nitrogen container through a German Silver pipe of diameter 13 mm, which is thermal insulator, so as to avoid thermal losses. The other end of copper pipe is at opening 'D' where it is connected to rotary pump, via needle valve (Edwards High Vacuum Ltd., Sussex), which is used to suck liquid nitrogen. The flow current of liquid nitrogen is checked from needle valve. The cylindrical walls as well as the lids are nickel polished from inner side so as to avoid radiation losses. Temperature losses due to atmosphere are minimised by keeping the covering chamber under a vacuum of at least 10^{-4} torr.

The sample holder, of copper, has been shown in Fig.3.10. Its height is 25 mm with diameter 40 mm and is held in the centre of covering chamber with the help of three legs of perspex. These legs have been used to eliminate temperature losses. The sample is kept at the middle of the holder, in the form of pellet made inside a copper ring. One junction of thermocouple is kept near the pellet as is shown in Fig.3.10. The pellet is kept fixed at its position with the help of spring which is pressed by copper cover put at one end of the sample holder. This copper cover is having a hole, of the dimensions of pellet, for the passage of gamma-rays and is covered with an aluminium foil so as to minimise temperature loss. This foil is pasted also on the other end of sample holder for the same purpose.

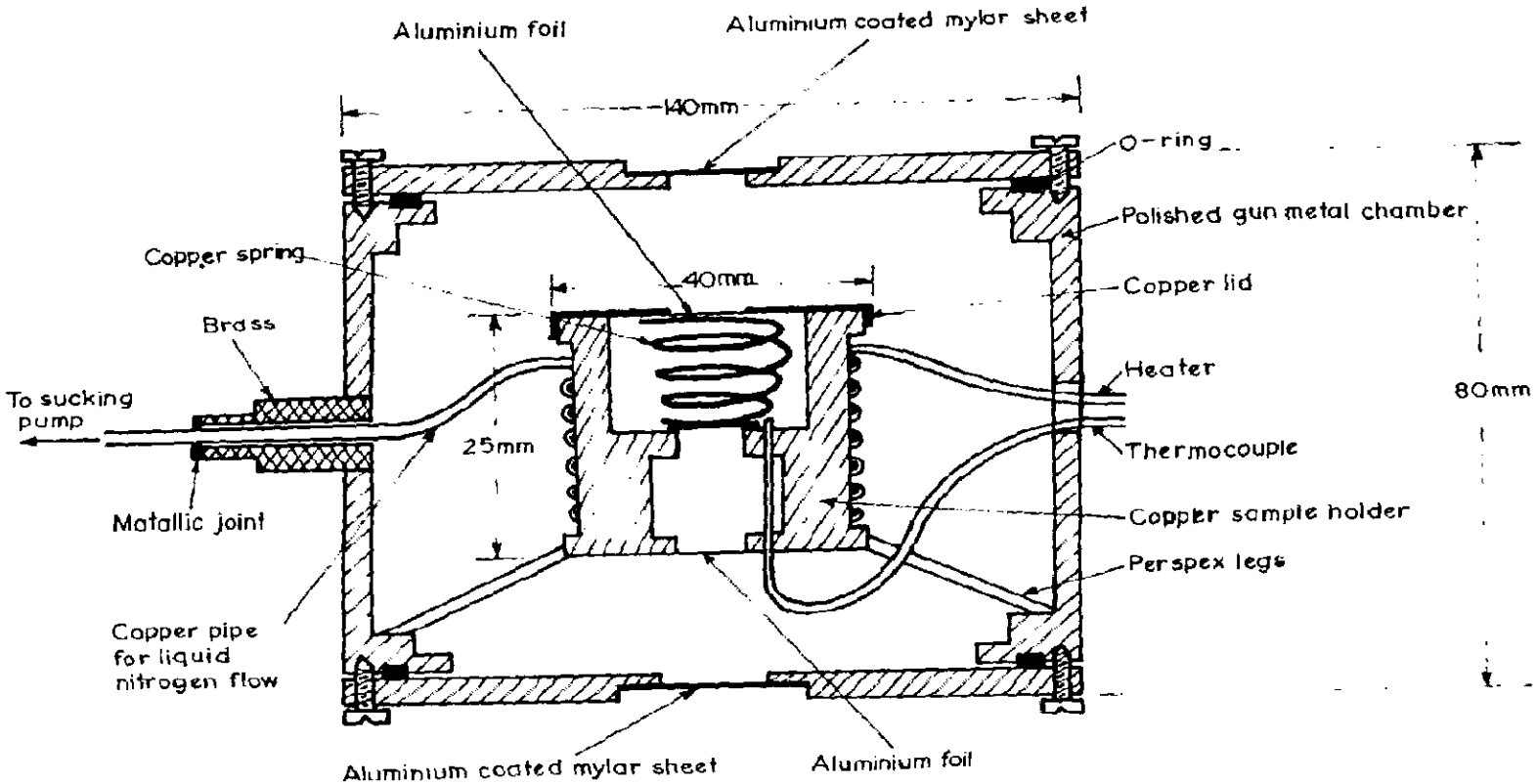

FIG. 3.10 - SECTIONAL VIEW OF CRYOSTAT .

To cool the sample down to liquid nitrogen temperature, first of all the covering chamber is evacuated, after putting the sample at its place and screwing the lids, upto at least a vacuum of $\sim 10^{-4}$ torr. Liquid nitrogen is then allowed to flow through the copper pipe. At first the current is kept low, later on it is increased until liquid nitrogen temperature is reached. The variation in the temperature can be done coarsly by decreasing the flow rate and finely by allowing required electric current in heating filament. A temperature controller has been used to keep the temperature controlled to within $\pm 0.05^{\circ}K$.

In this cryostat all precautions have been taken to keep the losses to minimum possible extent as has been described above. Dead time is very short between experiments. Warm up, sample change, pumping and cooling down is performed within about half an hour. The consumption of liquid nitrogen is very low and is about 0.5 litre/hour in summers and about 0.35 litre/hour in winters. The specifications of this cryostat have been given separately in Table 3.1.

3.4.II FURNACE

The use of high temperature furnace for Mossbauer work [97-99] has received much less attention than the cryogenic system. A simple oven can be constructed by using a carbon cloth heater [103] while that reaching to temperature of $1700^{\circ}C$

TABLE 3.1: SPECIFICATIONS OF CRYOSTAT

Temperature range	77 to 300°K
Thermocouple	Iron-Constantan
Heating element	Nichrome wire, Resistance 26 Ω
Radiation transmission angle	20° Conical (maximum)
Dimension of sample	15 mm diameter
Dimension of Cryostat	140 mm dia., 80 mm height
Main materials	Nickel polished Gunmetal
Windows	Aluminium coated Mylar sheet
Direction of radiation	Horizontal

has also been fabricated by using a helium filled oven with Berillium windows |104|. The furnace described here is capable of heating up to 900^{0}K.

Fig. 3.11 shows the furnace used in the present studies. The cylindrical chamber of gunmetal has got one lid on its either side and can be screwed vacuum tight with the help of O-rings. Each lid has got a window of aluminium coated mylar sheet which does not absorb low energy Mossbauer gamma rays and is thermal insulator. These windows are for the incidence and transmission of gamma rays. One of the two openings on its cylindrical surface is for the speedivalve (Edwards High Vacuum Ltd., Sussex) wherefrom it is connected to vacuum unit for evacuation. The other opening is for male-female connector for thermocouple and heating elements as well. The joint is made of bakelite so as to avoid heat loss. The sample holder with dimensions 40 mm diameter, 40 mm height has been shown in Fig. 3.11. Its material is perfulite (an african clay) which can be machined easily but after heating becomes brittle. This material is electrically insulator but a good heat conductor and has replaced metallic holder so as to avoid the electric insulation problems. Cylindrical holes have been drilled, in material, along the circumference and heating element, Nichrome wire, has been passed through it. Thus heating element has been wound round the sample holder. The resistance of this wire is 14Ω. The sample holder is kept inside a stainless steel cover. With the help of this oover the sample holder is kept at the middle

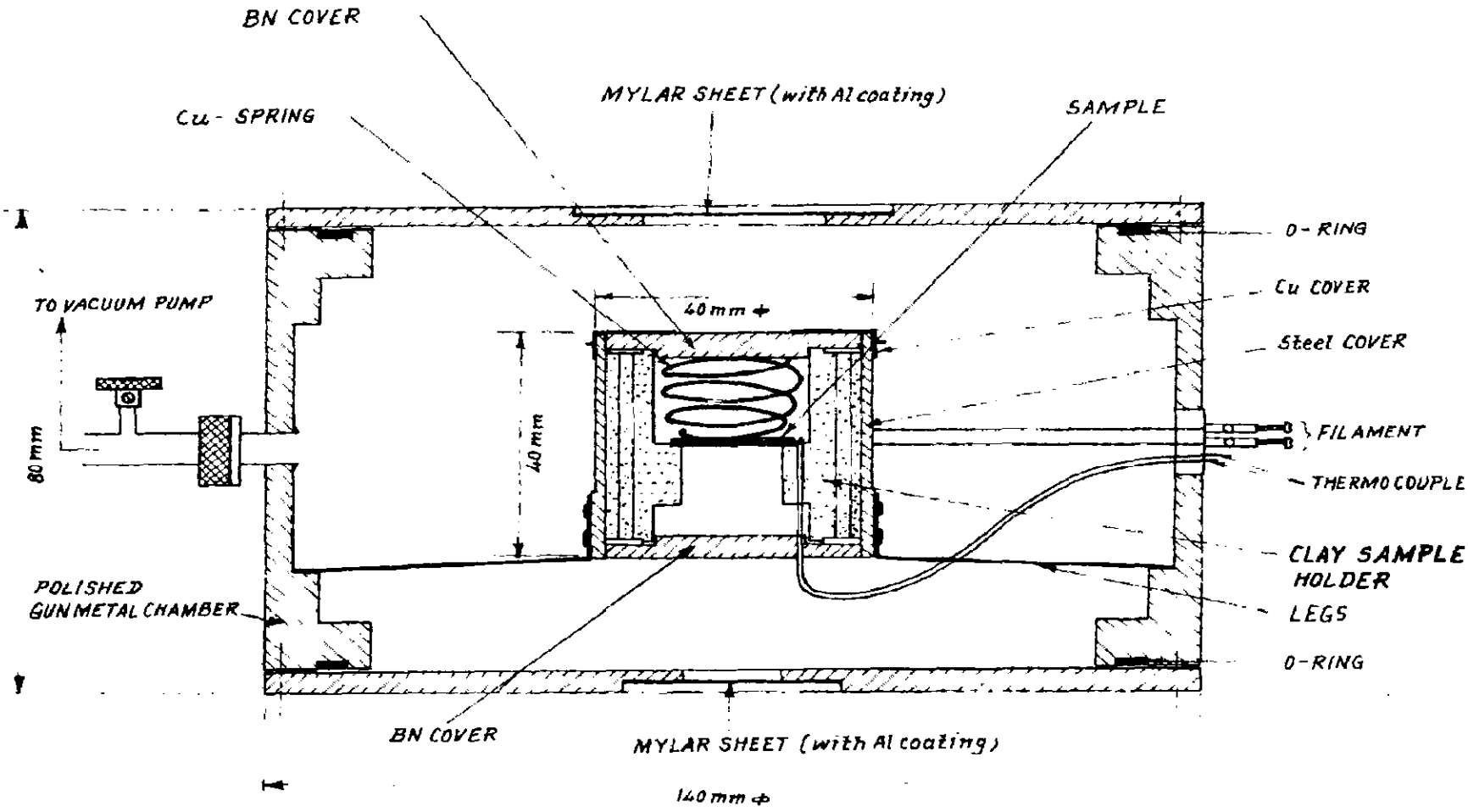

Sectional elevation of Mössbauer Furnace

FIG. 3.11

of vacuum chamber with the help of three metallic legs which are welded at the chamber's surface. The metallic legs replace perspex legs (used in cryostat) because of high temperature, where perspex starts melting. The sample is kept in middle in the form of pellet made inside copper ring. The ring is kept fixed in its position by spring but here this is pressed by Boron Nitride cover which acts as thermal insulator without attenuating low energy gamma-rays. The other end of the sample holder is also closed by a boron nitride cover. The inner and outer walls of the chambers are polished by nickel so as to avoid radiation loss. The losses due to atmosphere are minimised by evacuating the chamber to about 10^{-4} torr. The specifications of this furnace have been described in table 3.2. The temperature in this furnace can be controlled to within $\pm$ 0.05°K with the help of temperature controller which will be described in following section.

3.5 TEMPERATURE CONTROLLER

Since Mössbauer spectrum of a mineral takes at least about one or two days to build up with sufficient absorption, it becomes necessary to use a temperature control device while recording spectrum at low or high temperatures. A temperature controller was, therefore, fabricated in the laboratory, where present investigations were carried out. The details of this controller have been given elsewhere [94], only a brief account of it will, therefore, be given in the following lines.

TABLE 3.2: SPECIFICATIONS OF FURNACE

Temperature range	300 - 900^{0}K
Thermocouple	Iron-Constantan
Heating element	Nichrome wire, Resistance 14 Ω
Radiation transmission angle	20^{0} Conical (maximum)
Dimension of sample	15 mm diameter
Dimension of Furnace	140 mm diameter and 80 mm height
Main material	Nickel polished Gunmetal
Windows	Aluminium coated Mylar sheet
Direction of radiation	Horizontal

Several types of temperature controller have been described in literature [82,105,106]. In all these controllers external voltage was applied only when the temperature was lower than the required value. However, with this technique the variation in the value of temperature was larger than is required in some of the studies e.g. phase transition etc. The reason was the long thermal time constant due to large thermal capacity of the system where temperature control is required. To overcome this fault, the temperature controller fabricated was dynamic type where the furnace is kept on and off at a preset frequency (5 times a minute).

The block diagram of circuit is shown in Fig. 3.12. The difference of standard D.C. voltage and emf across thermocouple, designated as error-signal, is preamplified 50 times. This signal is then passed through a low pass filter, with gain 10, to filter out 50 Hz and pick-ups generated across the thermocouple junction. After filteration, the signal is amplified in a linear amplifier with various gains. The maximum gain thus obtained is 10^5. This signal is then finally passed through voltage follower. In the next step it is compared with triangular waveform generated separately with frequency 5 cycles/min. and voltage $\pm$ 0.7 V in a comparator which gives gated output. The gate opens whenever the error signal is negative whereas the time upto which it opens depends upon its magnitude. Thus if error signal is more negative, gate will be opened for more time and closed for less time and vice-versa if signal is less

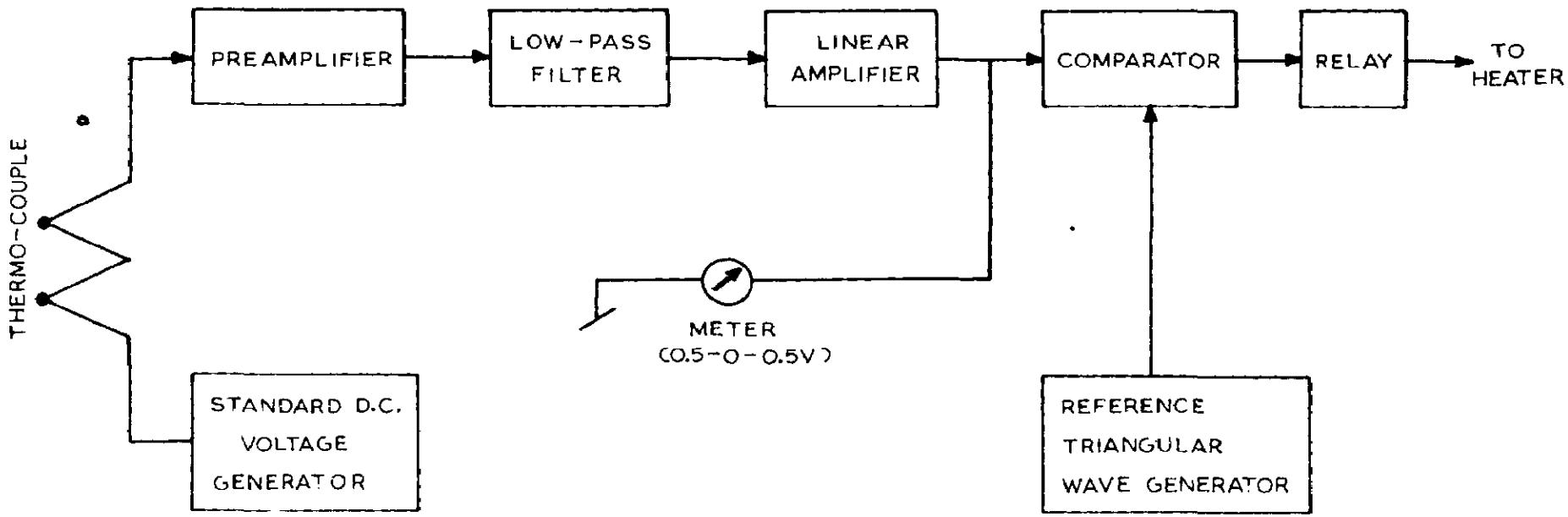

FIG. 3.12 - BLOCK DIAGRAM OF TEMPERATURE CONTROLLER.

negative. This gated output operates a relay which is connected further to heater. In this way the temperature control to within $\pm$ 0.05^{o}K has been achieved from 77 to 900^{o}K, with iron-constantan thermocouple, for sufficiently long time of continuous run.

3.6 EXPERIMENTAL PROCEDURES FOR DIFFERENTIAL THERMAL AND INFRARED ABSORPTION ANALYSIS

3.6.I DIFFERENTIAL THERMAL ANALYSIS

The equipment used in differential thermal analysis was Fisher's differential thermal analyser model 260. For analysis both alumina (used as inert material) and the sample were powdered and then about 100 mg. of their amount was weighed separately. Both the substances were then put in quartz tubes used as sample blocks. Each tube was of diameter 3 mm and length 3.8 cm. Temperature measurements were done with Pt-PtRh thermocouple. The maximum temperature attained in each sample was 1000^{o}C. Kaolinite was used for calibration purpose. An X-Y recorder supplied with the whole assembly was used for recording differential thermal curves of various samples.

3.6.II INFRARED ABSORPTION ANALYSIS

IR-20 Beckmann's spectrometer was used for recording IR absorption curves of various samples. In each case the sample was ground to a particle size below the wavelength

range of the radiation. About 25 mg of sample was weighed and then mixed with KBr in required amount. The KBr used here was kept at about 80 or 90°C for one or two days so that absorbed water is removed and does not interact with the OH group of samples. Pellet is formed of KBr and sample mixture by putting it under a hydraulic press. This pellet was then used as absorber for taking IR-absorption spectrum.

CHAPTER 4

MOSSBAUER STUDIES OF NATURALLY OCCURRING RED OCHRE AND YELLOW OCHRE*

* Based on 'Mossbauer studies of naturally occurring red ochre and yellow ochre'. A.K.Singh, B.K.Jain and K.Chandra. To appear in J.Phys. D- Appl. Phys. 11 (1978).

4.1 INTRODUCTION

Application of Mossbauer effect in geological and mineralogical problems have been of immense potential in certain aspects. Its ability to distinguish between Fe^{2+} and Fe^{3+}, without affecting their amounts at the same or different sites, and to estimate site populations puts Mossbauer spectroscopy to be at superior place than other analytical methods while studying iron minerals.

Red and yellow ochre are natural pigments. Pigment is an important raw material in paint industry. Naturally occuring pigments include iron oxides, ochres, siennas, umbers and graphite. With increase in iron contents ochres pass into siennas while the latter pass into umbers with increase in manganese oxide |107|.

Ochres were widely used as colouring material in paintings and pottery in ancient times. A study of ancient paintings and wares through Mossbauer spectroscopy and the comparision of spectra with those of clays and ochres, fired at various temperatures, may lead one to tell about the technological development of a particular race. It appears that certain artists and craftsmen were more skilled in the management of their furnaces and thus produced a more evenly fired work and at a high temperature. Attempts have been made in this direction by Cousins et. al.|2|, Gangas et.al.|55| in studying ancient Greek pottery. Bouchez et. al.|108| has studied grey and red ware of Tureng-Tepe, Janot et.al.|109| has tried to

determine the provenance and manufacture of ancient french ceramics. Keisch [110] studied iron bearing pigments for classifying different artists work.

In the present chapter, studies on red and yellow ochre have been described. The studies were performed by taking Mossbauer spectra at room temperature before and after annealing the samples at various temperatures in air. Chemical analysis was done to find out Fe,Si and Al contents. Infrared (IR) and differential thermal (DTA) analyses were also performed to support the results obtained through Mossbauer spectroscopy.

4.2 MINERALOGICAL DETAILS

Ochres are mixture of clays and oxide or oxyhydroxide mineral of iron. The presence of a particular clay mineral and impurity in mineral structure depends upon the locality of ochres. Large variations in the grain size have also been observed. Ochres should contain between 15 to 60% of iron oxide. Characteristics of both the studied ochres will now be outlined briefly.

4.2.I RED OCHRE

This red colour pigment is derived from hematite in which iron contents are present as αFe_2O_3. It is most earthy variety of hematite. This material can also be produced by heating the corresponding yellow form in air. It is very soft, having dull luster and often contains a considerable amount of sand or clay which may contain iron in silicate mineral structure [110,111].

4.2.II YELLOW OCHRE

It is yellow iron bearing earthy form of limonite containing varying amounts of alumina and silica. This material owes its colour principally to α-FeOOH. It is amorphous and of colloidal origin |110,112|.

4.3. OCCURRENCE

4.3.I RED OCHRE

Red ochre is a most earthy form of hematite. It is rare in igneous rocks and has formed when magma was poor in FeO. However, it chiefly occurs in sediments and their metamorphosed equivalents. Direct neutralization of Fe^{3+} ion solutions results in hydrous ferric oxide which upon aging or autodehydration forms hematite |113|. In metamorphic rocks it may result from the metamorphism of such materials as magnetite, siderite, iron silicates and the hydrated iron oxides. Hematite ores associated with sediments are related to the metasomatic introduction of hematite by solutions, the iron often having been derived from the weathering of overlying sediments. This pigment occurs widely in India.

4.3.II YELLOW OCHRE

It is an earthy variety of limonite, a name given to hydrated oxides of iron with poorly crystalline characters. Limonite results from the alteration of other iron minerals, from a highly ferruginous rock there may be formed by its degradation weathered residual deposits, consisting largely of

ferric hydroxide, mixed with clay and other impurities. It is common as a biogenic precipitate in swamps etc. It is often associated with hematite |114| . Like red ochre, yellow ochre is known to occur practically in every state of India in larger or smaller quantities.

4.4. STRUCTURE OF CONSTITUENT MINERALS

Main minerals occurring in red and yellow ochre are hematite and limonite respectively. Clay mineral may also be associated with these. A brief account of the structure of hematite, limonite and a general introduction of clay mineral structure is given below:

4.4.I HEMATITE

Pauling and Hendricks |115| determined the crystal structure of hematite. The lattice is rhombohedral hexagonal, isomorphous with corundum, having lattice parameters a=5.418 A^{o}, $\alpha=55^{o}17'$, space group $R\bar{3}c$. Thus oxygen ions in the anion layers are arranged in a slightly distorted hexagonal packing, while successive cation layers contain equal number of ions all in six fold coordination.

4.4.II LIMONITE

This mineral describes hydrated oxides of iron with poorly developed crystalline characters (The structure of hydrated oxide of iron has been outlined in a later section of chapter V). On occasion a water content determination has led to allocation of a molecular formula such as $2Fe_2O_3.3H_2O$.

Such limonites are generally composed of goethite with crystal size so small as to mask its external crystalline characteristics.

4.4.III CLAY MINERALS

Two structural units are involved in most of the clay minerals. One unit consists of two sheets of closely packed oxygen or hydroxyls in which aluminium, iron and magnesium atoms are embedded in octahedral coordination (Fig.4.1a). The second unit is built up of silica tetrahedra, in each unit of which silicon atom is equidistant from four oxygens or hydroxyls arranged in the form of tetrahedron (Fig.4.1b).

Normally the structure of clay minerals are of two types. The two sheet structure is composed of one sheet of silica tetrahedra with tips pointing in same direction and one sheet of octahedra such that tips of silica tetrahedra and one of the layers of the octahedral sheet form one common layer (Fig.4.2a). It, thus, contains one tetra-and one octahedral site |116|. Kaolinite comes in this category. Another is three sheet structure which is composed of one octahedral sheet sandwitched between two tetrahedral sheets of silica tetrahedra in such a manner that all the tips of silica tetrahedra point in same direction and the tips of tetrahedra of each silica sheet and one of the hydroxyl layers of the octahedral sheet form a common layer (Fig. 4.2b) |71| . It has got, thus, two octahedral and one tetrahedral cation sites. Montmorillonite mineral belongs to this category. This type of structure is also known as mica like.

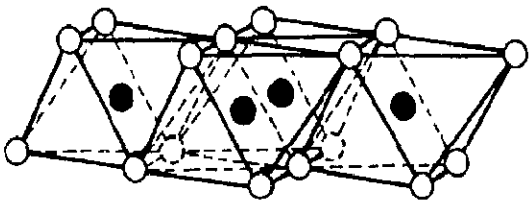

○AND ◌ — HYDROXYLS

● — ALUMINIUM, MAGNESIUM ETC.

(a)

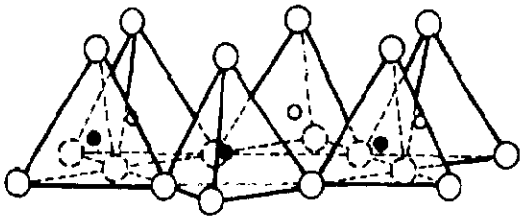

○AND ◌ — OXYGENS

oAND● — SILICONS

(b)

FIG. 4.1 – DIAGRAMMATIC SKETCH SHOWING SHEET STRUCTURE OF (a) OCTAHEDRAL UNITS AND (b) SILICA TETRAHEDRONS.

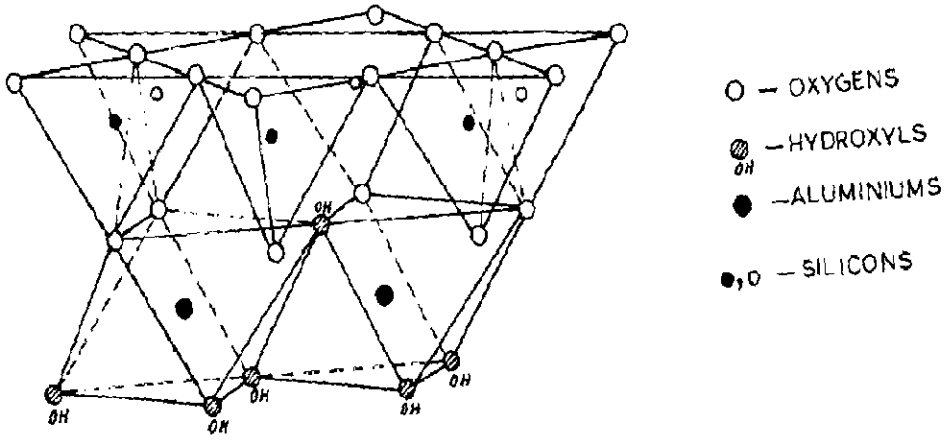

(a)

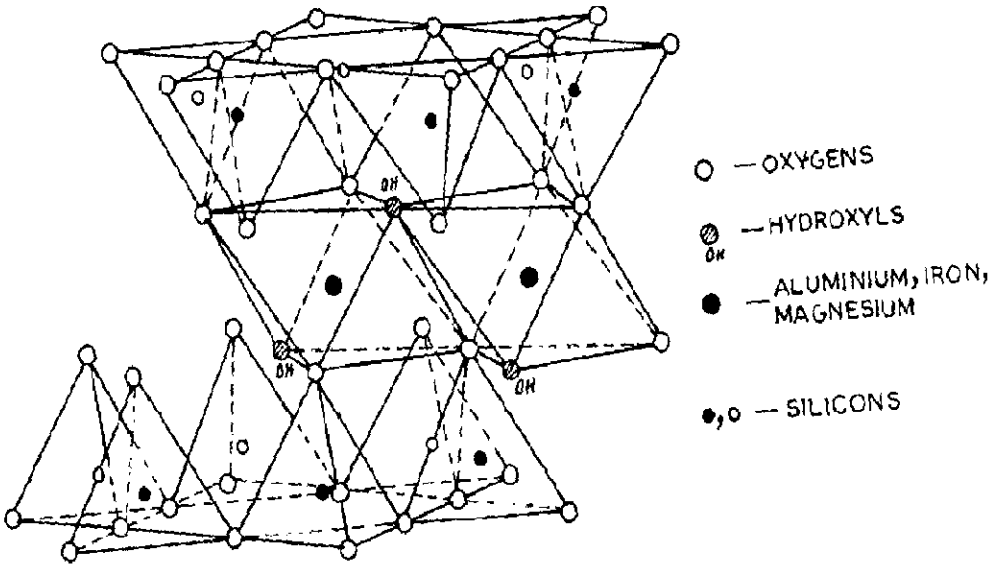

(b)

FIG. 4.2 - DIAGRAMMATIC SKETCH OF (a) TWO SHEET STRUCTURE AND (b) THREE SHEET STRUCTURE.

4.5 EXPERIMENTAL PROCEDURE AND RESULTS

The samples, yellow and red ochre, were obtained from Geology Department, University of Roorkee where they had already been identified through petromineralogical and textural studies.

Amounts of iron, aluminium and silicon were estimated gravimetrically, in these samples, through chemical analysis. Standard procedure given by Vogel|117| were adopted for their determination. The results are given in Table 4.1.

For studying the effect of annealing, the samples were heated for three hours in air at temperatures 200,400,600,800 and 1000°C and were cooled down to room temperature gradually.

The Mossbauer spectra of unannealed as well as annealed samples were taken, at room temperature, on a spectrometer described in chapter 3 . The gamma-ray source was $\sim$3.5 mCi Co^{57} in copper matrix. To prepare the absorber, 80 mg. of powdered sample was weighed and thoroughly mixed with the required amount of boron nitride. The latter is an inert matrix and practically does not attenuate the 14.4 KeV gamma rays. The mixture of sample and boron nitride was then pressed inside a copper ring of diameter 16 mm., under a hydraulic press. Thus obtained pellet was used as absorber. All the measurements were taken in transmission geometry. The spectra obtained for red ochre and yellow ochre have been shown in Fig. 4.3 and Fig. 4.4 respectively. The spectrum of unannealed red ochre at 113°K was obtained by putting the pellet in cryostat (described in chapter 3) and flowing liquid air through it and is

TABLE 4.1- WEIGHT PERCENTAGE OF IRON, SILICON AND ALUMINIUM IN THE SAMPLES

Sample	Weight percentage		
	Fe	Si	Al
Red Ochre	12.42	33.95	4.74
Yellow Ochre	44.98	3.25	14.48

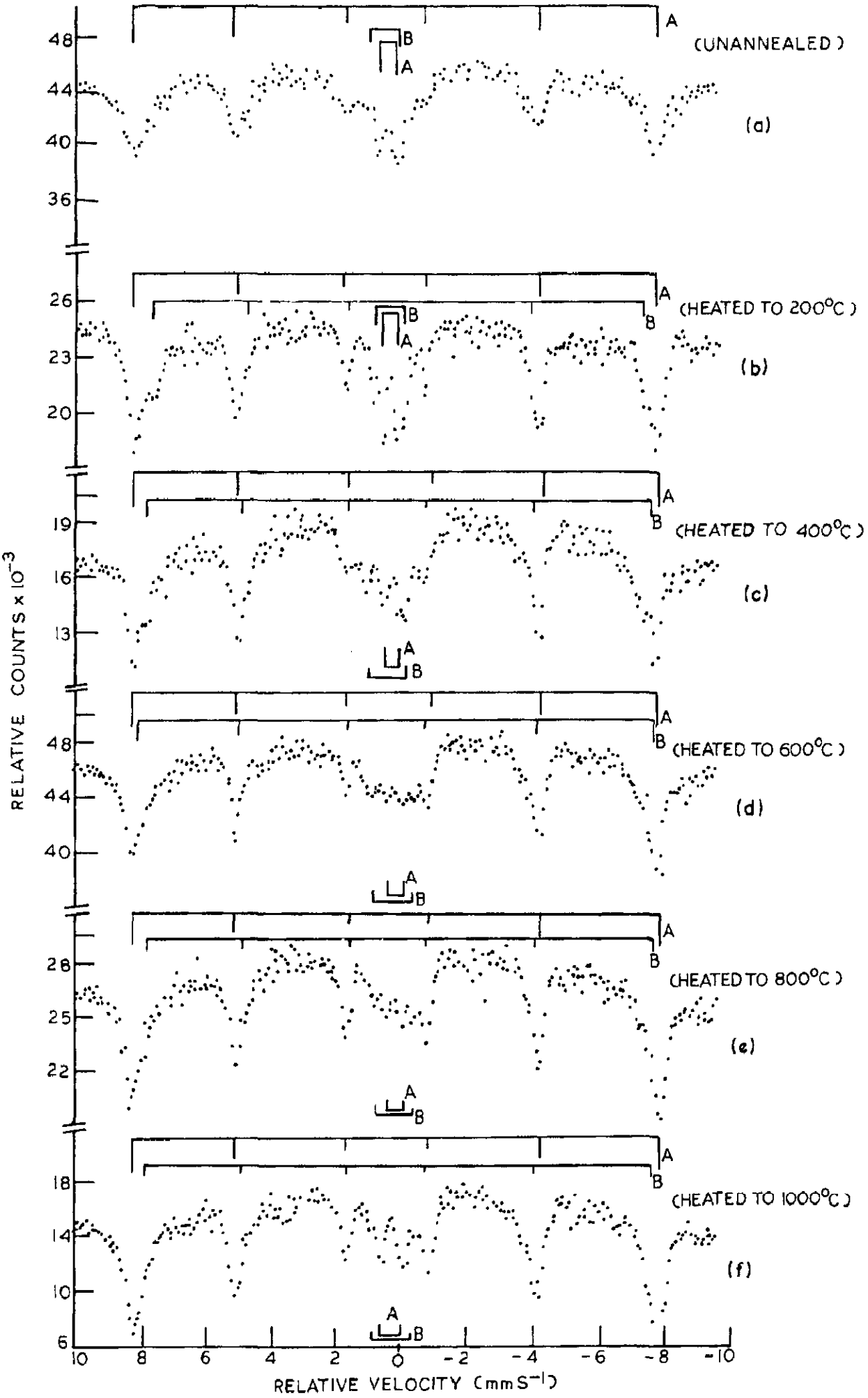

FIG.4.3 - MÖSSBAUER SPECTRA OF RED OCHRE AT ROOM TEMPERATURE.

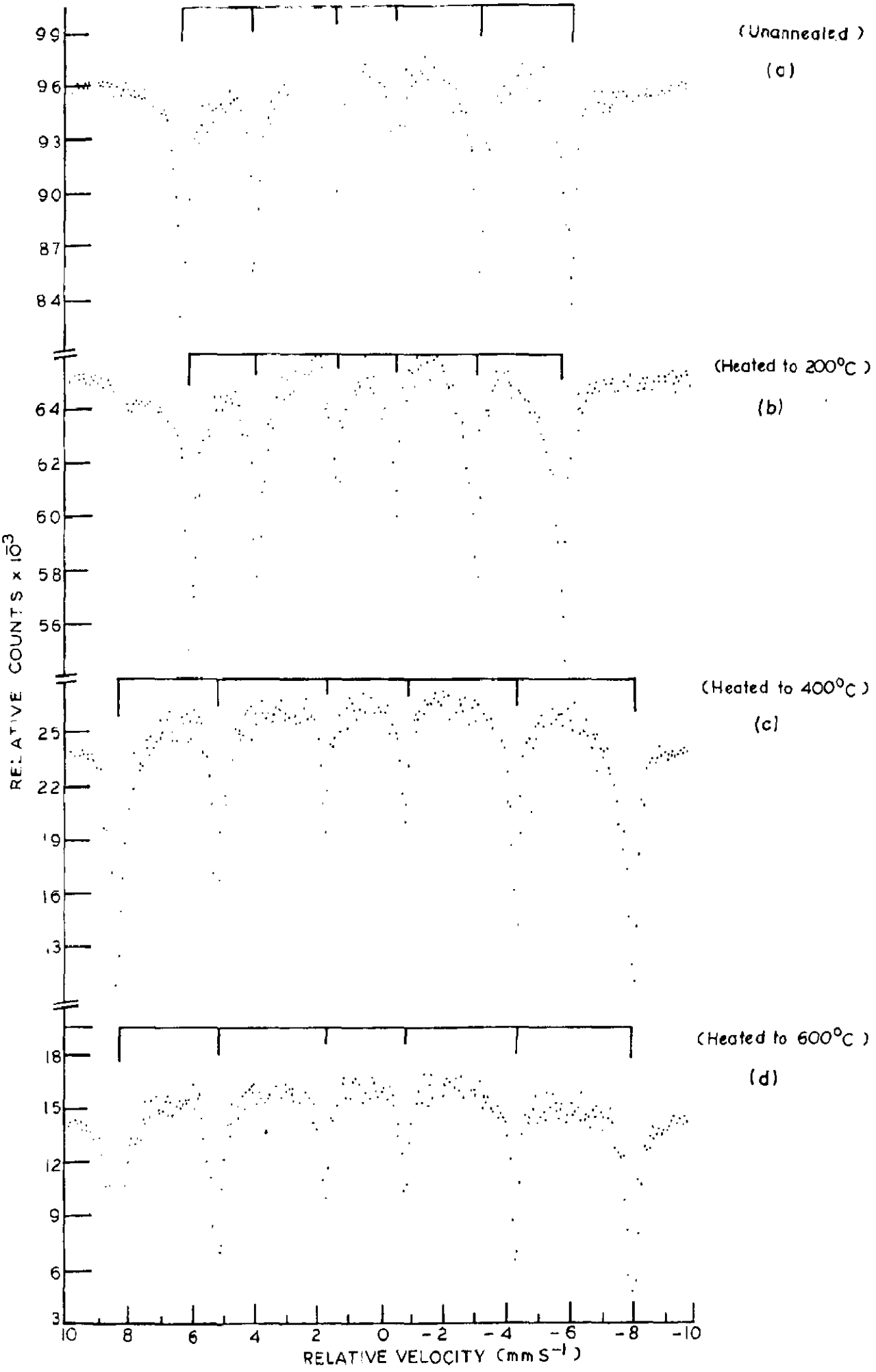

FIG. 4.4_ MÖSSBAUER SPECTRA OF YELLOW OCHRE AT ROOM TEMPERATURE.

shown in Fig. 4.5a. The spectrum of yellow ochre at 400°K was taken using furnace described in preceding chapter and has been shown in Fig. 4.5b. The spectra were analysed with a least square fitting programme on dec-10 computer and the analysed parameters have been given in Table 4.2 and 4.3.

Infrared absorption spectrum of unannealed red ochre has been shown in Fig. 4.6 while Fig. 4.7 depicts that of unannealed yellow ochre.

Differential thermal curves ofred ochre and yellow ochre have been given in Fig. 4.8 a and b respectively.

4.6 DISCUSSION

The discussion of the results obtained through Mossbauer spectra and supported by IR and DTA studies will be given for both the samples under separate subsections.

4.6.I RED OCHRE

The Mossbauer spectrum of unannealed sample (Fig.4.3a) consists of one magnetically splitted six line hyperfine pattern and two quadrupole doublets. The lines of sextet are broad and a better computer fit could not be obtained. The magnetic pattern and the quadrupole doublet (doublet A) are due to α-Fe_2O_3. IR spectrum of unannealed red ochre, apart from other peaks, shows peaks at 590, 530, 470 cm^{-1}. The peaks for synthetic α-Fe_2O_3 occur at 585, 550, 485 cm^{-1} in IR spectrum |118|.Hence the above mentioned peaks of red ochre can be attributed to α-Fe_2O_3. The value of the internal magnetic

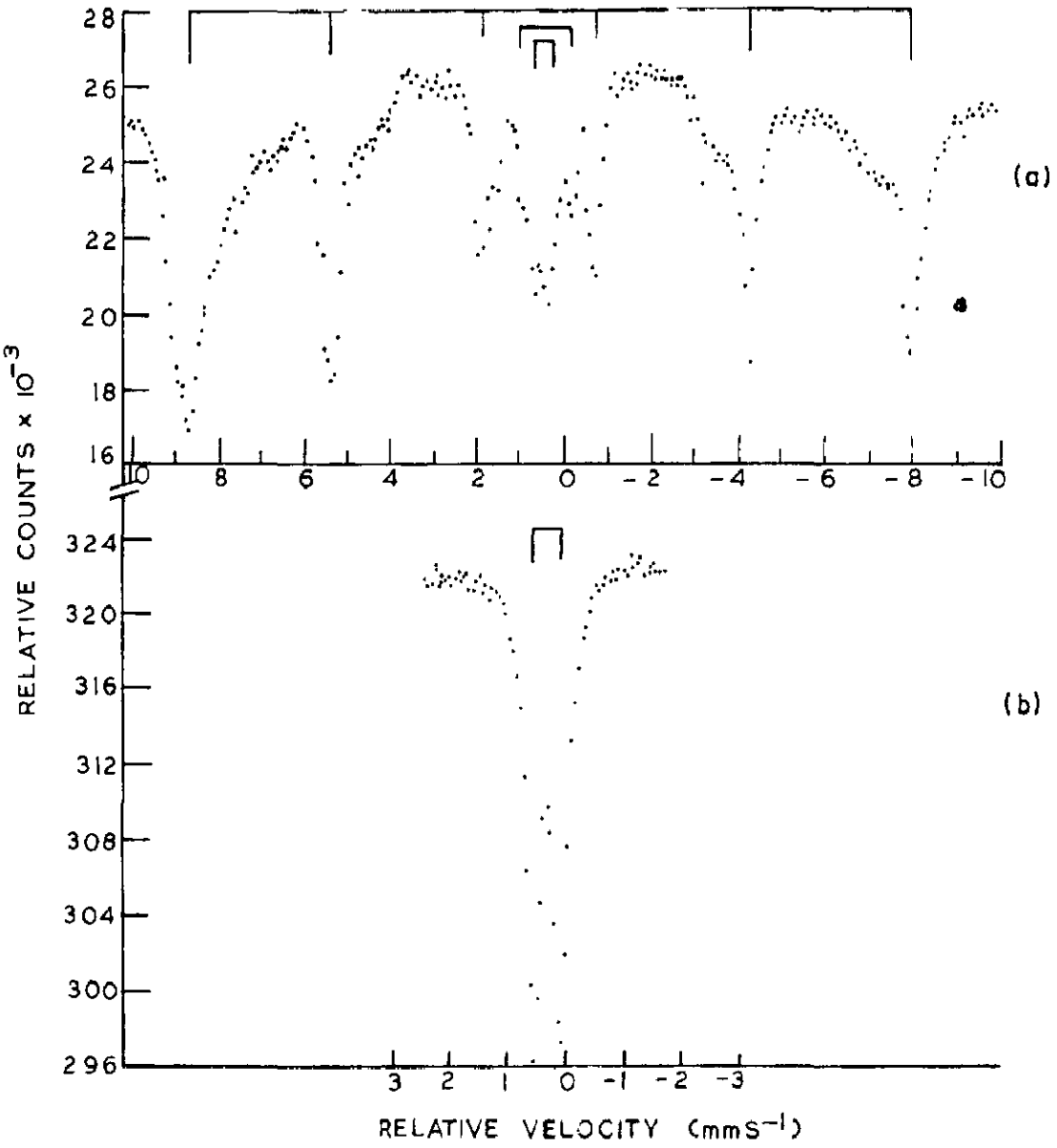

FIG.4.5 _ MÖSSBAUER SPECTRUM OF (a) RED OCHRE AT 113°K AND (b) YELLOW OCHRE AT 400°K.

TABLE 4.2- MOSSBAUER PARAMETERS OF RED OCHRE AT VARIOUS TEMPERATURE OF ANNEALING

Annealing Temperature	Magnetic Site						Quadrupole Doublet			
	A			B			A		B	
	H_{eff} (KOe)	δ (mm/s)	2ϵ (mm/s)	H_{eff} (KOe)	δ (mm/s)	2ϵ (mm/s)	δ (mm/s)	2ϵ (mm/s)	δ (mm/s)	2ϵ (mm/s)
Unannealed	506	+0.32	0.42	-	-	-	+0.34	0.50	+0.34	1.04
200	500	+0.41	0.46	470	+0.32	0.46	+0.29	0.38	+0.29	0.92
400	503	+0.40	0.38	480	+0.30	0.60	+0.19	0.50	+0.36	1.23
600	503	+0.24	0.40	496	+0.31	0.68	+0.15	0.46	+0.17	1.23
800	505	+0.31	0.51	484	+0.28	0.66	+0.15	0.46	+0.17	1.16
1000	504	+0.31	0.51	485	+0.31	0.64	+0.25	0.54	+0.29	1.08

'δ' measured with respect to atomic iron.

TABLE 4.3- MOSSBAUER PARAMETERS OF YELLOW OCHRE AT VARIOUS TEMPERATURE OF ANNEALING

Annealing Temperature (^{o}C)	H_{eff} (KOe)	δ (mm/s)	2ϵ (mm/s)
Unannealed	388	+0.34	0.62
200	371	+0.34	0.54
400	514	+0.33	0.46
600	511	+0.33	0.46

'δ' measured with respect to atomic iron.

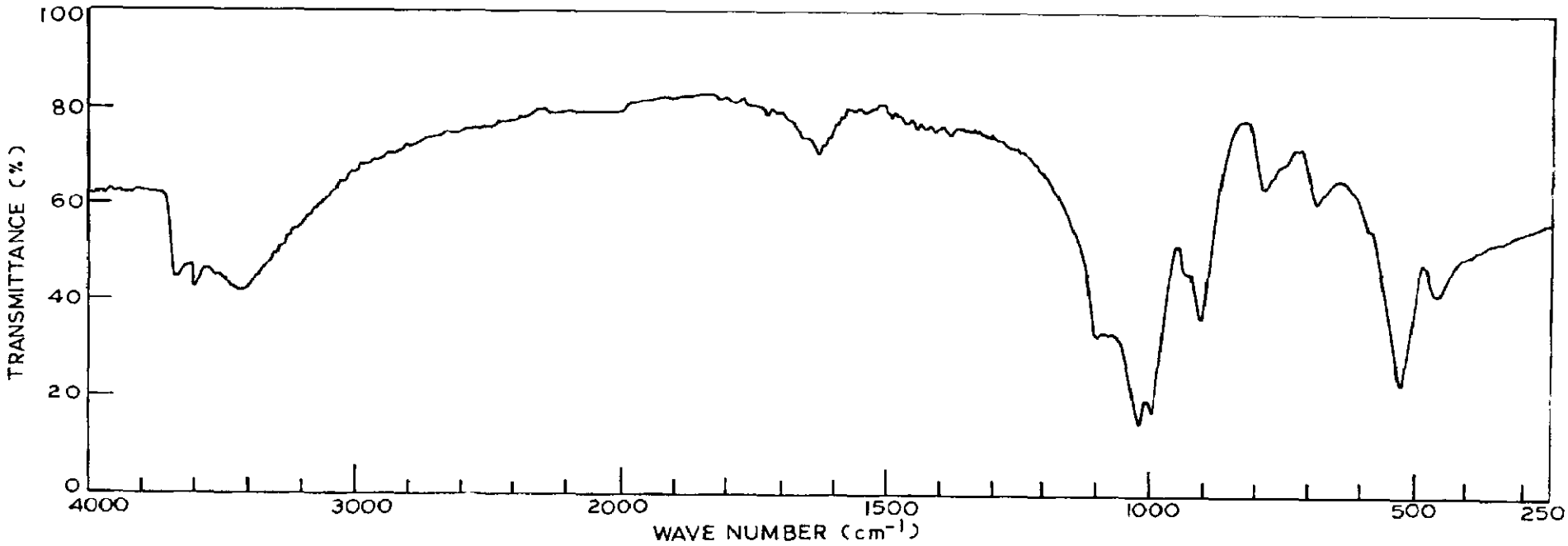

FIG.4.6 - INFRA-RED ABSORPTION SPECTRUM OF RED OCHRE.

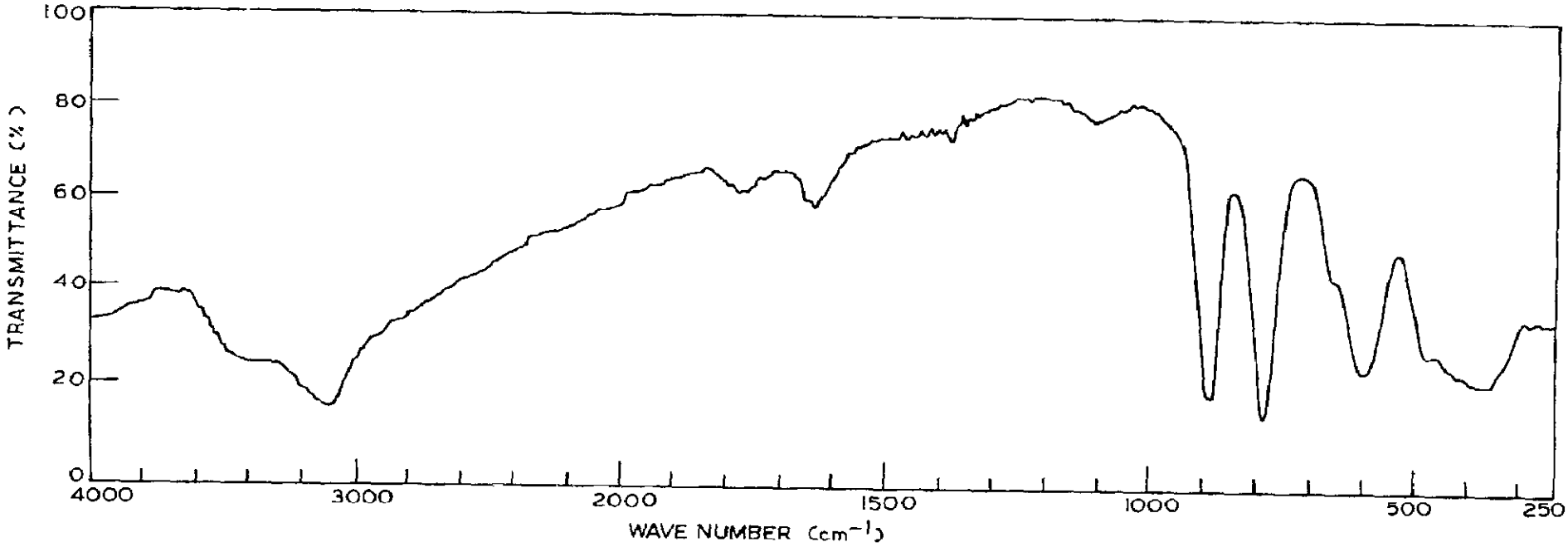

FIG.4.7 _ INFRA-RED ABSORPTION SPECTRUM OF YELLOW OCHRE.

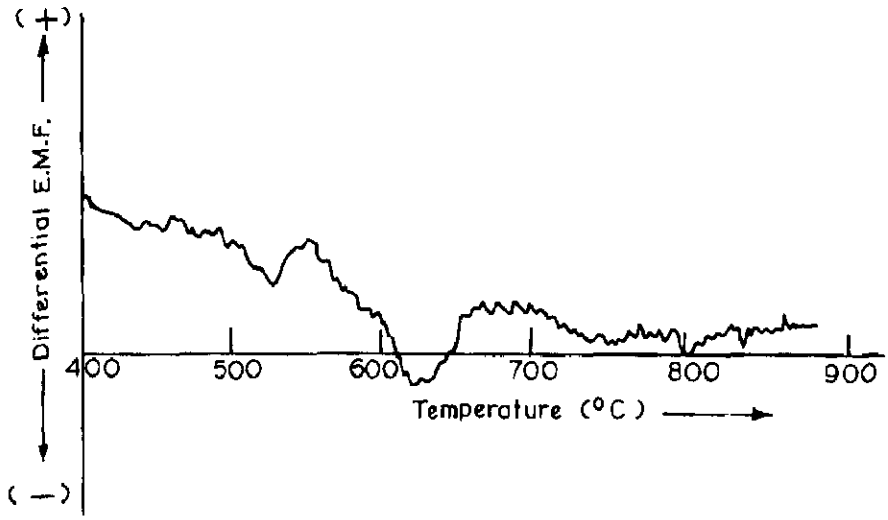

(a)

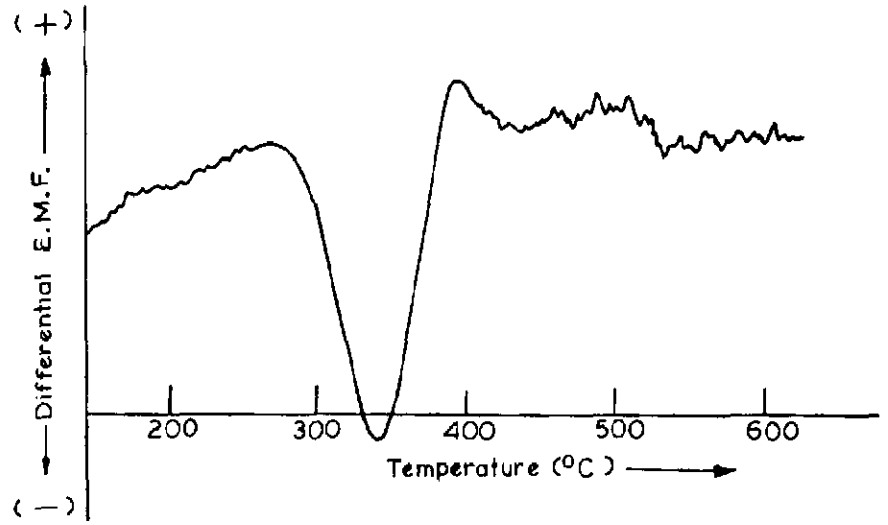

(b)

FIG.4.8 - DIFFERENTIAL THERMAL CURVE OF (a) RED OCHRE AND (b) YELLOW OCHRE.

field , H_{eff}, (~506 KOe) and the broadening of lines can be assigned to the presence of impurities such as silicon and aluminium in the neighbourhood of iron |109 |. The differential thermal curve of red ochre (Fig. 4.8a) shows two endothermic peaks. The one appearing at 624°C can be attributed to α-Fe_2O_3. The pure α-Fe_2O_3 peak appears at 680°C and low value of temperature of this peak in red ochre suggests the presence of impurities in the lattice sites |119 |.

Upon annealing the samples at various temperatures, the Mossbauer spectra show two sextets apart from two doublets (Fig. 4.3). The comparison of parameters indicates sextet B to be due to α-Fe_2O_3 with high degree of impurities. Variation in the value of H_{eff} of this sextet, with temperature of annealing, can be attributed to different amount of impurities associated with iron lattice.

The particle size is such that a superparamagnetic (spm) doublet(A) and a six line pattern are present simultaneously. The nearly constant value of quadrupole splitting, 2ϵ, with temperature of annealing suggests doublet A to be due to spm effects. This has been checked by recording the spectrum of unannealed red ochre at 113°K (Fig. 4.5a). Due to increase in spin relaxation time at 113°K, in comparison to that at room temperature, an increase in the intensity of magnetic pattern at the cost of decrease in intensity of doublet A is observed which lends support for this doublet to be due to superparamagnetic effects. The comparison of 2ϵ of sextet (due to α-Fe_2O_3)

at room temperature and at 113°K, in the case of unannealed sample, shows the absence of Morin transition. In bulk α-Fe_2O_3 it has been observed at 263°K, below which the spins lie along the EFG axis and show collinear antiferromagnetism whereas above this temperature the spins flip to a direction making 90° angle with EFG axis and show weak ferromagnetism due to canting|120 |. The absence of Morin transition may be attributed to fine particles |121,122|. Kunding et.al.| 121 | has attributed it to surface defects which pins the spins in the case of fine particles. The intensity of spm doublet goes on decreasing as the annealing temperature of sample is increased which can be attributed to increase in particle size. Such an observation has also been noted earlier by Srivastava and Sharma | 123 | and Simopoulos et.al.| 124|. The spm doublet is present even in the spectrum of sample annealed at 1000°C (Fig. 4.3f), however, with lower intensity indicating that particle size has not grown enough (> 200 A°) so as to show only the magnetic pattern.

The presence of two sextets in the spectrum of sample annealed at 1000°C suggests that impurities remain more or less unaffected even at this high temperature.

The other doublet, 'B',corresponds to another site in which iron is in the +3 oxidation state as is evident from value of isomer shift, δ (Table 4.2). The value of 2ϵ corresponding to this doublet suggests the presence of iron in a distorted alumina octahedra |109 |. The presence of absorption peaks at 3700, 3620, 1100, 1020,1000, 925,900,785 and 680 cm^{-1},

apart from the peaks characteristic of α-Fe_2O_3, in the IR spectrum of red ochre indicates the presence of clay mineral when the same is compared with the IR spectra of clay minerals | 71 |. The peaks at 3700, 3620 cm^{-1} correspond to water occluded in silicate structure, peaks around 1000 cm^{-1} correspond to Si-O stretching vibration, those at 925 and 900 cm^{-1} correspond to octahedral alumina sheet while the cause of remaining two peaks is not yet well understood | 71 |. The presence of clay mineral is also suggested by the appearance of an endothermic peak at 528°C, apart from that of α-Fe_2O_3, in DTA curve. Upon annealing, 2ϵ first remains practically constant then starts increasing from 400°C. From 800°C the value starts decreasing (Fig. 4.9). This type of variation, in 2ϵ, is in agreement with that obtained by Bouchez et.al.| 108 | and Janot et.al.| 109 |, while studying clays and ancient pottery. When the sample is heated, the impurity atoms partly get precipitated creating a variety of defects and thus leave the lattice in a very disorganized manner. The result is that a more asymmetric environment is created around iron ions and hence an increase in 2ϵ is observed. The same effect also appears in the IR spectrum of sample annealed at 600°C which shows broadening of peaks due to clay mineral. The observation of broad lines is an indication of asymmetry in the mineral structure. At higher temperatures (from 800°C in our sample) gradual recrystallization of disordered clay mineral occurs thus causing a decrease in the 2ϵ value. The variation of δ with temperature of annealing (Fig. 4.10) is in fair agreement with that obtained

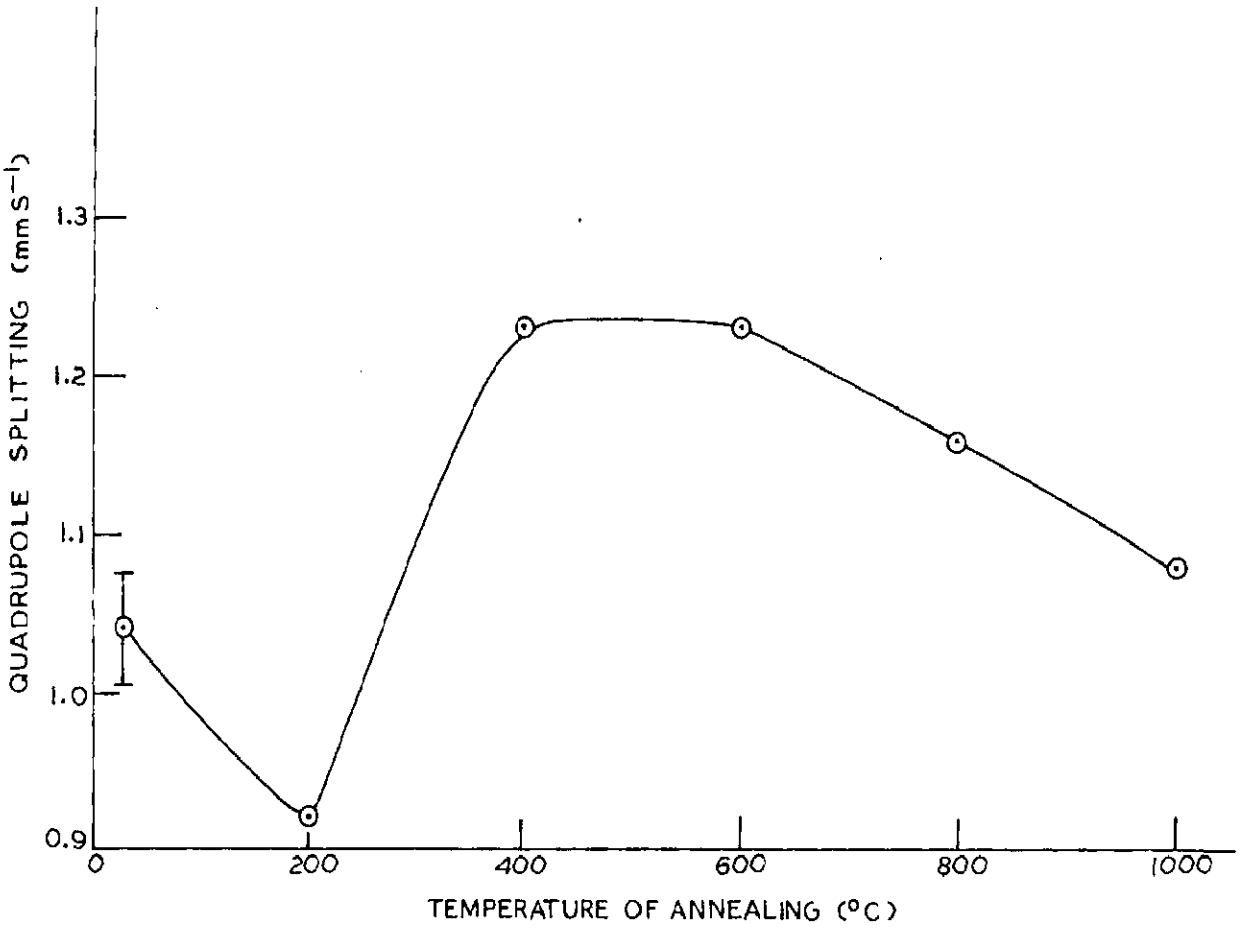

FIG. 4.9 _ VARIATION OF QUADRUPOLE SPLITTING WITH TEMPERATURE OF ANNEALING IN THE CASE OF CLAY MINERAL.

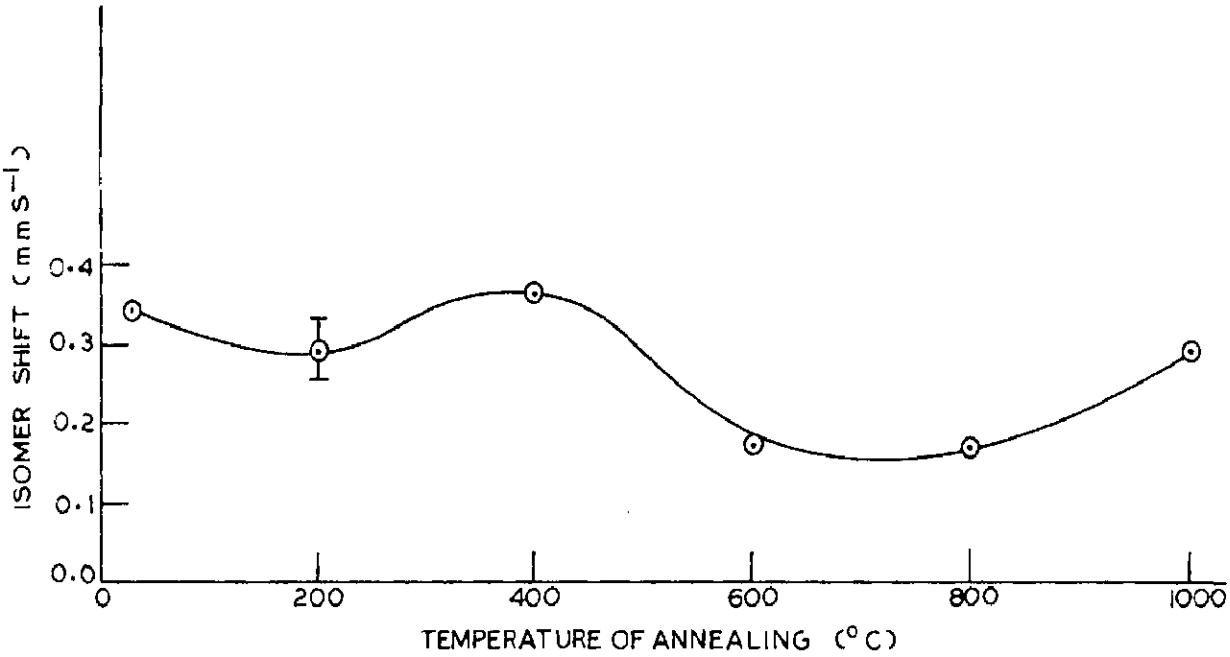

FIG. 4.10 _ VARIATION OF ISOMER SHIFT WITH TEMPERATURE OF ANNEALING IN THE CASE OF CLAY MINERAL .

by Janot et.al.|109 |.

4.6.II YELLOW OCHRE

Mineralogically yellow ochre has been reported to consist of α-FeOOH and α-Fe_2O_3. However, the Mossbauer spectrum of unannealed sample (Fig. 4.4a) shows only one six line pattern corresponding to α-FeOOH phase. The IR spectrum of sample shows peaks at 650, 785, 890 and 3120 cm^{-1}. These peaks are characteristic of α-FeOOH |118 |. Of these the peaks at 785 and 890 cm^{-1} correspond to lattice O-H bending vibrations while that at 3120 cm^{-1} apparently represents a strongly hydrogen bonded O-H stretching vibration. The 650 cm^{-1} peak has been reported without any specific assignment |125 |. Peaks at about 3440 and 1640 cm^{-1} are due to water of KBr which has been used in making pellets for IR study. Apart from these, the IR spectrum shows four more peaks which may be due to presence of silica and would not be discussed as they lie beyond the scope of present study. The Mossbauer spectrum of yellow ochre taken at 400°K shows only a quadrupole doublet. The transformation of a magnetically splitted six line pattern into a two line pattern confirms yellow ochre to be containing α-FeOOH whose Neel temperature is $\sim$400°K |126 |. Since the Mossbauer spectra of sample, taken at room temperature, does not show any quadrupole doublet or even a slight lowering of central portion, it has been concluded that grain size is large enough not to show spm effects. The spm effects have been observed in some samples of different origin by other workers previously |110 |.

The six fingered pattern of Mossbauer spectrum shows asymmetric lines which may be due to the presence of impurities such as Al^{3+}, in the neighbourhood of iron. The differential thermal curve of yellow ochre shows an endothermic peak at about 350°C corresponding to α-FeOOH, while the peak for pure α-FeOOH appears at about 405°C | 78 |. The lower value of temperature of this peak can once again be attributed to the presence of impurities in the lattice site |78 |.

After heating the sample at 400°C, α-FeOOH is converted to α-Fe_2O_3 | 127 | and a sextet for α-Fe_2O_3 is observed in the Mossbauer spectrum (Fig. 4.4c). This transformation was also observed in the IR spectrum which shows peaks corresponding to α-Fe_2O_3 while those corresponding to α-FeOOH disappear. On heating the sample at 600°C, the mobility of impurity ions increases so much that they are separated out from iron lattice and form a separate phase. The Mossbauer spectrum of sample annealed at 600°C, therefore, shows a neat six line pattern with symmetric lorentzians (Fig. 4.4d).

A decrease in the value of H_{eff} has been observed in the Mossbauer spectrum of sample annealed at 200°C (Table 4.3). This change can be attributed to change in spin relaxation time which decreases on heating the sample at 200°C and does not return to its original value, due to some rearrangement in the lattice, even on cooling down to room temperature. A decrease in the value of H_{eff} with decrease in spin relaxation time has also been suggested by Vander Kraan et.al.| 51 |.

Note that the above mentioned effect has not been observed in case of red ochre where magnetic pattern is due to α-Fe_2O_3. The effect can, therefore, be either due to change in the lattice or due to change in the geological conditions under which the two, red and yellow ochre, have formed. It is, however, quite premature at this stage to say anything conclusively.

4.7 CONCLUSIONS

After discussing various aspects with the help of Mossbauer spectra, IR and differential thermal analyses, following conclusions can be drawn:

(i) Iron, in red ochre is mainly in the form of α-Fe_2O_3 (with impurities in its neighbourhood) and in a clay mineral structure in which it is in distorted alumina octahedra. Simultaneous appearance of a magnetic pattern and an spm doublet, corresponding to α-Fe_2O_3, indicates that particle size was not more than 200 A°.

(ii) Upon heating, the clay mineral structure first distorts and then returns to less asymmetric structure at higher temperature. The impurities present in the α-Fe_2O_3 structure do not separate out even after heating the sample at 1000°C.

(iii) In case of yellow ochre, iron content has been found to be more than that in case of red ochre and mainly in the form of α-FeOOH.

(iv) After heating at 400°C, transformation of α-FeOOH to α-Fe_2O_3 has been observed in case of yellow ochre. Whereas the heating

at 600°C causes the mobility of impurity ions, in this transformed α-Fe_2O_3, to increase enough which results in the separation of these ions as another phase leaving pure α-Fe_2O_3.

(v) The exit of impurity ions from iron lattice at 600°C in the case of yellow ochre and not in red ochre even at 1000°C suggests that the two ochres are not of the same origin. The possibility that red ochre and yellow ochre may be of same origin, the former being the altered form of latter, has also been suggested by the geologists. It seems that red ochre has formed under high temperature (above 1000°C) conditions whereas yellow ochre is a sample formed in low temperature environments.

(vi) Yellow ochre is more rich in iron than red ochre which further suggests that the former has formed under low temperature conditions than the latter because the product which has crystallized at higher temperature is not iron rich.

CHAPTER 5

MOSSBAUER STUDIES OF NATURAL GOETHITE AND BOG IRON ORE*

* Based on ' Mossbauer studies of natural goethite and bog iron ore'. A.K. Singh, B.K.Jain and K.Chandra. To appear in Phys. Stat.Solidi(a) 44 (1977).

5.1 INTRODUCTION

The applications of Mossbauer spectroscopy in solving the mineralogical problems are no more stranger. Goethite and bog iron ore are natural samples containing mainly hydrated iron oxide. There have been number of studies on goethite. First of all Hrynkiewicz et.al. [128] proposed the existance of two internal fields. This result was further supported by him in a later communication [129]. Oosterhout [130], however, suggested the presence of only one internal field which has been observed by other workers also [131, 132], later. This controversy seems to have been solved by Deszi et.al. [133] and Govaert et.al. [134] in favour of one internal field. They have related the asymmetry of lines, appearing in some samples of natural goethite, to an excess of water present in the structure. Shinjo [50] and Van der Kraan et.al. [51] have done measurements on fine particles of goethite to examine Mossbauer spectra in fluctuating fields produced by the relaxation of electron spins. However, there is hardly any study of goethite through Mossbauer spectroscopy which had correlated the results with its occurrence. Bog iron ore has not been studied through Mossbauer effect previously. The purpose of the present study was, therefore, to study goethite and bog iron ore and to examine the type of deposit and also the conditions which were present at the time of their formation.

Both the samples are of Indian origin and were mainly studied through Mossbauer effect by recording spectra of

unannealed as well as annealed (at various temperatures) samples. Gravimetric chemical analysis was done to find out Fe, Si, Al contents. Differential thermal (DTA) and Infrared (IR) absorption analyses were also done to support the Mossbauer results. Variation of particle size with the temperature of annealing, has also been discussed.

5.2 BRIEF MINERALOGICAL AND STRUCTURAL INFORMATION

Both of these natural samples are essentially hydrated iron oxides. The distinction between them is made on the basis of their occurrence in nature.

5.2.I GOETHITE

It is one of the most common mineral typically formed as a weathering product of iron bearing minerals e.g. siderite, magnetite, pyrite etc. It is normally formed under oxidising conditions and is the stable soil iron oxide in humid climates. Iron is in the form of α-FeOOH |135|. The structure of goethite was shown by Goldsztaub |136| to be similar to that of diaspore (α-AlOOH), the unit cell containing four molecules of FeOOH. The oxygen lattice is hexagonally close packed with iron ions in the octahedral interstices.

5.2.II BOG IRON ORE

This natural product contains largely $FeO(OH).nH_2O$ with small amounts of $Fe_2O_3.nH_2O$. The water content varies widely and it is probable that the mineral is essentially an amorphous form of goethite with adsorbed water |135|. In some of the

bog ore deposits iron occurs as siderite ($FeCO_3$) whereas other contain siderite and vivianite $|Fe_3(PO_4)_2.8H_2O|$ in minor amounts, apart from goethite. The structure of goethite has been outlined in preceding subsection, those of other two minerals are not worth mentioning as the same were not observed in present studied sample.

5.3 OCCURRENCE

5.3.I GOETHITE

This mineral may be formed by the aging of brown gel formed by the slow oxidation of certain ferrous compounds or slow hydrolysis of certain iron salts e.g. ferric acetate, nitrate, bromide and oxalate. The brown gel of hydrous basic iron oxide are colloidally transported alongwith Al^{3+}, which is separated during precipitation due to properties different from the hydrous iron oxide colloids. Thus iron and aluminium are separated by geochemical conditions during weathering processes |113|. In some sedimentary iron ores of economic importance it may be the principal constituent.

5.3.II BOG IRON ORE

It is principally in the swamps and lakes constituting the centres of such systems that bog ores develop. According to Harder |137|, bog ores can be classified into two types. The first are Marsh or Peat ores. These are common in swamps and peat bogs in cool areas. Under Marsh conditions, the accumulation of decaying plants induces reducing conditions in the surface waters and leads to the formation of abundant CO_2,

Any iron in surface waters is thus reduced and combines to form ferrous-bi-carbonate. If, however, the ground water moves fairly freely and contains oxygen, interaction of this with the descending ferrous-bicarbonate solution leads to the local oxidation of latter and formation of a layer of marsh or peat bog ore along the water table. The other one is lake ore type. The development of this is possible if marshy conditions are of regional extent and incorporate lakes. In this case, the ferrous-bi-carbonate solutions move underground for considerable distances, eventually to discharge through bottom sediments into the body of a lake. Where such lakes waters are well oxygenated, the discharging ground waters are oxidised and iron precipitated on lake floor as limonite. Since such discharge, in most cases, tends to occur near the margins of lakes, bog ores of this kind are commonly developed near the edges of the lakes and may be absent in the centre |138 |.

5.4 EXPERIMENTAL PROCEDURE AND RESULTS

The samples, goethite and bog iron ore, were obtained from Geology Department, University of Roorkee. Their identification had already been done through standard geological methods.

The determination of iron, aluminium and silicon was carried out following standard procedures given by Vogel |117 |. Laboratory grade reagents and distilled water were used in the analysis. The results have been given in Table 5.1.

TABLE 5.1- WEIGHT PERCENTAGE OF IRON, SILICON AND ALUMINIUM IN GOETHITE AND BOG IRON ORE

Sample	Weight percentage		
	Fe	Si	Al
Goethite	47.36	7.06	8.66
Bog Iron Ore	13.37	34.91	0.08

The heat treatment to the samples was given by heating them separately at 200, 400, 600, 800 and 1000^{0}C for three hours in air atmosphere and then cooling down to room temperature gradually.

The Mossbauer spectra of the samples unannealed as well as annealed were recorded on a spectrometer already described in chapter 3. The gamma-ray source used was Co^{57} in copper matrix with initial activity of 3.5 mCi. The pellets were formed by mixing 80 mg. of the sample with the required amount of boron nitride, an inert matrix and transparent for gamma-rays, and then pressing the mixture inside a copper ring of 16 mm. diameter. Thus obtained pellets were used as absorber for recording spectra in transmission geometry. The spectra for goethite and bog iron ore have been shown in Figure 5.1 and 5.2 and the analysed Mossbauer parameters are given in Table 5.2 and 5.3 respectively.

Infrared absorption spectra of goethite and bog iron ore have been shown in Fig. 5.3 and 5.4 while differential thermal curves of the two have been depicted in Fig. 5.5a and 5.5b respectively.

5.5 DISCUSSION

5.5.I GOETHITE

The Mossbauer spectrum of unannealed goethite exhibits two six fingered patterns and a quadrupole doublet (Fig.5.1a). Internal magnetic field, H_{eff}, of the sextet A (site A in Table 5.2) is 354 KOe and is lower than that for synthetic

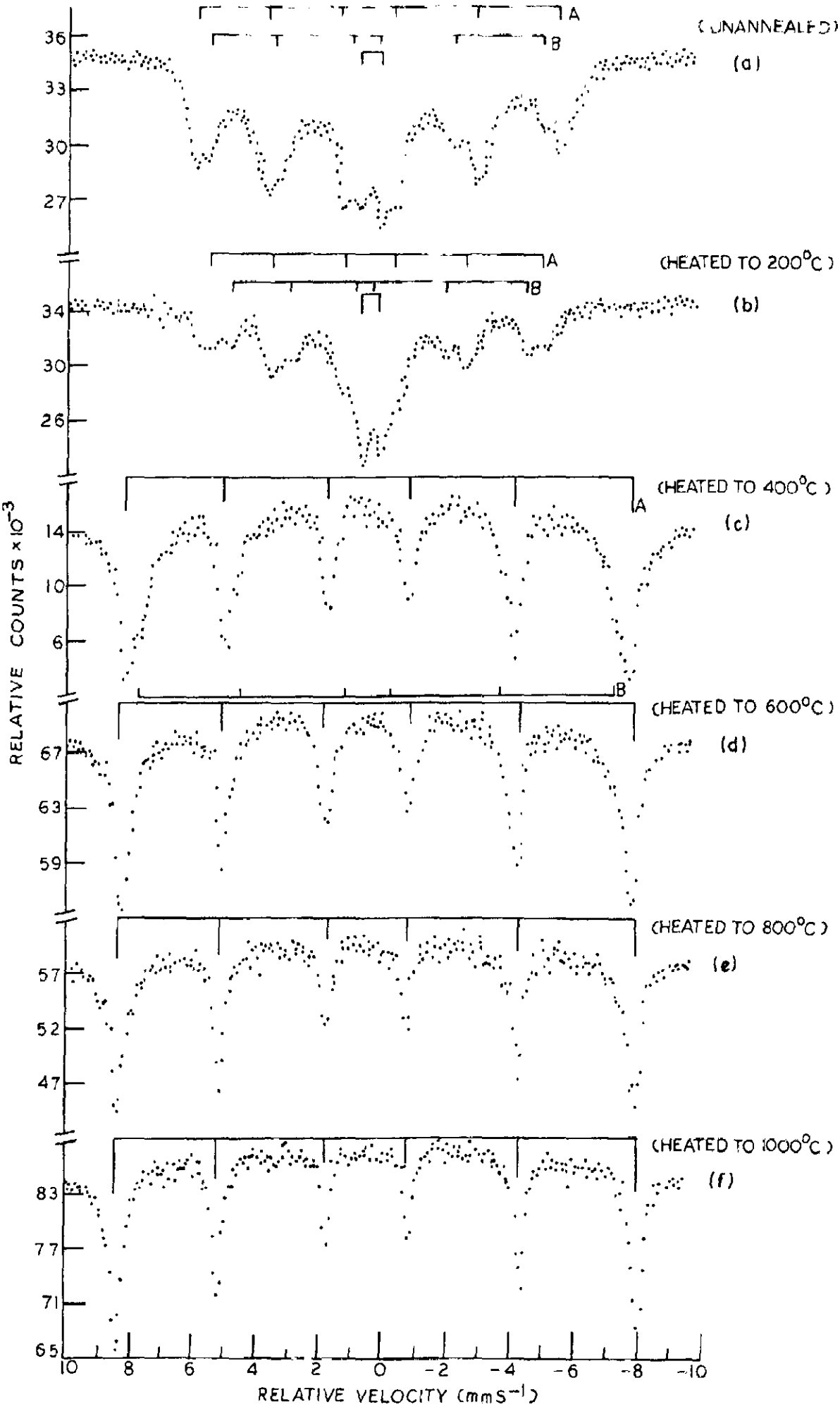

FIG.5.1 _ MÖSSBAUER SPECTRA OF GOETHITE AT ROOM TEMPERATURE.

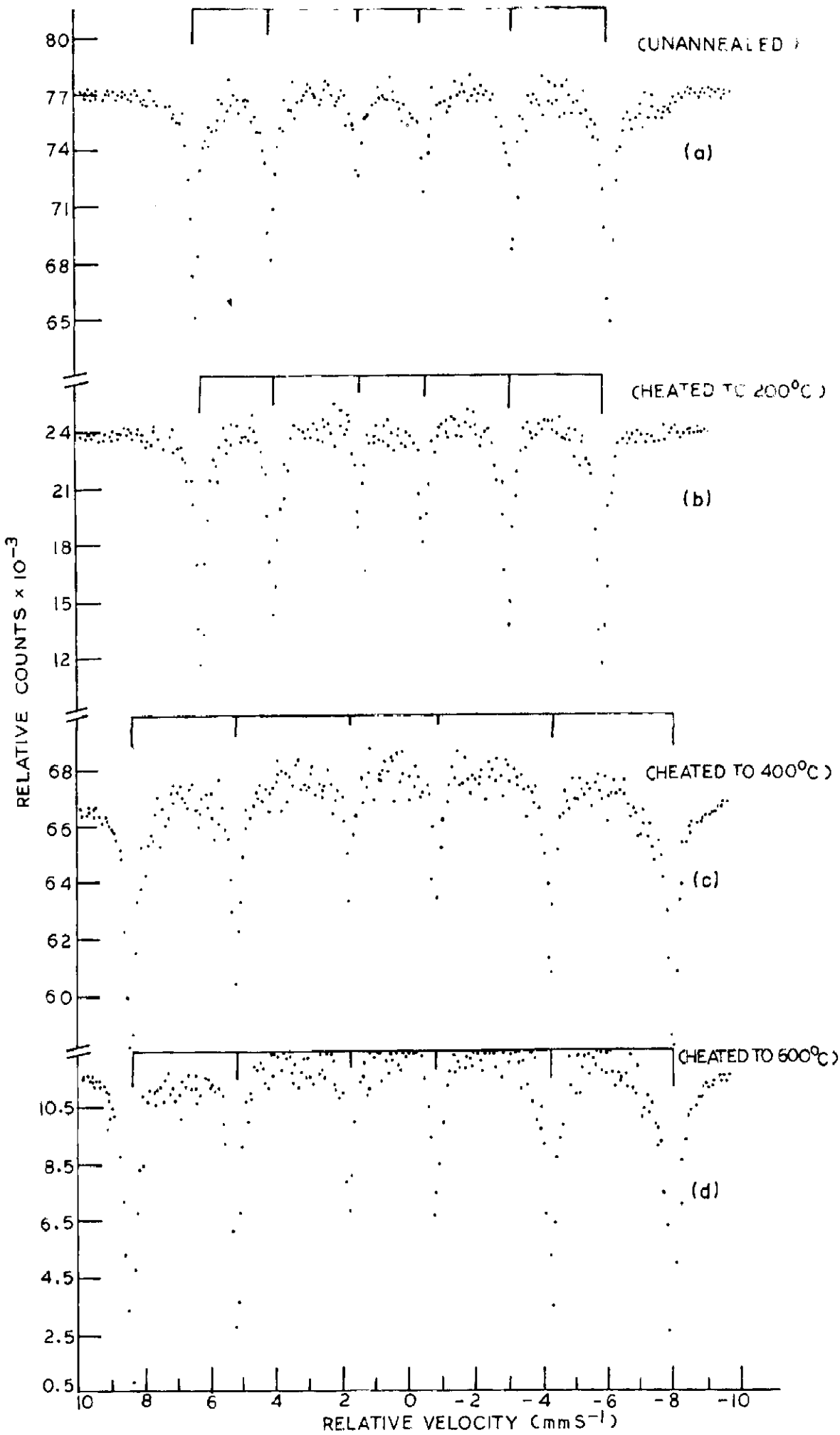

FIG.5.2 _ MÖSSBAUER SPECTRA OF BOG IRON ORE AT ROOM TEMPERATURE.

TABLE 5.2- MOSSBAUER PARAMETERS OF GOETHITE AT VARIOUS TEMPERATURE OF ANNEALING

Annealing Temperature (°C)	Magnetic Site						Quadrupole doublet	
	A			B				
	H_{eff} (KOe)	δ (mm/s)	2ε (mm/s)	H_{eff} (KOe)	δ (mm/s)	2ε (mm/s)	δ (mm/s)	2ε (mm/s)
Unannealed	354	+0.34	0.42	325	+0.45	0.57	+0.40	0.69
200	325	+0.39	0.50	288	+0.39	0.42	+0.38	0.58
400	497	+0.34	0.50	469	+0.34	0.42	-	-
600	505	+0.34	0.42	-	-	-	-	-
800	510	+0.33	0.46	-	-	-	-	-
1000	512	+0.33	0.46	-	-	-	-	-

'δ' measured with respect to atomic iron.

TABLE 5.3- MOSSBAUER PARAMETERS OF BOG IRON ORE AT VARIOUS TEMPERATURE OF ANNEALING

Annealing Temperature (°C)	H_{eff} (KOe)	δ (mm/s)	2ϵ (mm/s)
Unannealed	389	+0.33	0.61
200	379	+0.34	0.54
400	511	+0.35	0.50
600	511	+0.35	0.46

'δ' measured with respect to atomic iron.

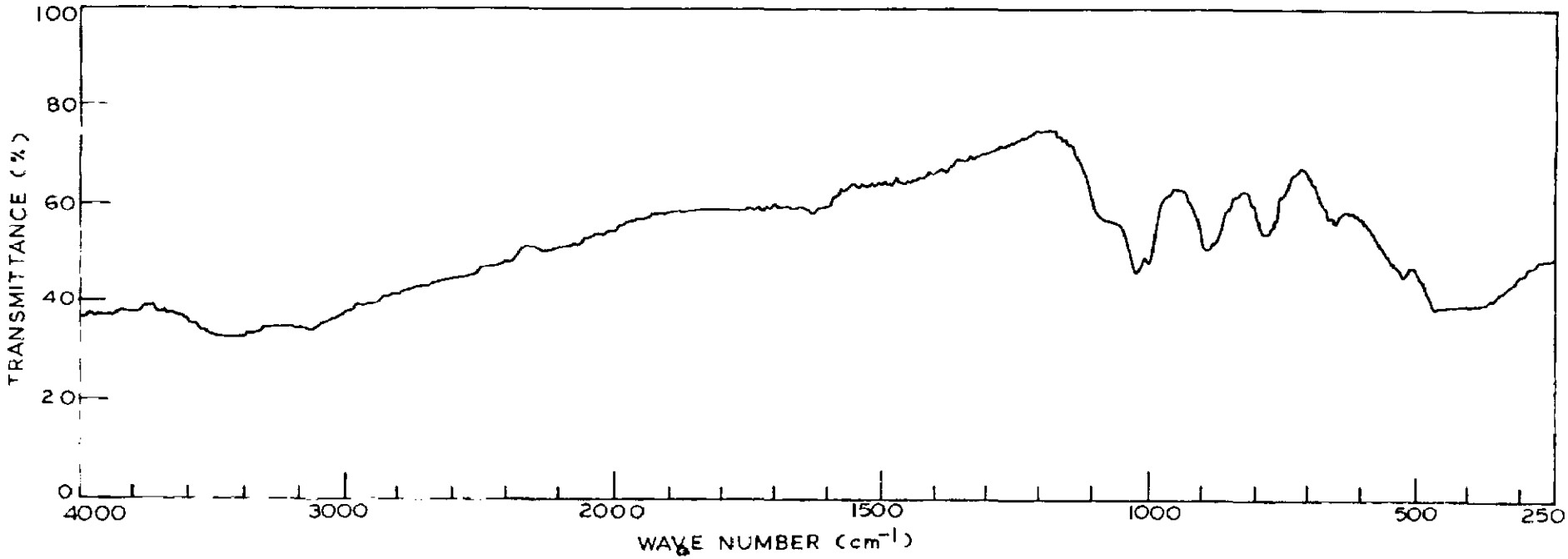

FIG.5.3 - INFRA-RED ABSORPTION SPECTRUM OF GOETHITE.

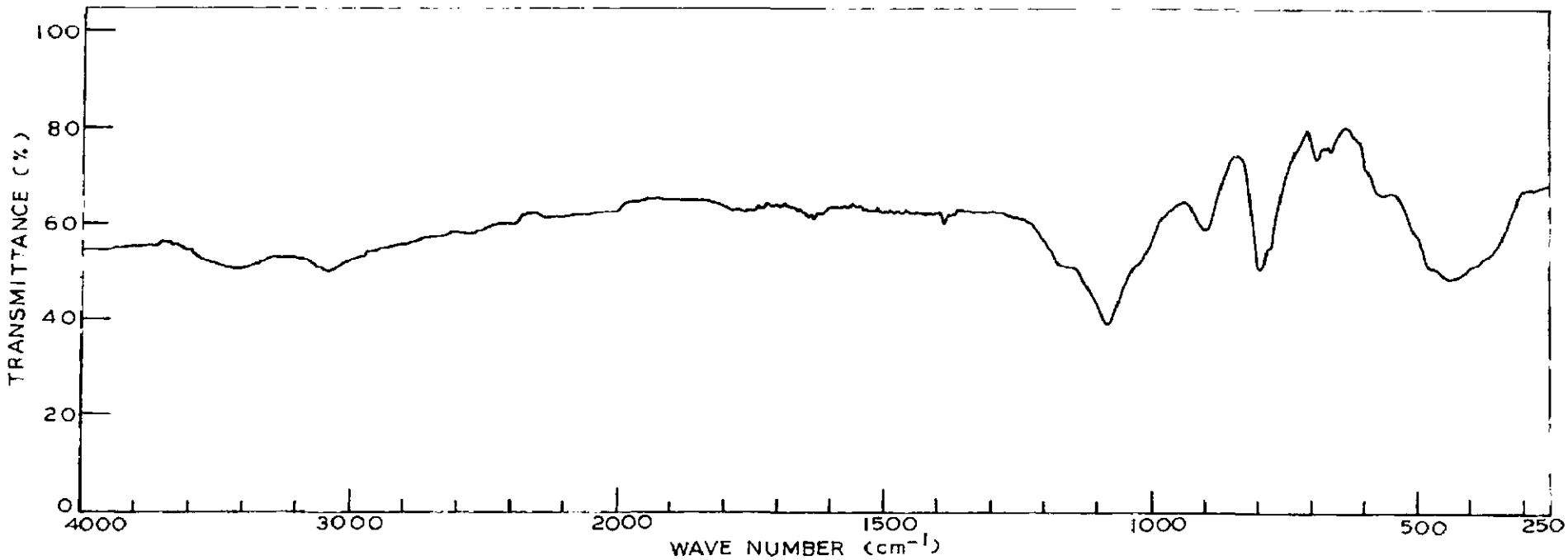

FIG. 5.4 - INFRA-RED ABSORPTION SPECTRUM OF BOG IRON ORE.

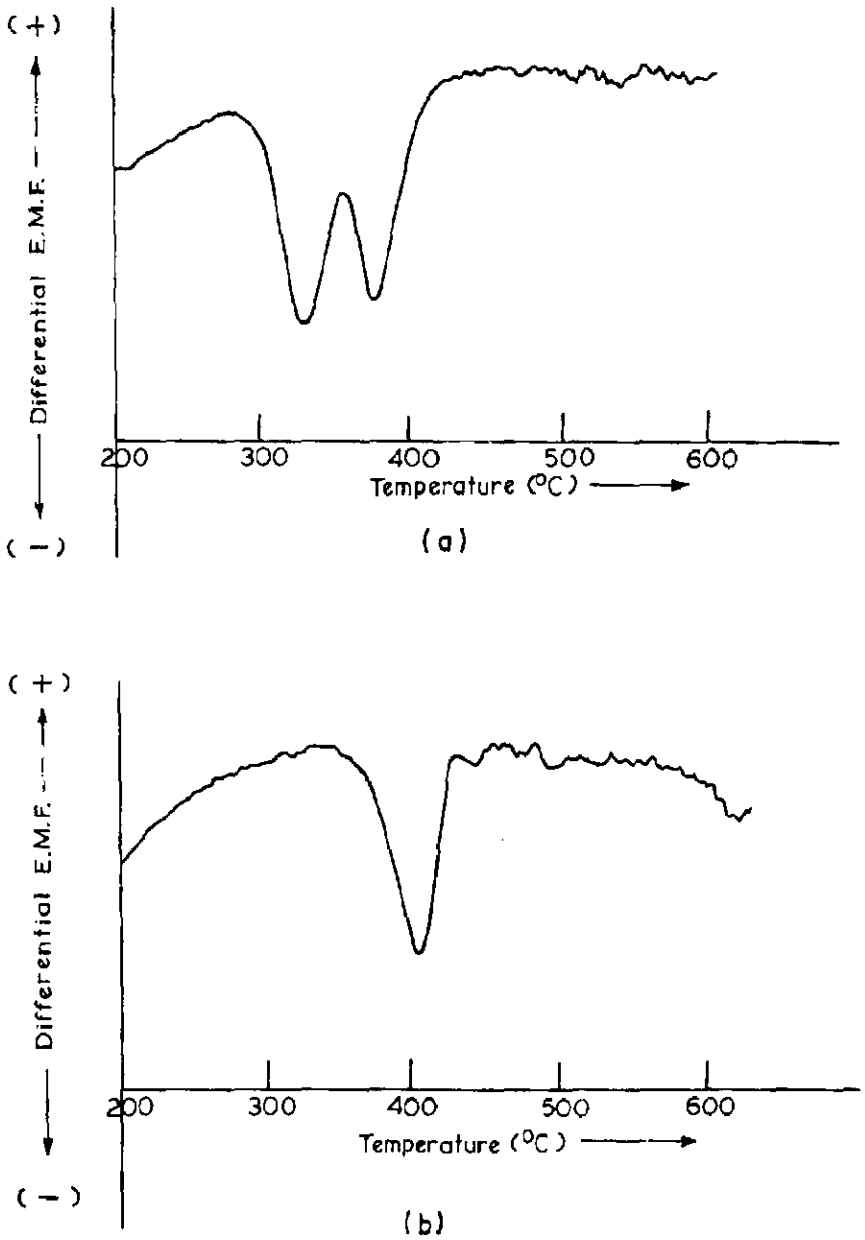

FIG. 5.5 _ DIFFERENTIAL THERMAL CURVE OF (a) GOETHITE AND (b) BOG IRON ORE.

α-FeOOH (388 KOe) | 51 |. This lowering in value can be attributed to small particle size as has been suggested by Van der Kraan et. al. |51 |. The other six fingered pattern, designated as site B, has got still lower H_{eff} (325 KOe). It can be assigned to fine particles of α-FeOOH with impurities in its lattice (site B in Table 5.2). The differential thermal curve shows two endothermic peaks centered at about 330 and 375°C (Fig. 5.5a) which supports the above view point regarding the presence of two sextets |113 , 119|. IR spectrum of unannealed goethite shows peaks at 650, 780, 890 and 3120 cm^{-1} which are close to characteristic peaks of α-FeOOH | 118 |. Apart from these, two weak peaks appear at 1630 and 3420 cm^{-1} which are due to presence of water in KBr (used in forming pellets for IR study), whereas peaks at 525, 1000, 1020 and 1090 cm^{-1} correspond to silicate mineral | 71 |.

Isomer shift, δ, for sextet A (0.34 mms^{-1}) is characteristic of low spin Fe^{3+} and remains practically constant with the temperature of annealing. 'δ' for sextet 'B' is larger (0.45 mms^{-1}) than that of sextet A. This may be due to the presence of impurities e.g. Al^{3+} | 139 |. Upon heating, the impurities separate out and thus result in the decrease of isomer shift.

The simultaneous appearance of six line and two line patterns suggests the presence of superparamagnetism which in turn is due to small particles (< 500 Å) of α-FeOOH | 51 |. This doublet can be confused with that due to lepidocrocite (γ-FeOOH), which can also be found to coexist with

goethite | 113 |. But its presence has not been shown by differential thermal curve of goethite which, in an otherwise case, should show an endothermic peak followed by an exothermic peak showing the conversion of γ-Fe_2O_3 into α-Fe_2O_3 | 113 |. IR spectrum also does not exhibit peaks at 730 and 1025 cm^{-1} which are characteristic of lepidocrocite | 118 |. When goethite is heated upto 400°C, α-FeOOH transforms to α-Fe_2O_3 | 127 |. Since α-Fe_2O_3 needs finer particles than α-FeOOH to exhibit superparamagnetism, the spm doublet vanishes completely. In the case of α-Fe_2O_3, superparamagnetism is observed for particle size of $\sim$ 200 A° or smaller | 45, 51, 121 |. The particle size of unannealed goethite can, therefore, be estimated to be lying in between 200-500 A°. The Mossbauer spectrum of this transformed sample contains two sextets with H_{eff} as 497 and 469 KOe (Fig. 5.1c). The former sextet (site A) is due to small particle size of α-Fe_2O_3 and the latter (site B) is due to fine particles of α-Fe_2O_3 with impurities in its lattice site. On heating the sample at 600°C, the mobility of impurity ions increases fast enough to get out of lattice structure and to separate out into another phase. This causes the appearance of single six line pattern in the Mossbauer spectrum of sample annealed at 600°C . The anomalous line shapes and smaller value of H_{eff} (505 KOe) can be attributed to smaller particle size. An increase in the value of H_{eff} is observed with increase in temperature of annealing. This happens due to increase in particle size as the annealing temperature is raised. The value of H_{eff} approaches that for

normal α-Fe_2O_3 (515 KOe) in the Mossbauer spectrum of sample annealed at 1000°C.

5.5.II BOG IRON ORE

The Mossbauer spectrum of the unannealed sample shows a six line hyperfine splitted pattern for which the value of H_{eff} is 389 KOe, close to that of normal α-FeOOH. The other two possible iron compounds which may be present in bog ore deposits are siderite and vivianite. Siderite shows one quadrupole doublet at room temperature | 140 | whereas vivianite exhibits two quadrupole doublets corresponding to two crystallographically inequivalent Fe^{2+} sites | 141 | . The Mossbauer spectrum, therefore, suggests the presence of iron as α-FeOOH only. The presence of α-FeOOH is also evident from IR absorption spectrum in which peaks at 660, 795, 895 and 3080 cm^{-1} appear. The peaks at 3420, 1630 cm^{-1}, in IR spectrum of bog iron ore, are due to water present in KBr whereas the peaks due to silicate mineral are at 570, 690, 1020, 1080 and 1170 cm^{-1}. The differential thermal curve of bog ore shows an endothermic peak at 405°C (Fig. 5.5b) which is characteristic of pure α-FeOOH | 113 |. The isomer shift δ is characteristic of Fe^{3+} and remains constant with various temperature of annealing. The particle size in present sample is large enough not to show superparamagnetic effects in Mossbauer spectrum. When the sample is heated at 400°C, α-FeOOH is converted to α-Fe_2O_3 corresponding to which a sextet with H_{eff} of 511 KOe is observed in the Mossbauer spectrum (Fig. 5.2c). Further heating at 600°C, of sample, does not show any change in the spectrum as is evident from Mossbauer parameters (Table 5.3).

5.5.III RELAXATION EFFECTS

A common feature has been noted in the spectra of goethite and bog iron ore after having given heat treatment at 200°C. The H_{eff} value has decreased from that of unannealed samples (Table 5.2 and 5.3). Heating of the samples at 200°C, it seems, decreases the relaxation time and even on cooling down, to room temperature, the same does not return to its original value due to some rearrangement in the lattice structure. Consequently a Mossbauer spectrum may show all or any of the three peculiarities (a) broadening of the component peaks | 50 |, (b) decrease in the value of H_{eff} | 51 |, and (c) increase in the superparamagnetic fraction | 51 |. Since particle size in the case of goethite is smaller (as suggested by the presence of a superparamagnetic doublet) than that in bog iron ore, heating should affect spin relaxation time more in goethite than in bog iron ore. Consequently all the three changes given above are observed in the spectrum of goethite annealed at 200°C (Fig.5.1b, Table 5.2). Whereas the effect of heating in case of bog iron ore is just to decrease the value of H_{eff} (Fig. 5.2, Table 5.3).

5.6 CONCLUSIONS

Having discussed the various results of Mossbauer spectra of the samples and supplementing them from IR and differential thermal studies, following conclusions may be drawn:

(a) Iron in case of goethite has been detected in the form of fine particles of α-FeOOH. Some of the α-FeOOH sites also contain impurities such as Al^{3+}.

(b) Upon heating at 400°C, α-FeOOH is converted to α-Fe_2O_3. While the annealing at 600°C forces the impurity ions to leave the lattice structure and let them separate out into another phase. Annealing at progressively higher temperatures helps in developing the particle size also.

(c) As has already been discussed, Al^{3+} is also transported alongwith the brown gel containing Fe^{3+} iron, yet it is generally separated during precipitation due to geochemical conditions. The presence of impurities in α-FeOOH structure and the small grain size suggest that crystallisation of present studied goethite is not complete.

(d) The bog iron ore studied here contains iron as α-FeOOH only without any impurity and with grain size large enough not to show superparamagnetic effects.

(e) The presence of iron as α-FeOOH only and not as carbonates or phosphates suggests the bog iron ore studied in present investigations, to be not of Marsh or peat ore type but is a lake ore type deposit. Furthermore, α-FeOOH present in this bog ore deposit is pure and with larger grain size (atleast equal to the size of normal α-FeOOH) hence the bog iron ore is of hard type.

CHAPTER 6

MINERALOGY AND GENESIS OF IRON ORE BAND ASSOCIATED WITH THE META-ACIDIC INTRUSIVE OF CARBONATE SUITE OF CHAMOLI, GARHWAL HIMALAYA*

* Based on 'Mossbauer studies of iron ore' A.K.Singh, B.K.Jain and K.Chandra.
Proc. NP and SSP Symp., India 19C, 420 (1976).

and

'Mineralogy and genesis of iron ore band associated with meta-acidic intrusive of carbonate suite of Chamoli, Garhwal Himalaya.
A.K.Singh, G.C.S. Gaur and K.Chandra
Can. J.Earth Sci. (Communicated).

6.1 INTRODUCTION

Iron is a metal of universal use. Its applications have increased thousandfold since man discovered steel. Iron is extracted mostly from its ores magnetite, hematite which are oxides of iron. The chief minerals of iron which may be considered as ores are tabulated below.

Mineral	Composition	Iron (%)
Magnetite	Fe_3O_4	72.4
Hematite	Fe_2O_3	70.0
Turgite	$2Fe_2O_3.H_2O$	66.3
Goethite	$Fe_2O_3.H_2O$	62.9
Limonite	$2Fe_2O_3.3H_2O$	59.8
Siderite	$FeCO_3$	48.3
Pyrite	FeS_2	46.6
Pyrrhotite	Fe_nS_{n+1}	38.0
Ilmenite	$FeTiO_3$	36.8
Greenlatite, Chamosite etc.	Hydrous Iron silicates	20 to 35

Among these magnetite is the richest ore, hematite is the most common ore whereas turgite, limonite, goethite and siderite are important ores in some countries only. Rest are only minor

sources of iron. For modern industrial purposes it is necessary to know whether the ore is of the Bessemer or non-Bessemer type. This is determined by the amount of phosphorous in the ore, since practically all the phosphorous goes into iron or steel manufactured from it. In general, a content of 0.1% of phosphorous in the pig iron is considered as the safe upper limit in the acid process. The bessemer limit in ore is taken roughly as .001% phosphorous for each percent of iron content. Thus a 60% ore should not contain more than .06% phosphorous to be classed as Bessemer ore |142|.

The iron ores of India can be divided into three major groups |142| on the basis of their origin:

(a) Banded ferruginous formations of pre-cambrian age are most important type of ores. In the unmetamorphosed type, which includes the majority of larger deposits, the ore bodies have been derived from the concentration of the iron contained in the original banded hematite-jasper formation. When subjected to metamorphism, these ores convert into banded quartz-magnetite rocks, magnetite being derived from original hematite. Some times the magnetite is associated with amphiboles of the grunerite-cummingtonite group.

(b) Sedimentary iron ores of sideritic or limonitic composition comes in this category. The examples are ironstone shales of the eastern coal fields occurring in the tertiary formations in parts of Himalayas and Assam. The sideritic ore is often

hydrated and changed to limonitic iron-stone near the surface.

(c) This group consists of lateritic ore derived from the sub-aerial alteration of iron-bearing rocks such as gneisses, schists, basic lavas etc., under humid tropical conditions, resulting in the concentration of the hydrated oxides of iron often associated with those of Al and Mn. Lateritic caps cover large stretches of the Deccan traps, the gneisses in the western ghats, the schistose rocks of many areas, the impure line formation etc. However, they are low graded containing only 25 to 35% iron.

Iron ores occur in different geological formations in India but by far the most of important deposits belong to the pre-cambrian. These ores are derived from the enrichment of the banded-ferruginous rocks by the removal of silica. The ore bodies generally form the tops of ridges and hillocks. The later formations contain some ore, especially the Gondwanas and the Laterites but these are of comparatively little importance at present.

Iron ore beds especially hematitic have been described by various workers from the different stratigraphic horizons of Himalayas |143 - 149|. The regional geology of lesser Himalaya in Garhwal-kumaon region has been systematically worked out by Medlicott | 150|. Contributions of Wadia |151| and Heim and Gansser |152| have thrown light on the geology, stratigraphy and structure of Garhwal-Kumaon Himalaya. A

sketch of the geology of Chamoli district was given by Valdiya |153|. O'Rourke |154| discussed the stratigraphic implications of occurrences of hematite iron ore beds and regarded them geosynclinal sediments.

In the carbonate suite of chamoli, widespread hematitization of the schistose and phyllitic rocks are observed along the main central thrust. A one meter thick band of iron ore is also found associated with the green meta-acidic intrusive near the core of the Pipalkoti anticline. The present chapter is the outcome of the studies done on this iron ore band to find out the minerals present in it and to correlate the variations with the geological setting of the band. The investigations were carried with the help of thin sections and polished samples in the preliminary stage. In the secondary stage chemical analysis was done to find out its composition and Mossbauer effect studies were done to study the variation in the amount and structure of respective minerals. Attempt has also been made to suggest about the genesis of this band.

6.2 GEOLOGICAL SETTING

The rocks of the 'carbonate suite of Chamoli' of Garhwal group |155,156| consists of alternating sequence of slates and dolostones and occur as broad doubly plunging anticline|149,157|. To the north of this anticline the high grade crystalline rocks are found thrusted over these low grade sedimentaries along

the main central thrust. Close to this thrust the slates/phyllites of carbonate suite show wide spread hematitization. In the southern limb of this anticline a thin concordant meta-acidic unit, described as chloritoid slate, is found within the dolostone. At the base of this unit, a 1 meter thick iron ore band is encountered. From the field observations a fault has been inferred along this band |149|.

The iron ore band shows a sharp contact with the meta-acidic unit, whereas, it has a corroded lower contact with the dolostones. Along the lower contact a slight discordance is also observed with the country rock. Within the ore band, mainly in the central portions, coarse octahedral and cubic magnetite crystals are found embedded in fine hematitic ground mass. Along the margins long flakes of hematite are common.

6.3 MICROSCOPIC OBSERVATIONS

Two types of microscopic studies were carried out: Polished samples and thin section studies.

For polished samples' studies three rock samples were taken from the top, middle and bottom of this 1 meter thick band. Their polished sections were made for ore microscope analysis. The preparation of polished surfaces is an important part of the technique of ore microscopy. For satisfactory examination , a plane polished surface of an ore, with a minimum of pits, scratches, fractures, and pores is desirable.

In such a surface minute details e.g. mineral occurrence, form and texture are observable. The production of polished surface commonly involves three stages - preparation of specimen, grinding and polishing. The specimen is prepared by cutting a slab of desired size from the rock. This is done with a diamond saw, which consists of a motor driven disc having its edges set with small diamonds. The piece, cut from the rock sample, is then ground on motor driven lap of cast-iron, copper or bronze. After fine grinding, polishing is done in few stages on metal laps covered with silk cloth. In this manner polished sections are prepared. Details regarding the preparation of polished surfaces have been nicely given by Cameron |158|.

The polished section of the rock sample, from the bottom part of ore band, shows foliated texture by lepidoblastic hematite and contain porphyroblastic ideoblasts of magnetite. The foliations, in general, show bending around porphyroblasts, whereas, at places the truncation is also observed. The alteration of magnetite crystals by oxidation into fine fibrous laths of hematite is common,whereas, the secondary recrystallisation of hematite is usual along veins and fine cracks. Ilmenite and goethite occur in minor amounts (plate 6.1a).

The sample from the upper portion of the ore band shows, in its polished section, highly folded foliations marked by hematite flakes, and having the octahedral scattered porphyroblasts of magnetite and titaniferrous magnetite (containing

inclusions of iron oxide). The development of martite is peculiar. Magnetite generally alters into hematite and goethite. The flakes and laths of hematite are also found surrounding the gangue porphyroblasts (plate 6.1b).

The central portion of the band shows slightly massive nature and contains euhedral to subhedral porphyroblasts of magnetite. Hematite occurs as cementing material or along the weak planes and interstitial spaces. Magnetite commonly alters to hematite and goethite. Pyrite and ilmenite occur as sporadic minor grains (plate 6.1c).

In general the grain size varies from place to place. Hematite occurs as recrystalised flakes and also as amorphous cement.

The ore samples were also studied by forming their thin sections. For making thin section of a rock, its chip is ground perfectly flat on one side, with carborundum powder on a glass plate. The grinding is began with a coarse powder and continued with finer powders until a very smooth flat surface is obtained. Care is being taken to avoid mixing of grinding powder, of different grades, on the chip. A glass slide is taken and a small amount of Canada balsam put in its centre and heated gently until sufficient turpentine or xylol has been driven off to cause the balsam to become hard and compact when cool. The chip of the rock is then placed on the slide with the flattened side in contact with the balsam and

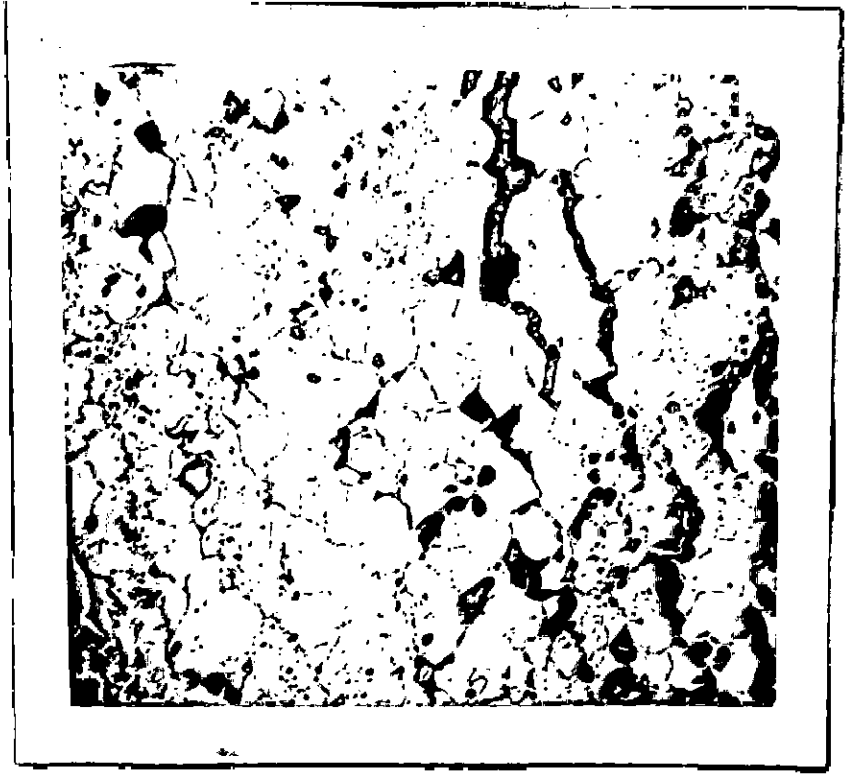

PLATE 6.1 a-Microphotograph of sample from Bottom part of the Ore Band.

Magnification- 45 X
Enlarged ×2

PLATE 6.1 b-Microphotograph of sample from Top part of thr Ore Band.

Magnification- 45 X
Enlarged ×2

PLATE 6.1 c-Microphotograph of sample from Middle part of the Ore Band.

Magnification- 45 X

Enlarged x2

glass. Air bubbles are removed from the film of balsam between the chip and the glass slide. On cooling, the chip is cemented firmly on the glass. The resulting thick chip is then ground as previously, beginning with the coarse and ending with the finest powder. The thickness of slice is judged by the polarisation colours given by some recognisable mineral e.g. quartz, and grinding is continued until this mineral shows its usual polarisation colours e.g. grey and yellow for first order. After final grinding, the slice is covered with fresh balsam and heated again to slightly less extent than before. When balsam is of right consistency, a very thin slide of glass-the cover glass slide - is carefully placed over the rock slice and pressed down so that no air bubbles are present. The resulting slide is known as thin section of the rock.

In thin sections the identifiable gangue minerals are dolomite, calcite, quartz, stilpnomelane, rutile and chlorite. The dolomite grains occur as inclusions in the iron minerals, whereas calcite grains contain numerous inclusions of iron oxide and occur as porphyroblasts. Chamosite is also oftenly observed.

A general survey by the studies of polished and thin sections taken from a very close interval of 10 cms. indicate that hematite predominates in the upper portions and is minimum in central portion. Contrary to this, magnetite predominates in the central portion. Ferruginous chlorite and chamosite are well developed at the base, whereas stilpnomelane is widespread.

Ilmenite, goethite and lepidocrocite are sporadic and scattered throughout. The mineralogical variation in the band and its setting in the rocks has been depicted in Fig.6.1 and the paragenetic sequence of the minerals are given in Table 6.1.

6.4 CHEMICAL ANALYSIS

Chemical analysis of the iron ore samples was undertaken following the standard procedures adopted by Vogel [117]. For determining Fe^{2+} and Fe^{3+} iron in ore samples, first of all total iron was determined and then amount of Fe^{2+} iron. The difference of the two gives Fe^{3+} iron. AR grade reagents were used in the analysis. The results have been given in table 6.2. The sample obtained from top part of the band shows least amount of Fe^{2+} iron indicating that it is most oxidised. Amount of manganese, calcium and magnesium is maximum in the sample taken from the bottom part of the band. Among the impurities, titanium is in very small amount, however, a comparison of its amount in the three samples showsit to be least in the sample from middle part of the band. This is in agreement with microscopic observations also.

6.5 STRUCTURE OF CONSTITUENT MINERALS

Through microscopic studies the three samples, taken from the iron ore band, have been found to contain hematite, magnetite, lepidocrocite, stilpnomelane and chlorite minerals in fairly good amount. Of these, the first three minerals are

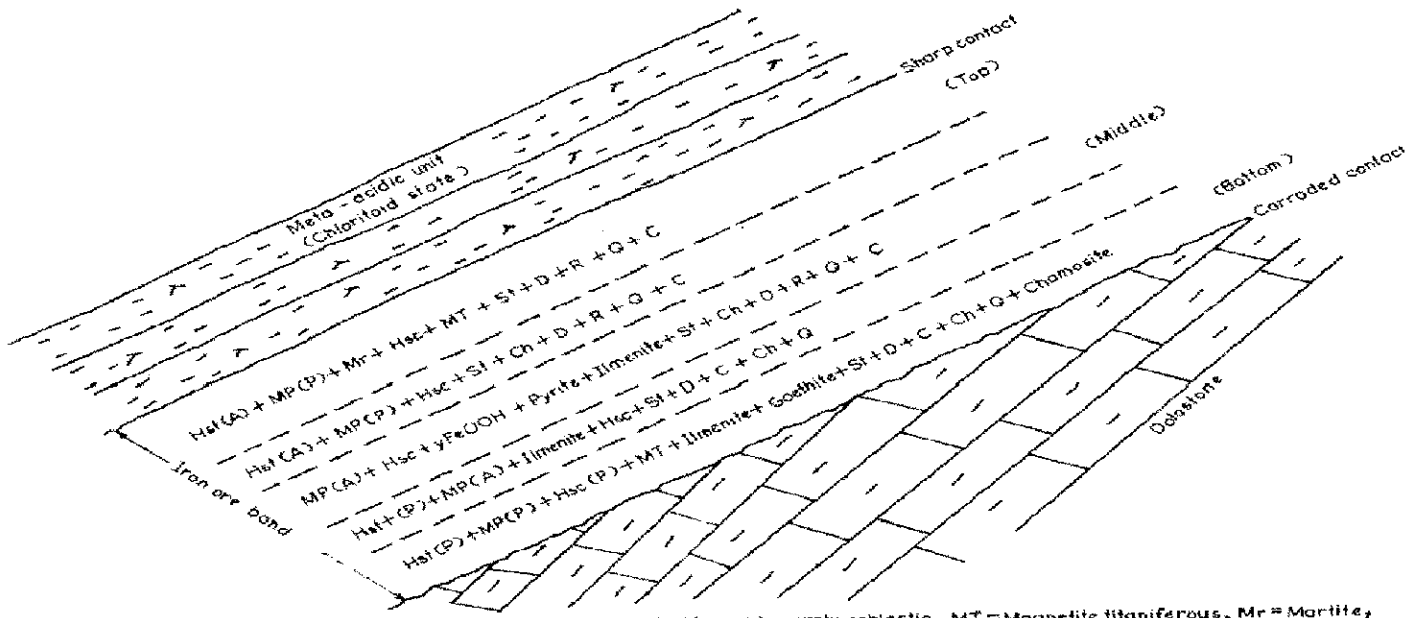

Hst = Hematite (Stress generated), Hsc = Hematite secondary, MP = Magnetite porphyroblastic, MT = Magnetite titaniferous, Mr = Martite, St = Stilpnomelane, Ch = Chlorite, D = Dolomite, R = Rutile, Q = Quartz, C = Calcite, A = Abundant, P = Prominent.

FIG.6.1 - MINERALOGICAL VARIATION IN THE ORE BAND -

TABLE 6.1- PARAGENETIC SEQUENCE OF THE MINERALS OBSERVED IN IRON ORE BAND

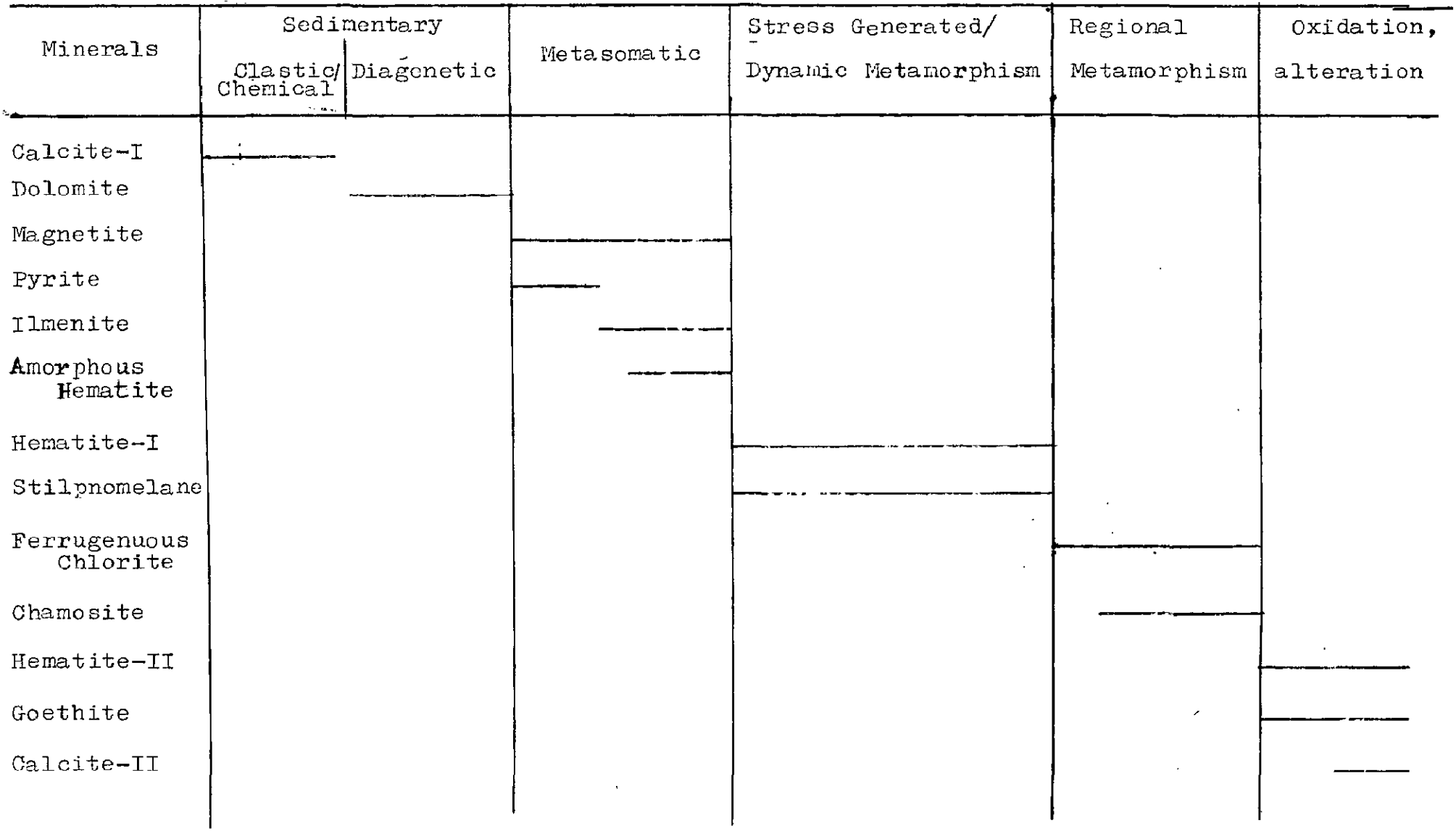

TABLE 6.2- CHEMICAL ANALYSIS OF SAMPLES OBTAINED FROM TOP, MIDDLE AND BOTTOM PART OF IRON ORE BAND

Elements' Oxides	Top	Middle	Bottom
Fe^{++}(ous)	5.77	9.83	11.40
Fe^{+++}(ic)	54.88	58.02	50.27
SiO_2	5.10	9.10	7.00
Al_2O_3	3.60	2.42	2.50
TiO_2	0.24	0.12	0.36
MnO	4.10	3.41	5.72
CaO	5.32	4.20	6.16
MgO	7.24	6.80	9.31

essentially of iron whereas rest two may contain iron in detectable amount. These minerals are, therefore, expected to show their characteristic patterns in the Mossbauer spectrum of iron ore samples. The structure of these minerals have been given briefly in the following lines.

6.5.I HEMATITE

The structure of this α-Fe_2O_3 mineral has been described in section 4.4.I. Possible impurities in its structure are Ti^{4+} and Mn^{3+} whereas the presence of SiO_2 and Al_2O_3 represents contamination. Large percentage of Ti in natural sample of hematite represents intergrowth of ilmenite ($FeTiO_3$) |114|.

6.5.II MAGNETITE

This mineral is (Fe^{3+}) $[Fe^{2+}, Fe^{3+}]$ O_4 i.e. Fe_3O_4. It is having an inverse spinel structure with half of ferric iron at tetrahedral and rest at octahedral sites and ferrous at octahedral sites. The details of spinel structure are given in a later section 7.4. A considerable amount of Ti can enter the magnetite structure, there being a continuous relationship between magnetite and the ulvospinel molecule, Fe_2TiO_4. Mg, Mn and some Ca are impurities of divalent group which may enter in the structure of natural magnetite |114|.

6.5.III LEPIDOCROCITE

This mineral is γ - FeOOH. The oxygen lattice is

orthorhombic with cubic close packing. The lattice parameters are

$$a = 12.4\ \text{Å}^{o},\quad b = 3.87\ \text{Å}^{o},\quad c = 3.06\ \text{Å}^{o}$$

Iron is present here in octahedral surrounding of oxygen and hydroxyl ions. The octahedra are nearly regular and have four corners occupied by oxygen and two by hydroxyl group |114,159|.

6.5.IV STILPNOMELANE

This mineral comes under the category of sheet silicates. Preliminary details about silicate mineral structure have been described in section 4.4.III. It has got mica-like layer structure and hence has got one tetra-and two octahedral sites|116|. Two hydroxyls and four oxygens form the apexes of the octahedron. The O_a site has hydroxyls on opposed apexes and the O_b site has the hydroxyls on adjacent tips | 160|. Trivalent iron may be present in both tetra-and octahedral sites, however, bivalent iron is generally believed to be in octahedral coordination only |71,116|.

6.5.V CHLORITE

Chlorite is also a member of sheet silicate minerals' group. Its structure consists of alternate mica-like and brucite-like layers (Fig. 6.2). In brucite-like layers metallic ions e.g. $Al^{3+}$and Mg^{2+} are surrounded octahedrally

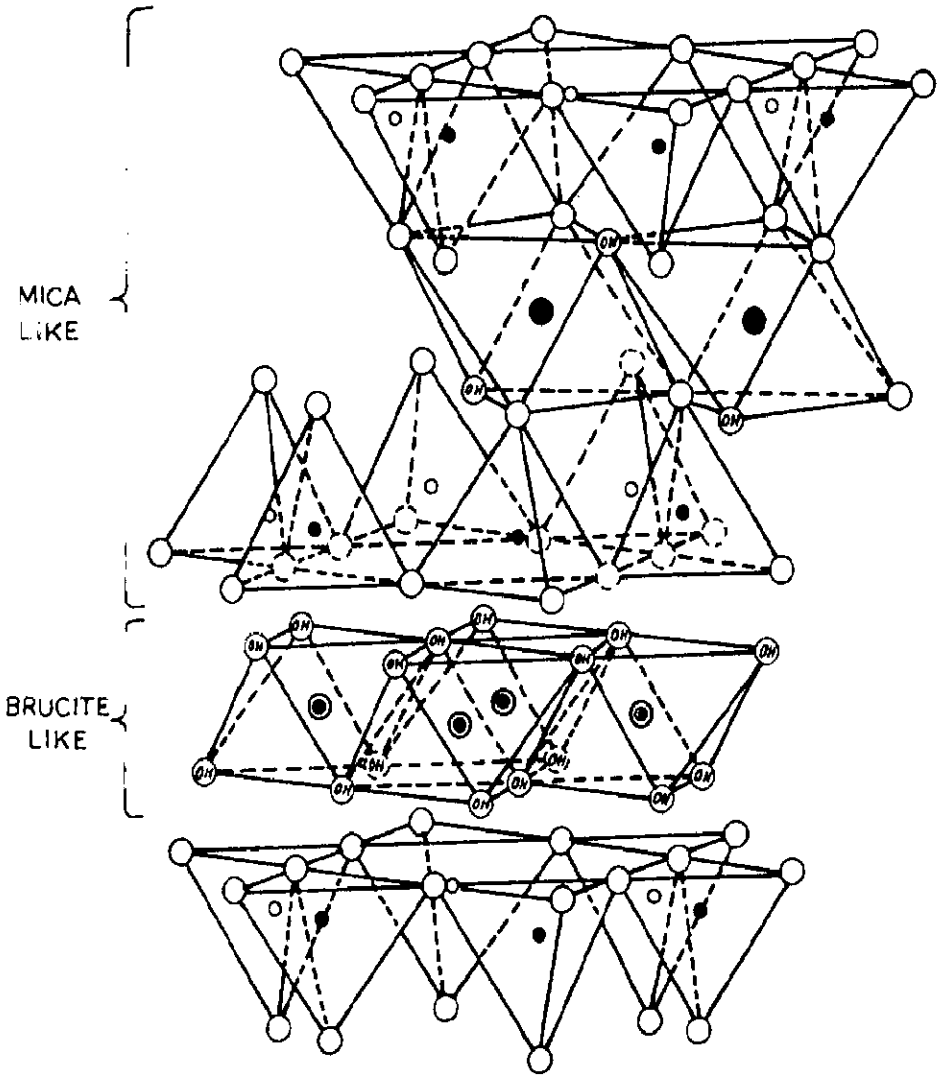

○ — Oxygen , ⓞ — Hydroxyls , ○ and ● — Silicons (some of them replaced by aluminiums),

◉ — Magnesiums (partially replaced by aluminiums), ● — Aluminium, Iron, magnesium.

FIG.6.2 - STRUCTURE OF CHLORITE .

by hydroxyl ions. In this structure, hence, there are three octahedral and one tetrahedral site in each unit |71|.

6.6 MOSSBAUER STUDIES

Three samples from top, middle and bottom of the iron ore band, referred to as T,M and B respectively hereafter, have been subjected to this study. Their Mossbauer spectra were observed at room temperature. The gamma-ray source used was $\sim$5.5 mCi Co^{57} in palladium matrix. The absorbers were prepared by weighing 50 mg of powdered samples and forming their pellets after thoroughly mixing with the required amount of boron nitride. The Mossbauer spectra were analysed on IBM 370/155 computer using a least square fitting programme. The results are given in Table 6.3. The spectra of all the three samples show three six line patterns and one or two quadrupole doublets. Two six line patterns (A and B in Fig. 6.3, 6.4 and 6.5) are characteristics of tetra- and octahedral sites of magnetite |161| while third (site C) corresponds to hematite |121| . Comparison of parameters of these sextets (site A,B and C in Table 6.3) with those of respective synthetic compounds |161,121| shows the presence of impurities in these structures. Apart from these two, stilpnomelane (site D) |116| is also present in all these samples whereas the presence of lepidocrocite in sample M (site E in Fig. 6.4) and that of feruginous chlorite in sample B (site E in Fig. 6.5) has been identified by their representative

TABLE 6.3- MOSSBAUER PARAMETERS OF SAMPLES OBTAINED FROM TOP, MIDDLE AND BOTTOM PART OF THE IRON ORE BAND

Sample	Mineral	Relative Intensity (%)	Site	H_{eff} (KOe) ±0.5KOe	δ (mm/s) ±0.01 mm/s	2ε (mm/s) ±0.06 mm/s
Top	Magnetite	31.9	A	488	+0.38	0
			B	457	+0.73	-0.03
	Hematite	64.6	C	514	+0.45	-0.46
	Stilpno-melane	3.5	D	-	+0.45	0.47
Middle	Magnetite	68.3	A	492	+0.41	-0.10
			B	459	+0.74	0
	Hematite	25.2	C	512	+0.45	-0.43
	Stilpno-melane	2.4	D	-	+0.35	1.04
	Lepido-crocite	4.1	E	-	+0.40	0.53
Bottom	Magnetite	51.6	A	500	+0.27	-0.31
			B	454	+0.68	0.01
	Hematite	36.3	C	502	+0.54	-0.27
	Stilpno-melane	5.2	D	-	+0.42	0.73
	Chlorite	6.9	E	-	+1.32	1.98

'δ' measured with respect to atomic iron.

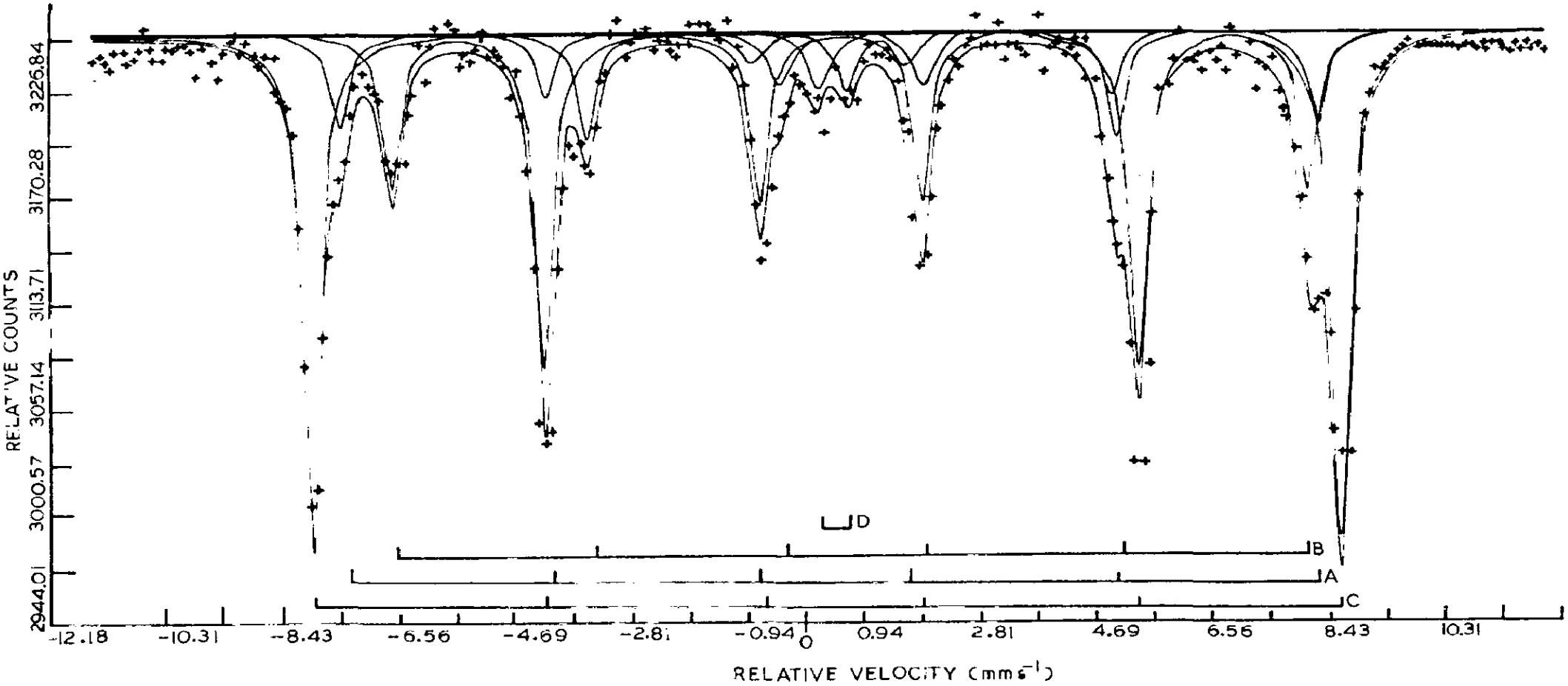

FIG. 6.3 - MÖSSBAUER SPECTRUM OF SAMPLE FROM TOP PART OF THE ORE BAND.

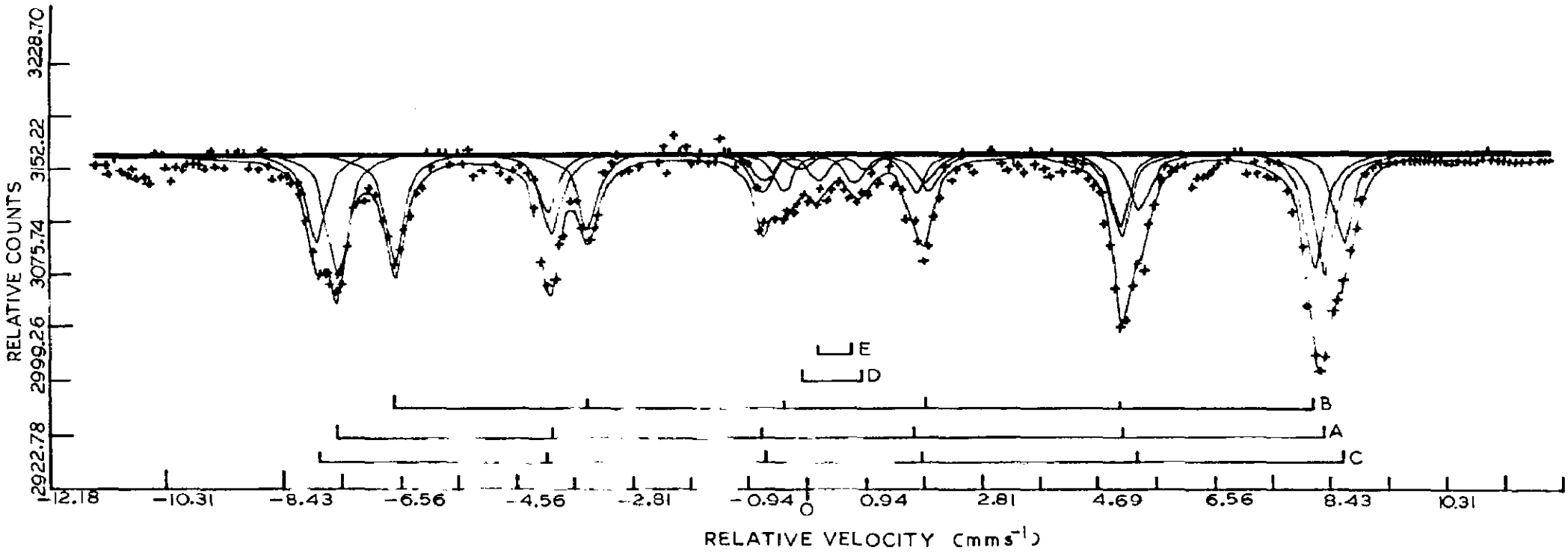

FIG.6.4 - MÖSSBAUER SPECTRUM OF SAMPLE FROM MIDDLE PART OF THE ORE BAND .

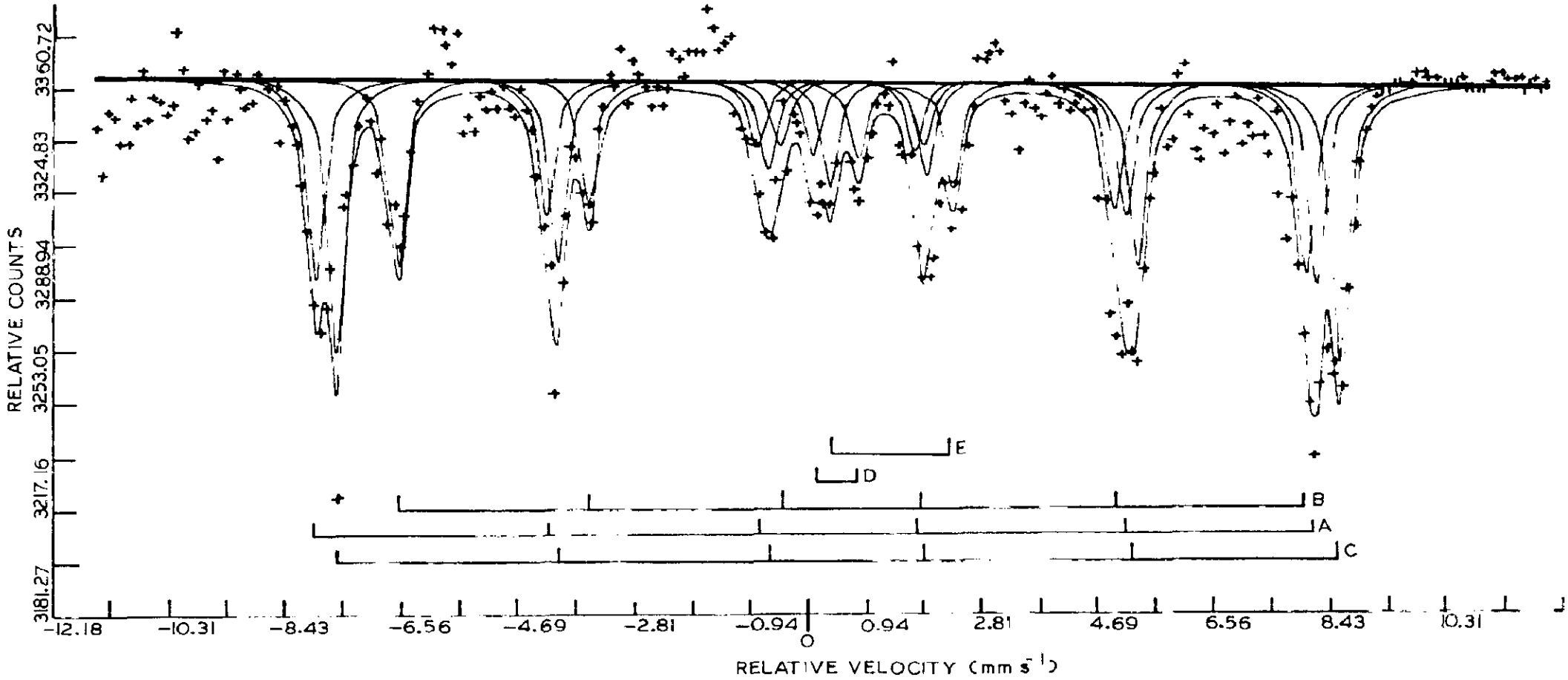

FIG.6.5_ MÖSSBAUER SPECTRUM OF SAMPLE FROM BOTTOM PART OF THE ORE BAND.

doublets |162, 163|.

A comparison of intensity (Table 6.3) corresponding to each mineral gives a considerable variation from top to bottom. The spectrum of sample T shows it to be hematite rich whereas sample M is observed to be dominant in magnetite. The spectrum of sample B shows decrease in the amount of magnetite and an increase of hematite. These observations are in close agreement with microscopic studies. Stilpnomelane has been observed in all the spectra whereas lepidocrocite in sample M and ferruginous chlorite in sample B only are observable. Minor phases of ilmenite, goethite and pyrite (observed in microscopic studies) do not show their representative patterns in the Mossbauer spectra.

6.7 GENESIS OF IRON ORE BAND

The field occurrence and petro-mineralogical evidences suggest that the iron ore band has been metasomatically emplaced along the contact between acidic intrusive mass and dolostone. Later movement along this band (faulting) has caused the remobilization of iron ore and resulted in the development of hematite, porphyroblastic magnetite, martite, stilpnomelane, chlorite etc. The assimilation and replacement of dolostone is evidenced by the inclusion of unreplaced dolomite within the iron phases. The low grade metamorphism suffered by rocks gave rise to minerals like chamosite and chlorite.

The mode of genesis can be further elaborated with the laboratory studies of Holser and Schneer |164|. They synthesised hydrothermal magnetite from iron chloride solutions having 1000 ppm Fe^{3+} and 500 ppm Fe^{2+} with a pH of 2. They used calcite to neutralise the solutions and for crystallisation of magnetite At 320°C the principal product observed was crystalline magnetite whereas at temperatures 240°C and 150°C, approximately 70 and 90 % hematite respectively with remainder magnetite was observed. It was concluded that if the iron is transported in HCl solutions the deposition of magnetite in carbonate rocks can be explained by the reaction between acidic solutions and $CaCO_3$.

A similar situation can be visualised here as well. The iron rich acidic solutions, probably released from the acidic intrusive body, came in contact with the carbonate country rock and thus resulted in crystallisation of magnetite and cementing hematite at moderate temperatures by the reaction between $CaCO_3$ and the solutions. The calcite grains of the band contains fine magnetite octahedra and filling along cleavages and fractures (also observed by Holser and Schneer |164|).

The different mineral phases of this ore band show wide variation in the Mossbauer parameters and need explaination.

HEMATITE

Hematite in sample T and M has nearly same Mossbauer

parameters (site C in Table 6.3). The internal field, H_{eff}, in these is close to that of synthetic hematite |121|,showing a structure nearly free from impurities. On the contrary, H_{eff} in sample B is quite low indicating higher degree of impurities present in the structure. The probable impurities in hematite structure are manganese and titanium |114|. Higher isomer shift, δ, and lower quadrupole splitting,2ϵ, in this case (sample B) suggests Mn^{3+} as the impurity |165, 166|. This is in accordance with the chemical analysis result (Table 6.2).

These variations of Mossbauer parameters can be well correlated with physical observations. The impurity free structure of hematite at the top is due to high energy level of its crystallisation under stress conditions. In the base of the band not much recrystallisation of hematite (under stress) has taken place and Mn-rich hematite is common as stresses were less effective at the base of the ore band.

MAGNETITE

The tetrahedral site (site A in Table 6.3) of sample M seems close to that of pure magnetite. The parameters of samples from margins (T and B) indicate insertion of impurities into the lattice (Mg^{2+}, etc.) which were introduced into the mineralizing solutions by the assimilation of dolostone rocks occurring at the base of the band. Higher value of 2ϵ and lesser value of δ, in the case of sample B, indicate it containing Mg^{2+} as impurity |20|.

The 2ϵ values for octahedral site (site B) of magnetite are slightly higher in the samples from top and bottom part of the band, whereas, it is zero for sample M. This can be correlated to the microscopic observation of the presence of titani-ferrous magnetite on the two sides and its absence in the central part. This is further supported by low values of H_{eff} in samples T and B than that in case of sample M. Least value of H_{eff} and δ in sample B indicate it to be most impure of the three samples, and the impurity is most probably Ti |167|, in agreement with the results of chemical analysis.

The relative ordered structure of magnetite in the sample M can be attributed to receipt of lesser amount of impurities from the country rocks as well as to remobilisation in the band.

STILPNOMELANE

Doublet D in the Mossbauer spectra of these samples can be assigned to presence of Fe^{3+} in octahedral sites on the basis of its Mossbauer parameters. These sites can be attributed to stilpnomelane which is the only non magnetic iron containing mineral, widespread within the ore band, as has been observed from microscopic studies. Fe^{2+} at octa- and Fe^{3+} at tetrahedral |116| are not detectable due to their very small amount. Such variations in this mineral are not uncommon |116,168|.

The decrease in the value of 'δ' and increase in '2ϵ' in

case of sample M can be attributed to presence of Mg^{2+} which is lesser electronegative and having larger ionic radius than iron |20,169|. Mg was made available by the assimilation of dolostone rocks at the base of the ore band (as discussed in geological setting and shown in Fig. 6.1).

6.8 CONCLUSION

The iron ore band associated with meta-acidic intrusive consists of hematite, magnetite, martite, lepidocrocite, stilpnomelane, dolomite, calcite, chlorite and chamosite. Ilmenite, goethite and pyrite are present in minor amount and are not detectable in the Mossbauer spectrum. This ore band was emplaced metasomatically along the contact of meta-acidic unit and dolostone country rock. The crystallisation of magnetite and minor hematite took place at moderate temperatures by the reaction between acidic mineralizing solutions (probably derived from the intrusive mass) and the calcite of country rock. Later, the susceptible upper surface of this band acted as plane of movement which caused the remobilisation of iron ore and resulted into the formation of long flakes of hematite, porphyroblasts of magnetite, martite and stilpnomelane. Low grade metamorphism resulted in the generation of chamosite and chlorite. The Mossbauer spectra of samples T,M and B reveal magnetite, hematite and stilpnomelane in varying amounts whereas lepidocrocite in sample M and ferruginous chlorite in sample B are also observable. The structures of magnetite

and hematite are comparatively more pure in sample M than those of sample T and B whereas inclusion of impurity in stilpnomelane of sample M is relatively more than that of sample T and B. These variations have been suggested to be due to the differential stresses and remobilisation experienced by even this small band and are correlated with the physical state of this ore band.

Thus Mossbauer effect in addition to other techniques may be useful in understanding the different processes, responsible for various changes in the minerals of the geologic past.

CHAPTER 7

STRUCTURAL AND COMPOSITIONAL STUDIES OF NATURAL CHROMITES OF INDIAN ORIGIN*

* Based on 'Structural and compositional studies of natural chromites of Indian origin'. A.K.Singh, B.K.Jain S.K.Date and K.Chandra.
J.Phys. D-Appl. Phys. (accep. for publication)

7.1 INTRODUCTION

Chromite ($FeCr_2O_4$) is a chromium rich spinel with Fe^{2+} at tetra - and Cr^{3+} at octahedral sites and is the only ore mineral of chromium. The chemical composition of natural chromites can be expressed by the formula (Mg, Fe) $[Fe,Cr,Al]_2O_4$ that is ferrous iron is partly replaced by magnesium and chromium partly by aluminium and ferric iron. Its relation to spinel group allows chromite a wide range in composition and physical properties. Palache et al.| 170 | divided the spinel group into three series based on trivalent elements:

	Spinel Series Al	Magnetite Series Fe	Chromite Series Cr
Mg	Spinel	Magnesio Ferrite	Magnesio Chromite
Fe	Hercynite	Magnetite	Chromite
Zn	Gahnite	Franklinite	Artificial
Mn	Galaxite	Jacobsite	-do-
Ni	Artificial	Trevorite	-do-

From numerous analyses natural chromites have been found to be essentially solid solutions, principally of Mg and Fe end members of spinel and chromite series, with a subordinate but persistent proportion of the magnetite series. The composition diagram for natural chromite may be depicted by a triangular prism |171,172,173 | (Fig. 7.1), known as Stevens' triangular diagram. The shaded portion of the prism indicates the composition field that includes most natural chromites |172 |. The analyses done on natural chromites show that these cover about

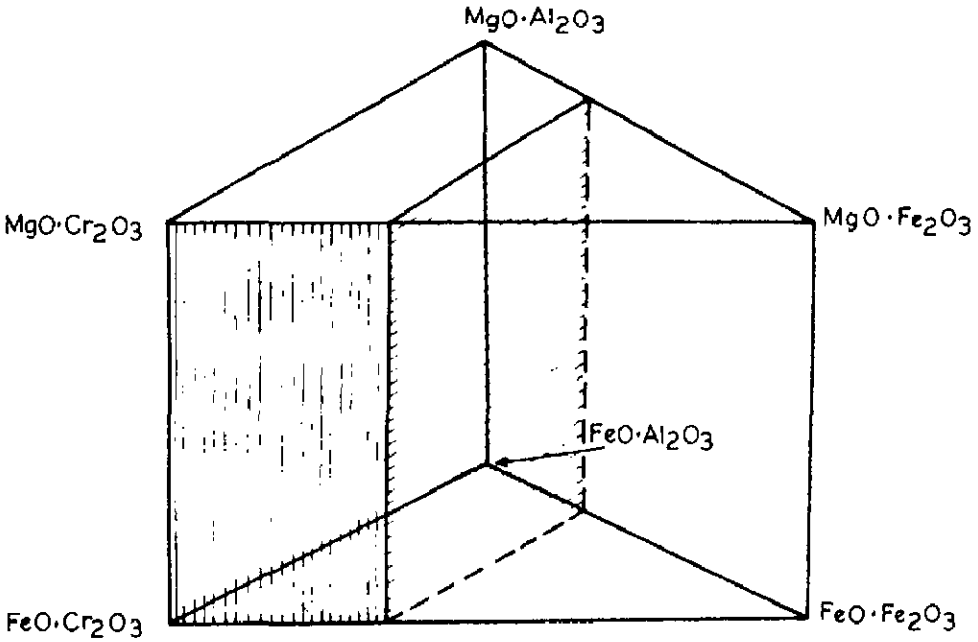

FIG.7.1 - STEVENS' TRIANGULAR DIAGRAM INDICATING COMPOSITION RANGE OF MOST NATURAL CHROMITES.

70% of the theoretical range from $(Mg,Fe)Al_2O_4$ to $(Mg,Fe)Cr_2O_4$. The content of Fe^{2+} has a wide range and appears to vary independently of Fe^{3+} |172 |. Thus observed wide compositional range in both di- and trivalent elements show it to be relatively sensitive to the chemical and thermal conditions which accompanied their formation |174 |. Chromite is, therefore, potentially an extremely important indicator of the physico-chemical and thermal conditions under which its host rocks have formed..

7.2 PAST STUDIES AND STATEMENT OF PROBLEM

In the past, studies of natural chromites have been done to find out their composition, cation distribution, cell dimensions etc. Clark and Ally | 175|,from a study of five chromites, suggested that the cell dimensions decreases with increasing Al_2O_3 contents. Malhotra et.al.|176 | has categorised Indian chromites (from different regions) on the basis of their compositional study. Chakraborty | 177| has done studies on the geology and mineralogical characters of Indian chromites through thin and polished sections and chemical analysis.

Cation distribution studies had been done through X-ray diffractometry in past. However, this technique becomes useless when one is interested particularly in finding out the sites of Fe^{2+} and Fe^{3+},which are expected at any or both of the octa (B)and tetrahedral (A) sites of spinel. This is because atomic scattering factor of these two ions,for X-rays, are very nearly same. It is here that Mossbauer spectroscopy of Fe^{57} plays a vital role. Natural chromites have been studied

through this technique only recently. Da Silva et.al.|178| has investigated ten samples from Brazil to study oxidation process of Fe^{2+} and the distribution of cations over A and B sites covering a temperature range from 25°C to 1200°C. Fe^{3+}/Fe^{2+} ratio in case of five samples from Madagascar, USSR, Iran and South Africa have been calculated and its variation, at both the sites of spinel, was obtained as a function of temperature by Fatseas et.al |179|. These studies have been correlated with hopping effect and activation energy associated with this effect has been discussed |179|.

The studies done on some natural chromites of Indian origin form the subject matter of this chapter. In all four samples were taken, two from different places of same Byrapur (Mysore) ore belt and one each from Ladakh (Kashmir) and Sukinda (Orissa). Microscopic studies of polished sections of chromite rocks were done to identify chromite, gangue minerals and to see whether scondary alterations have taken place. Chemical analysis of the separated chromite was done to find out their composition whereas Mossbauer analysis was done to study various physical aspects of spinel structure and hence to find out the type of spinel structure. Lastly attempt has been made to suggest some points about their genesis and conditions that led to their formation.

7.3 OCCURRENCE

Chromite deposits occur most commonly in highly basic or ultra-basic igneous rocks, containing predominantly olivine

and pyroxene, like peridotite, dunite and in their alteration product, serpentine rock. It also occurs in basic gabbros. Usually chromite occurs as small grains, but by the segregation of these grains, ore bodies may be formed. Its deposits are regarded as early or late magmatic segregation or injection product.

In Indian peninsula, chromite deposits occur quite extensively, on the eastern part, from Bihar to Madras. On the western coast chromite ores of appreciable size and concentration are present in Mysore and Maharashtra. Here chromite always occur with serpentinized dunite-peridotite and pyroxenites.

Following is given brief account of the chromite deposits wherefrom presently studied samples were taken:

(a) Sukinda - The Sukinda ultramafic is the largest single chromiferrous field mass in Orissa. The ultramafic field lies to the north-west of Sukinda 'Khas' near the trijunction of Cuttack, Dhenkanal, and Keonjhar districts. The extent of the field is about 40 sq. Km. These deposits are early magmatic. Both coarse and fine grained ores are noticed and they may be banded, massive or occur as disseminations. Their Cr:Fe ratio, being about 3:1, make them quite suitable for metallurgical purposes [180, 181].

(b) Byrapur - It is an important mining occurring place in Hassan district of Mysore. These mines lie in association with ultrabasic rocks within the Nuggihalli schist belt. High to low grade chromite deposits occur in the ultramafics. The schist

belt extends for a length of 40 Km. with an average width of 1.0 Km. The chromite ore body at Byrapur has a strike length of 60 meters and a maximum thickness of 12 meters |181 |. The deposits are confined to ultrabasic rocks and occur as both disseminated and massive ore bodies. Chemical analyses show Mg/Fe^{2+} ratio to be about 2:1 and Cr:Fe ratio about 2.5:1. Since this ore is having a relatively low alumina content, it is of chemical grade |182 |.

(c) Ladakh - From south of Astor to the Dras region and including the Burzil Pass, in Kashmir, the volcanics and pyroclastic sediments have been called the 'Dras Volcanics' of Ladakh region |183 |. Deposits of chromite in the form of pure olivine-chromite rock occur in dunite intrusions forming hill masses in this volcanic. As these deposits have been located only recently and are not important from economical point of view, not much literature exist about the chromite deposits of this region.

7.4 STRUCTURE OF CHROMITE

Chromite mineral is a spinel rich in chromium. Spinel is the name given to a category of oxide compounds having structure similar to that of $MgAl_2O_4$ (spinel mineral). In its structure oxygen lattice is fcc in cubic close packing with trivalent aluminium ions surrounded octahedrally by oxygen ions and divalent magneium ions occupying tetrahedral sites each surrounded by four oxygen ions. In this structure each oxygen ion also has tetrahedral coordination, its nearest

neighbours being three metal ions of octahedral coordination and one tetrahedrally coordinated metal ion |127| (Fig. 7.2), The crystallographic unit cell consists of thirty two cubic close packed oxygen atoms and 64 tetra (also known as A sites), 32 octahedral (also called 'B' sites) sites. Of these 8 tetra- and 16 octahedral sites are filled. In 'normal spinel structure' unit cell consists of 8 divalent ions at tetra and 16 trivalent ions at octahedral sites. Examples of normal spinel are $FeAl_2O_4$, $CdFe_2O_4$, $ZnFe_2O_4$ etc. Unit cell of 'inverse spinel structure' has a distribution of 8 trivalent ions at tetra- and 8 di-and 8 trivalent ions at octahedral sites. The oxides in this category are $NiFe_2O_4$, $CoFe_2O_4$, Fe_3O_4, $FeCrNiO_4$, $FeCuMnO_4$ etc.

Chemical formula for chromite is $FeCr_2O_4$. It is a normal spinel structure and has Fe^{2+} at tetrahodral or A sites and Cr^{3+} at octahedral or B sites. In mineral chromite, replacement of Cr^{3+} by iron, which causes variation in structure, is not uncommon. To understand this variation Fe-Cr spinel system, $Fe^{2+}Cr^{3+}_{2-x}\ Fe^{3+}_{x}O_4$ in the range $0<x<2$, has been studied through X-ray diffraction, Mossbauer effect and magnetic measurements |184- 187|. On the basis of structure changes three regions in this system have been suggested. Region I extends from $x=0$ to $x\sim0.7$, where structure is normal spinel i.e. all the Fe^{3+} goes at octahedral site. Region II begins from $x\sim0.7$ and terminates at $x\sim1.4$. Within this region some of the Fe^{3+} ions are at octa- and some at tetrahedral site and it is known as transition region from normal to inverse spinel structure. From

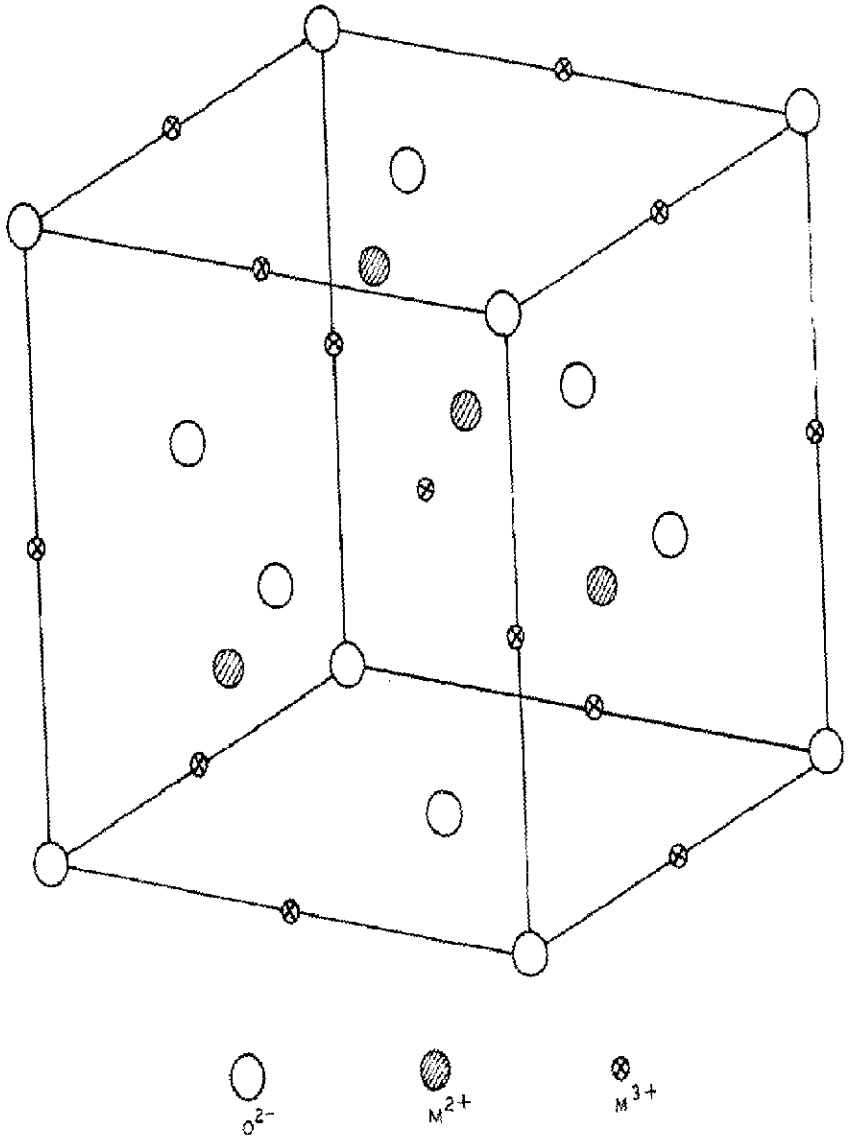

FIG.7.2- SPINEL LIKE STRUCTURE.

$x \sim 1.4$ to $x = 2$, Region III is defined where structure is purely inverse spinel.

7.5 EXPERIMENTAL DETAILS

Chromite samples taken from Ladakh (Kashmir) and Sukinda (Orissa) have been designated as L and S respectively whereas those obtained from different places of Byrapur (Mysore) chromite belt have been abbreviated as B_1 and B_2.

Microscopic studies of the chromite rocks were done on their polished samples. The polished specimens were obtained by smoothing the rock sample in an ordinary way and finally polishing them by rubbing it on a lap sprinkled with a fine polishing powder of chromium oxide. Microscopic observations were done on the ore microscope. The microphotographs of the polished samples have been shown in plates 7.1 and 7.2.

These chromite rock samples were poor in gangue minerals hence chromite mineral was separated under microscope by hand - picking after crushing the rock in an agate mortar. In the case of sample B_2 where gangue was present in slightly higher amount the mineral was separated using isodynamic magnetic separation method [188]. The instrument used for this purpose was Frantz isodynamic separator model L-1. All the analyses were done on these separated chromite samples.

Chemical analysis was done following procedure adopted by Mall [189]. Estimation of only MgO, FeO, Fe_2O_3, Al_2O_3, Cr_2O_3, apart from SiO_2, was done since these sum to more than 98 % in

chromium spinels |174|. The analysis estimating the above said five constituents (SiO_2 is excluded) is said to be 'complete'|174|. The spectrophotometer used in this analysis was spectronik-20 Bosch and Lomb make. All reagents used in the analysis were AR grade. The results showing percentage of different constituents in chromites have been given in Table 7.1.

Mossbauer spectra of powdered samples were taken at room temperature and at liquid nitrogen temperature in case of samples S and B_2. These spectra were analysed with a least square fitting programme on dec-10 computer.

7.6 RESULTS AND DISCUSSION

7.6.I MICROSCOPIC STUDIES

The chromite samples are from massive ore region. All are early magmatic hence have crystallised at high temperatures. The description of individual sample is as follows:

Sample L - In this sample, chromite grains are xemomorphic showing a reaction with gangue. Incipient alteration has been observed along the grain boundaries and fractures. The associated gangue mineral is enstatite (orthorhombic pyroxene), a primary constituent of basic igneous rocks.(plate 7.1a)

Sample S - The chromite crystals have grown with xemomorphic grains. The association of silicates with chromite ore is very less. Incipient alteration is observable along grain boundaries and fractures only under high magnification lenses. The gangue minerals are talc and serpentine which form by alteration of

TABLE 7.1- WEIGHT PERCENTAGE OF OXIDES IN CHROMITES FROM DIFFERENT ORIGIN.

Locality	SiO_2	FeO	MgO	Fe_2O_3	Cr_2O_3	Al_2O_3
Sukinda	0.63	0.70	19.35	7.72	66.30	1.53
Ladakh	1.23	4.97	17.33	9.68	60.61	4.08
Byrapur B_1	3.50	7.17	15.72	12.70	60.68	2.04
Byrapur B_2	5.46	8.49	15.32	30.83	39.57	4.79

PLATE 7.1 a-Microphotograph of Ladakh Chromite.

Magnification- 40 X

Enlarged ×2

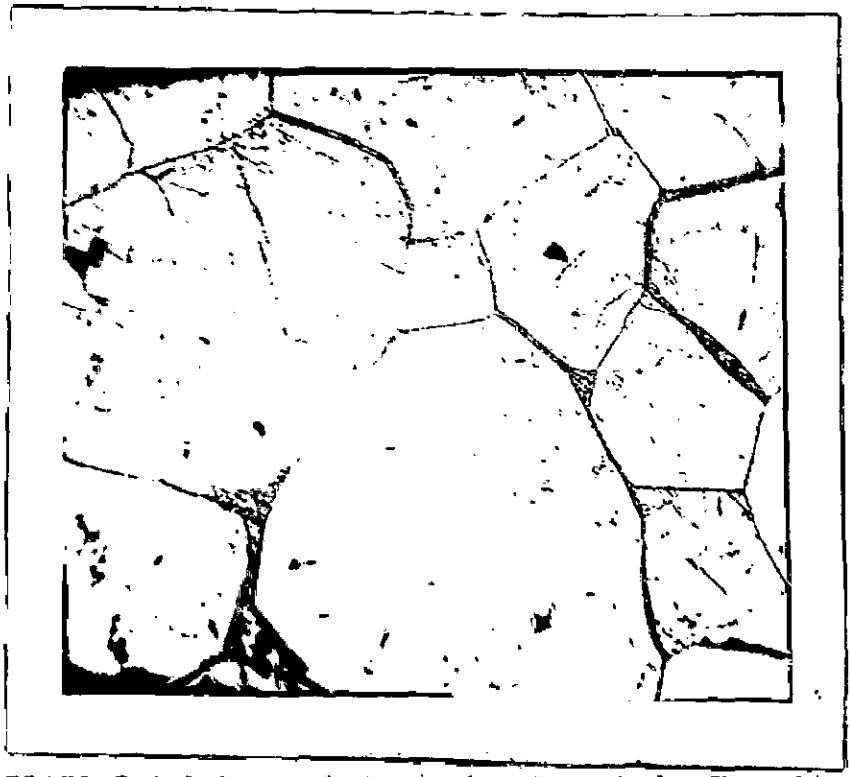

PLATE 7.1 b-Microphotograph of Sukinda Chromite.

Magnification- 40 X

Enlarged ×2

magnesium bearing rocks.(Plate 7.1 b).

Sample B_1 - The crystals of chromite have grown with ideomorphic grains indicating absence of reaction with gangue. The associated gangue mineral is serpentine (Plate 7.2 a).

Sample B_2 - The microscopic observations show chromite crystals grown up with corroded boundaries showing reaction with gangue. Most of the grains exhibit alterations along the grain boundaries (forming rims) and fractures. The associated gangue mineral is serpentine (Plate 7.2 b).

7.6 II CHEMICAL COMPOSITION AND CLASSIFICATION OF CHROMITES

The weight percentage of various oxides present in the samples (given in Table 7.1) show lesser amount of chromium content in case of sample B_2 in comparison to rest three samples. The amount of iron present in the former sample is maximum. Least amount of SiO_2 in the case of sample S supports the microscopic observation that association of silicate with chromite ore is least of all the samples (Plate 7.1 b). These chromites are very poor in aluminium contents.

In all the analysed chromite samples RO/R_2O_3 ratio has been calculated as follows: Molecular ratios of the oxides were first obtained by dividing percentage of each oxide by its molecular weight. The ratio was then calculated after subtracting silicate impurity, if it is there |171|. In present case, subtraction was done for enstatite impurity, which is $(Mg,Fe)O.SiO_2$, in case of chromite L. In other

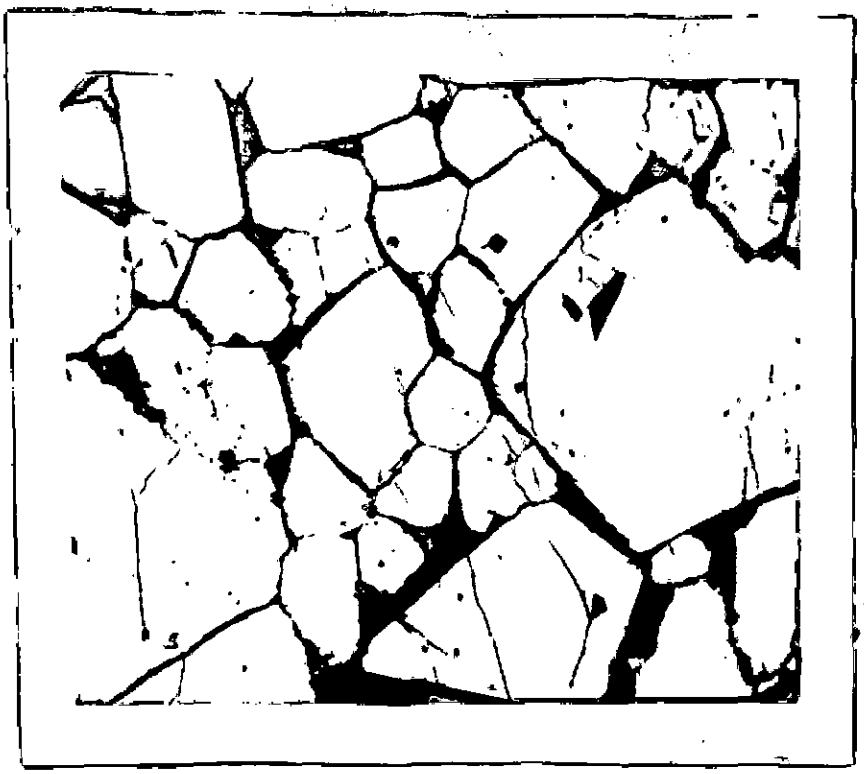

PLATE 7.2 a-Microphotograph of Byrapur B_1 Chromite.

Magnification- 60 X

Enlarged ×2

PLATE 7.2 b-Microphotograph of Byrapur B_2 Chromite.

Magnification- 60 X

Enlarged ×2

chromites, the silicate minerals present are talc and serpentine which do not contain iron, hence subtraction was not done. The calculated values of this ratio are about 1 (Table 7.2) which is indicative of balanced spinel structure. This result again supports these samples to be primary magmatic on theoretical petrologic grounds |171|.

The variation in the chemical composition of chromites and their classification can be best made out by plotting the unit cell values on Stevens' triangular diagram |171|. The unit cell of spinel structure consists of 8 di- and 16 trivalent elements (section 7.4). Assuming this unit cell content, the number of atoms of each metal per unit cell has been calculated (Table 7.2) and these values have been plotted on Stevens' triangular diagram (Fig. 7.3). The plot shows all of these chromites falling within the field of ferrian chromite. This field being defined by those chromites which are having a high chromium and a high total iron content.

7.6 III MOSSBAUER STUDIES

Mossbauer spectra of samples taken at room temperature have been illustrated in Fig. 7.4. Whereas Fig. 7.5 depicts the spectra of sample S and B_2 taken at liquid nitrogen temperature. The analysed Mossbauer parameters have been given in Table 7.3.

A look at the spectra of samples reveals them to be of two types, the one were containing paramagnetic quadrupole

TABLE 7.2- RO/R_2O_3 RATIOS AND ATOMS PER UNIT CELL IN CASE OF CHROMITES FROM DIFFERENT LOCALITIES

Locality	RO/R_2O_3	Cr^{3+}	Al^{3+}	Fe^{3+}	Fe^{2+}	Mg^{2+}
Sukinda	0.98	13.95	0.51	1.54	0.34	7.66
Ladakh	0.96	12.74	1.34	1.92	1.12	6.88
Byrapur B_1	0.98	12.77	0.70	2.53	1.76	6.24
Byrapur B_2	0.99	8.32	1.50	6.18	1.92	6.08

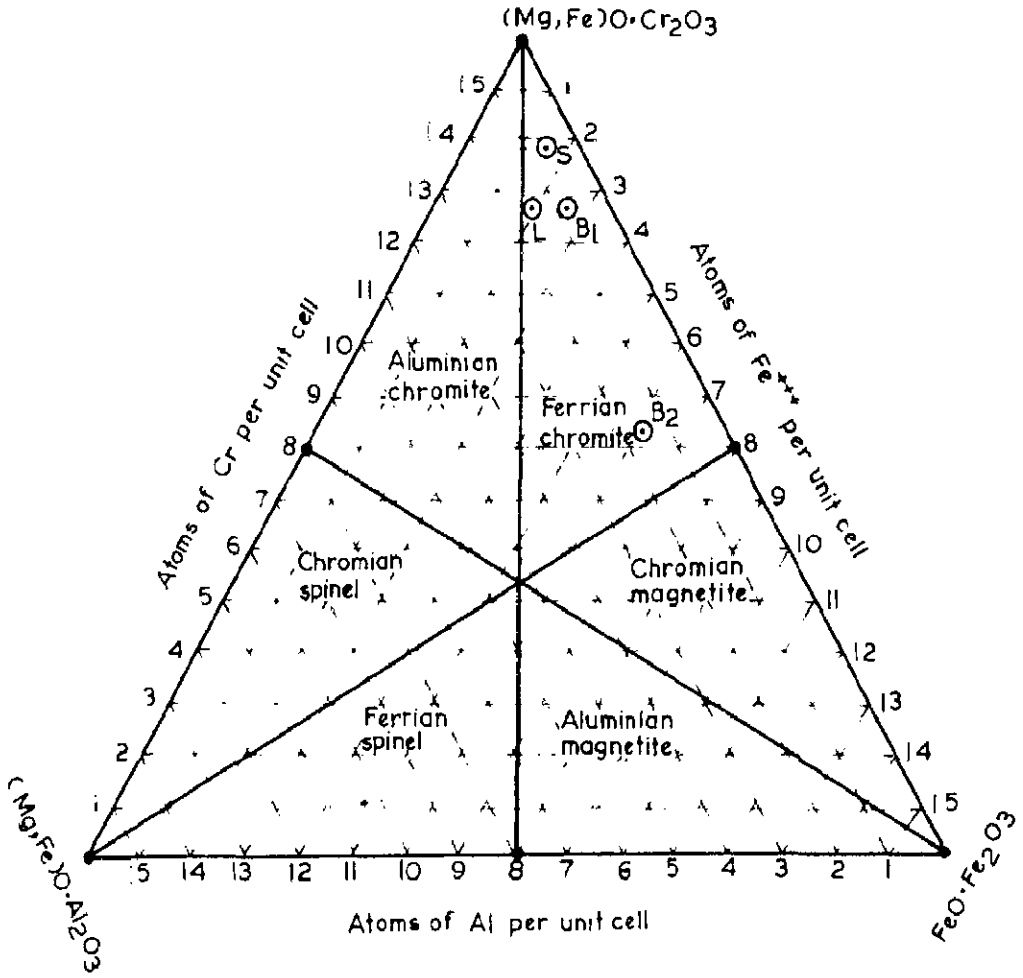

FIG.7.3 - STEVENS' TRIANGULAR DIAGRAM WITH UNIT CELL CONTENTS IN SUKINDA, LADAKH AND BYRAPUR B_1 AND B_2 CHROMITES.

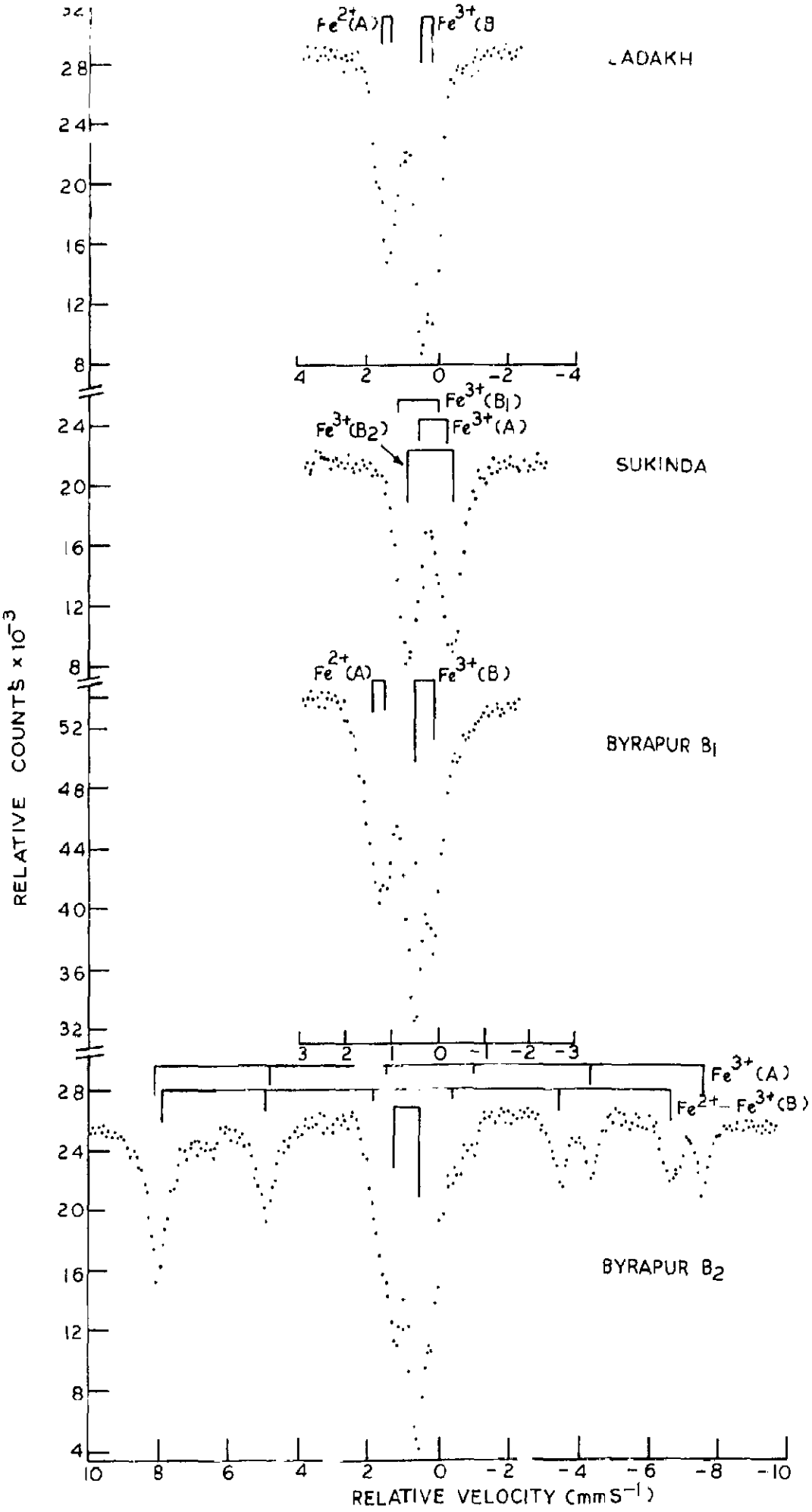

FIG.7.4- MÖSSBAUER SPECTRA OF CHROMITE SAMPLES AT ROOM TEMPERATURE.

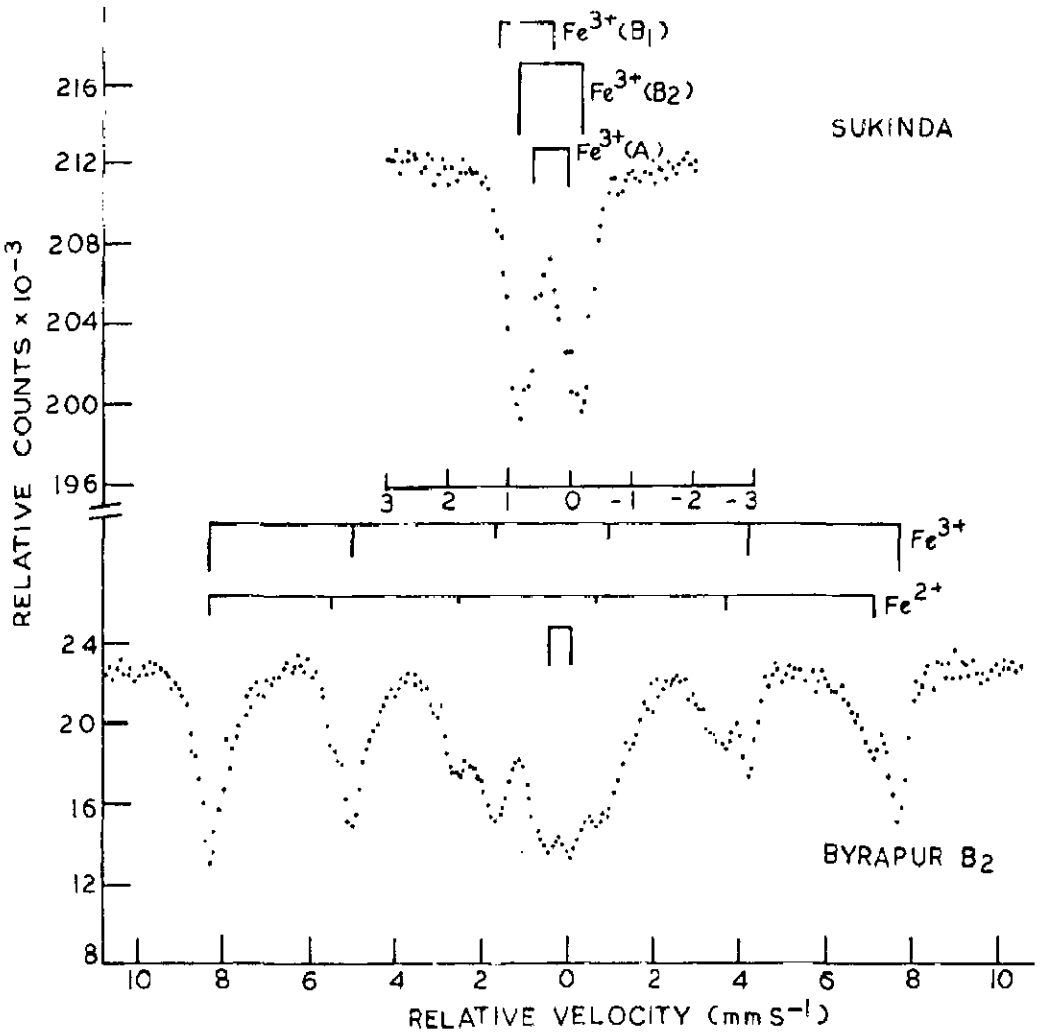

FIG.7.5 - MÖSSBAUER SPECTRA OF SUKINDA AND BYRAPUR B_2 CHROMITE SAMPLES AT LIQUID NITROGEN TEMPERATURE .

TABLE 7.3- MOSSBAUER PARAMETERS CORRESPONDING TO DIFFERENT SITES IN CHROMITES FROM VARIOUS LOCALITIES.

Locality	Site	H_{eff} (KOe)	δ (mm/s)	2ϵ (mm/s)	Fe^{3+}/Fe^{2+}
Ladakh	$Fe^{2+}(A)$	-	+1.47	0.25	1.82
	$Fe^{3+}(B)$	-	+0.35	0.36	
Byrapur B_1	$Fe^{2+}(A)$	-	+1.32	0.25	2.08
	$Fe^{3+}(B)$	-	+0.37	0.44	
Sukinda (Room Temperature)	$Fe^{3+}(A)$	-	+0.18	0.58	
	$Fe^{3+}(B_1)$	-	+0.50	0.88	
	$Fe^{3+}(B_2)$	-	+0.22	1.02	
Sukinda (Liquid N_2 Temperature)	$Fe^{3+}(A)$	-	+0.35	0.55	
	$Fe^{3+}(B_1)$	-	+0.73	0.88	
	$Fe^{3+}(B_2)$	-	+0.34	1.02	
Byrapur B_2 (Room Temperature)	$Fe^{3+}(A)$	489	+0.22	0.02	
	Fe^{2+} - $Fe^{3+}(B)$	453	+0.66	0.10	
		-	+0.73	0.52	

'δ' measured with respect to atomic iron.

doublets whereas the other was consisting of two sextets superimposed upon a quadrupole doublet. Accordingly the discussion may be divided into two sections.

Samples L, B_1 and S - The spectra of samples L and B_1 each show two quadrupole doublets. One of the doublets (doublet A in Fig. 7.4) is due to Fe^{2+} as is evident from its isomer shift, δ (Table 7.3). Comparison of δ and quadrupole splitting 2ϵ of this doublet with those of $Fe^{2+} \mid Fe_x^{3+} Cr_{2-x}^{3+} \mid O_4$ for $0<x<0.75$ |187| shows this doublet to be due to Fe^{2+} at tetrahedral sites (also called A sites) of normal spinel. The value of δ is, however, more in present case than that of Fe^{2+} observed in $FeCr_2O_4$ |190| and in $Fe^{2+}|Fe_x^{3+} Cr_{2-x}^{3+}|O_4$ |187|. This can be attributed to presence of Mg^{2+} |191| at tetrahedral sites, since presence of Fe^{3+} does not affect δ of Fe^{2+} much (evident from Table 1 of ref. |187|)and amount of Cr^{3+} at octahedral site is very nearly the same in both of these chromites (Table 7.1). The parameters of this doublet agree well with those of Fe^{2+} (A) reported, in natural chromites, by Da Silva et.al.|178|. The presence of more Mg^{2+} at tetrahedral site in the case of sample L (Table 7.1) is responsible for higher value of δ |191| than that for B_1. Quadrupole splitting at this site arises due to random strain developed as a result of presence of different cations at octahedral sites |187|. This strain causes lifting of three fold degeneracy of the low lying Fe^{2+} crystal field states and hence definite value of EFG at A sites.

The parameters of other doublet (doublet B in Fig.7.4)

in both of these samples (L and B_1) are about the same as those for $ZnFe_2O_4$ |192| where iron is in Fe^{3+} state at octahedral site. The doublet B can, therefore, be assigned to Fe^{3+} at octahedral site of spinel structure. The parameters agree well with the earlier reported values of Fe^{3+}(B) |179,187|. The value of δ in both the cases is about same whereas 2ϵ in the case of B_1 is more than that for chromite L and needs explanation. Although B site in spinel structure is surrounded by six O^{2-} ions nearly octahedrally, the point symmetry is trigonal with its axis in <111> direction. This trigonal field causes electric field gradient (EFG) at B sites |193|. The presence of more Fe^{2+} (having larger atomic radius) present at A sites creates more asymmetric environment at B-site |194| and hence larger value of 2ϵ in case of B_1 chromite.

Thus chromite L and B_1 have Fe^{2+} at A at Fe^{3+} at B sites which is characteristic of normal spinel structure. Since recoil-free fractions for both A- and B-sites are known to be similar in spinels |195|, the absorption area corresponding to both sites provides a good measure of site occupancy. The comparison of Fe^{3+}/Fe^{2+} ratios(from Mossbauer spectra) with those obtained from chemical analysis shows a close agreement (Table 7.3 and 7.4).

The Mossbauer spectrum of chromite S, recorded at room temperature shows three doublets. Doublets A (Fig.7.4) can be attributed to Fe^{3+} at A sites because of its low value of δ |179|. Distribution of cations at B sites may be

responsible for 2θ value of this doublet as in the case of $FeNiAlO_4$ and $FeNiCrO_4$ |193|. The other two doublets (B and C in Fig. 7.4) represent two different crystallographic Fe^{3+} B sites. The presence of more than one Fe^{3+} B sites has been demonstrated by Fatseas et.al. |179| also in natural chromites. The parameters of these doublets agree well with those reported earlier |178,179|. The spectrum does not indicate a doublet with parameters characteristic of Fe^{2+} (its presence has been observed from chemical analysis). This may be probably due to very small amount of Fe^{2+} in this sample (Table 7.1). To check whether the sample undergoes a phase transition, its spectrum was taken at liquid nitrogen temperature. The spectrum still showed three doublets. 'δ' has been found larger than the room temperature values and can be attributed to second order Doppler shift whereas 2θ values remain unaffected for all the sites. Such observations have also been noted by Mizoguchi et.al.|193|. Thus one can conclude that this sample is not undergoing any phase transition upto liquid nitrogen temperature.

Sample B_2 - This chromite, although belongs to same Byrapur belt as B_1, shows quite large variations. Chemical analysis of the sample (Table 7.1) shows largest amount of iron and least amount of chromite of all the samples. The room temperature Mossbauer spectrum of this sample shows two six line patterns, thus indicating inverse spinel structure, similar to those of magnetite |196| alongwith a superparamagnetic (SPM) doublet. The pattern having larger internal magnetic field, H_{eff}, and

sharper lines (Fig. 7.4) are due to Fe^{3+} at tetrahedral (or A) sites while broader lines with lesser H_{eff} (Fig.7.4) may be due to Fe^{2+} - Fe^{3+} at octahedral (or B) sites. The broadening of B-sites lines and the value of δ (midway between δ's of Fe^{2+} and Fe^{3+}) shows the hopping of electrons between Fe^{2+} and Fe^{3+} ions at B-sites. It also indicates that hopping is sufficiently fast enough to give an effective average valence of +2.5, however, it is slow enough not to restore natural line width. The broadening of B-site lines can also be attributed to presence of impurity ions e.g. Cr^{3+}, Al^{3+} |187| and to small grain size which also slows down electron hopping |53|. The presence of impurities at A and B sites is also reflected in the definite values of 2ϵ (although very small) and lower value of H_{eff}'s than those in the case of synthetic magnetite |196|. The simultaneous presence of two sextets and a doublet gives an indication of spm effects due to small particle size. This has been checked by taking its spectrum at liquid nitrogen temperature (Fig. 7.5). It shows an increase in the intensity of six line patterns at the cost of that of spm doublet (Fig.7.5) due to increase in spin relaxation time.

7.7 CORRELATION OF COMPOSITION AND STRUCTURE WITH GENETIC CONDITIONS.

The value of Fe^{3+}/Fe^{2+} ratio is greater than one for all samples, indicating that all of these have formed under high oxygen fugacity, f_{O_2} |174|. A relative comparison of

this ratio (Table 7.4) suggests that f_{O_2} is highest for sample S and least in case of sample L, in latter case f_{O_2} is about the same as for sample B_1. Comparison of Fe^{3+}/Fe^{2+} ratio in case of samples B_1 and B_2 suggests that, although initially the magmatic conditions were same (since these are taken from same ore belt), later alterations led to higher value of this ratio in the case of B_2 (also evident from microscopic observations).

As the ionic radii of Al^{3+} and Cr^{3+} are smaller than those of Fe^{3+}, it should be expected that they are more abundant in the early formed crystals, while Fe^{3+} will become concentrated in the later crystals of an isomorphous series. Among the divalent cations in chromite Mg^{2+} (0.78 A^{0}) has a smaller radius than Fe^{2+} (0.83 A^{0}) hence an early formed chromite will have more of Mg^{2+} than Fe^{2+}. Thus early formed chromite should be expected to be rich in Cr^{3+}, Al^{3+} and Mg^{2+}, while the later segregations should be progressively enriched in Fe^{2+} and Fe^{3+} |176|. Thus on the basis of Mg/Fe^{2+} and Cr/Fe ratios, suggestions can be put about their time of genesis on a relative scale. Upon comparing these ratios (Table 7.4), the samples can be placed, according to their time of crystallisation, in following order: S,L,B_1 and B_2. Thus sample S is earliest crystallised while B_2 is of latest time.

Normal spinel structure in case of samples L,S and B_1 and inverse in case of sample B_2 suggests that the latter has

TABLE 7.4- SOME RATIOS IN CASE OF DIFFERENT CHROMITES

Locality	Fe^{3+}/Fe^{2+}	Mg/Fe^{2+}	Cr/Fe
Sukinda	9.66	48.0	8.16
Ladakh	1.75	6.14	4.21
Byrapur B_1	1.60	3.90	3.07
Byrapur B_2	3.27	3.22	1.03

crystallised at relatively higher temperature |180|. It is known that iron end members of spinel group have lowest melting point hence iron contents increase in chromites as the crystallising system becomes cooler |173|. Highest iron content in the case of sample B_2, therefore, suggests of alterations (also indicated by microscopic studies) which have taken place at later stage.

Smaller particle size in case of sample B_2, suggested from the appearance of superparamagnetic doublet in Mossbauer spectrum, indicates of comparatively faster rate of cooling of magma |197|.

7.8 CONCLUSION

The chromites investigated in the present study were all early magmatic and have been taken from massive ore region. All of these are having balanced spinel structure. The plot of number of atoms per unit cell on the Steven's triangular diagram shows them falling within the region of Ferrian chromite.

Among these, samples L and B_1 show large similarities. Both have normal spinel structure with Fe^{2+} at A and Fe^{3+} at B sites. Fe^{3+}/Fe^{2+} is not much different in both cases. Other constituents also do not differ much. The genetic conditions were probably very nearly the same in the case of both of these deposits. The sample L is of relatively earlier time than B_1. Sample S shows least amount of iron content with practically all in Fe^{3+} form distributed at A and B sites both.

The condition of genesis were such that oxygen fugacity was higher and the magma was poor in iron and rich in chromium. Further the association of silicates was very small as indicated from microscopic and chemical analyses.

Two samples B_1 and B_2 taken from same ore belt show large variations. Being derived from same belt, the magmatic conditions can be supposed to be the same, however, the crystallisation of B_2 took place at relatively higher temperature with faster cooling rate which resulted into inverse spinel structure with small particle size. Later alterations experienced by this sample led it to be iron rich and poor in chromium.

CHAPTER 8

EPILOGUE

Preceding chapters give an account of the attempts made in exploring the applicability of Fe^{57} Mossbauer spectroscopy in the fields of mineralogy and geochemistry. The technique has been used for identification of mineral phases, studying their structural variation, cation distribution at different sites in a mineral structure etc.

Mossbauer technique has following advantages; over others, in studying natural samples. It distinguishes clearly between Fe^{2+} and Fe^{3+} sites in a mineral phase. Other standard methods e.g. X-ray diffraction, electron probe are unable to differentiate between Fe^{2+} and Fe^{3+} whereas chemical analysis gives an unreliable data. The applicability of this technique in studying crystallized as well as poorly crystallized, amorphous and fine grained samples e.g. mud, clay etc., with equal efficiency, place it ahead of optical and X-ray techniques. The former of these two is time consuming and not workable always while the latter one shows broadened or diffuse lines for fine particles. The rapid determination of Fe^{2+} site populations and Fe^{3+}/Fe^{2+} ratios, in silicate minerals, through Mossbauer effect makes it quite useful for studying 'ordering'. Chemical analysis, together with optical density measurements, may suggest ordering but can not determine it quantitatively. Infrared spectroscopy does not appear to be a precise method and is limited to silicates containing hydroxyl group only.

It has, however, certain shortcomings also. While doing

identification type of work in case of a multi-phase assembly e.g. a rock, it might be very difficult to resolve different overlapping lorentzians unless information on the mineral content is available from other sources. The similarity of Mossbauer parameters for Fe^{3+} ions in silicate minerals makes it a relatively poor method in identifying ferric paramagnetic minerals . The relative amount of iron in various mineral phases is calculated by estimating the area lying under the absorption line which in turn is determined by number of iron atoms (in that particular site). The latter two quantities are related directly for thin absorbers only, hence corrections are needed for thick absorbers. Secondly, the primary data must be corrected for the background of non-Mossbauer radiation. Thirdly, there are still no suitable published measurements of resonant fractions for almost all the minerals which one has to deal with.

With present state of development,as regards the instrumentation and source strength, it is possible to detect 0.1% of magnetic and somewhat less of paramagnetic mineral in a natural sample. With further improvement in techniques, it should be possible in next decade to extend the detection range down to 100 ppm. At this range, it could be very difficult to detect minerals using other standard techniques even if the minerals are well crystallised.

In chapter 4 of this dissertation, effect of annealing

on ochres have been discussed. These natural pigments have been frequently used by ancient potters and hence the study finds possible application in archeology. Pottery wares are of prime importance in archeology as cultural items, indexes of artistic and technological skill, and objects of extensive trade in ancient world. These are made up of clays which is defined to be fraction of soil consisting of particles with diameter less than 4 μm. The relatively high abundance of iron in clays used in ancient pottery (ranging between 5 and 10%) allows one to use Fe^{57} Mossbauer spectroscopy. This technique is latest addition to the instrumental techniques, e.g. optical emission spectroscopy,neutron activation analysis, used so far in providing unambiguous interpretation of the results, about artifacts, derived through macroscopic criteria e.g. stylistic considerations and excavation systematics. Mossbauer spectroscopy is helpful in giving information about iron chemistry and constitution of unfired and fired clay. This creates a multiparameter function that could be used for provenance, classification and manufacturing techniques e.g. the firing temperature and the type of atmosphere in which firing took place, of these artifacts. Work has already begun in this direction by several groups |2,108,109,198|. The different temperature behaviour observed in spectra of modern and ancient pottery . | 199| shows evidence that ageing of the materials over several millenia may bring about alterations in the chemical and physical state of iron-containing phases

in the clay. It seems a disintegration process took place over such a large period which resulted into small particle size observed in ancient pottery sherds. The possible factors responsible for determining particle sizes may be: the daily temperature change, humidity and pH of soil in which pottery was buried. A possible mechanism, operative inside earth, responsible for disintegration may thus be worked out which may help in tracing out the history of ancient pottery with the help of Mossbauer effect. In later stages, Mossbauer spectra may well help in dating the artifacts of archeological interest. In this manner, it may come out as unique technique in supplying a time scale in formation of various ancient pottery.

Detailed and exact knowledge of the composition, cation distribution in ferromagnetic minerals e.g. hematite, ilmenite, magnetite, titanomagnetite, maghemite, pyrrhotite etc. in igneous rocks is becoming sufficiently useful as a geological thermometer for determining initial temperature and the rate of cooling at the time of formation of these rocks. All of these minerals contain fairly good amount of iron and are important from the view point of rock magnetism. A study of the magnetic rock samples (which are having above mentioned minerals) from Mossbauer and magnetic measurements would help to have an understanding of the physics of magnetism in these natural samples which find possible applications, apart from those mentioned above, in paleomagnetism, a field related with tracing the history of the intensity and direction of earth's

magnetic field at the time when materials were formed. The relation between composition and magnetism is not at all well understood in case of natural chromites which have wide variations in their compositions. Their magnetic properties vary strongly with oxidation state of iron and their site occupancy. Hence a careful estimation of Fe^{2+} and Fe^{3+} (with their site of occupation), for which Mossbauer technique is best suitable, and its correlation with magnetic measurements is very much needed.

Thus the author strongly feels that problems (outlined above) which were baffling the workers of respective fields till now may well be solved efficiently with the help of Mossbauer technique and hence leave lot of scope for Mossbauer spectroscopists to work in these challanging fields of earth sciences and archeology.

R E F E R E N C E S

1. R.L.Mossbauer: Z. Physik 151, 124 (1968); Naturwissenchaften 22, 538 (1958); Z. Naturforsch 14a, 211 (1959).

2. D.R. Cousins and K.G. Dharmawardena: Nature 223, 733 (1969).

3. J.W. Williams: New Sci. (1), 119 (1974).

4. N.H. Gangas, A.Simopoulos, A.Kostikas, N.J. Yassoglou and S. Filippakis: Clays and Clay Min. 21, 151 (1973).

5. U. Gonser and H.D. Pfannes: J. Physique Colloque , 35, C6-113 (1974).

6. N.A.Eissa, H.A. Sallam, B.A. Ashi, M.Y. Hassan and S.A.Saleh: J. Phys. D 9, 1391 (1976).

7. V.Kacena: Acta Mont 26, 37 (1974).

8. C.L.Herzenberg and D.L. Riley: Proc. Apollo 11 Lunar Sci. Conf., Geochim. Cosmochim. acta Suppl.1, Vol.3, 2221 (1970); C.L. Herzenberg, R.B. Moler, and D.L.Riley: Proc. 2nd Lunar Sci. Conf., Geochim. Cosmochim. acta Suppl. 2, Vol.3, 2103 (1971).

9. The Mossbauer Effect (Bibliography Series) Tech. Rept. Series No.16, IAEA, Vienna (1965).

10. A.H. Muir,Jr., K.J.Ando and H.M. Coogan: Mossbauer effect data Index, 1958-65, 1966-68 (Inter Science, New York); J.G.Stevens and V.E. Stevens: Mossbauer effect data Index, 1969-75 (Plenum Press, New York).

11. ''Mossbauer Effect Methodology'' Vols. 1-9, Ed. I.J. Gruverman (Plenum Press,New York). Published every year since 1965 except in 1972.

12. H. Frauenfelder: 'The Mossbauer Effect' (W.A. Benjamin, Inc., N.Y.,1962).

13. G.K.Wertheim: Mossbauer Effect, Principles and applications (Academic Press, N.Y.,1964).

14. V.I.Gol'danskii: The Mossbauer effect and its applications in chemistry. (Consultant bureau enterprises, Inc.,N.Y.,1964).

15. V.I. Gol'danskii and R.H. Herber (Eds.): Chemical applications of Mossbauer spectroscopy (Academic Press, N.Y.,1968).

16. L.May (Ed.): An introduction to Mossbauer spectroscopy (Plenum Press, N.Y., 1971).

17. N.N.Greenwood and T.C.Gibb: Mossbauer spectroscopy (Chapman and Hall Ltd., London, 1971).

18. Applications of Mossbauer Effect (International atomic Energy Agency, Vienna, 1972).

19. V.G. Bhide: Mossbauer Effect and its applications. (Tata McGraw-Hill Book Co. Ltd., N. Delhi, 1973).

20. G.M. Bancroft: Mossbauer Spectroscopy, An introduction for inorganic chemists and geochemists. (McGraw-Hill book Co. Ltd., Berkshire, 1973).

21. U. Gonser (Ed.):Topics in Applied Physics Vol. 5, Mossbauer spectroscopy (Springer-Verlag, Berlin, 1975).

22. R.L.Cohen (Ed.): Applications of Mossbauer spectroscopy, (Academic Press, N.Y., 1976).

23. Lord Rayleigh: The theory of sound (Reprinted by Dover Press, New York, 1894).

24. R.W.Wood: Physical Optics (McMillan Press, N.Y., 1934).

25. W. Kuhn: Phil. Mag. 8, 625 (1929).

26. P.B.Moon: Proc. Phys. Soc. 63, 1189 (1950).

27. K.G. Malmfors: Ark. F.Fysik 6, 49 (1952).

28. K. Ilakovac: Proc. Phys. Soc. 67, 601 (1954).

29. C.P.Swann and F.R. Metzger: Phys. Rev, 108, 982 (1957).

30. W.E. Lamb, Jr.: Phys. Rev. 55, 190 (1939).

31. R.L. Mossbauer; α -,β- and γ-ray spectroscopy (Ed.K. Siegnahn, North Holland Publishing Co., Amsterdam, 1965) p. 1293.

32. W.M. Visscher: Ann. Phys. 9, 194 (1960).

33. J. Petzold: Z.Physik 163, 71 (1971).

34. M.K.F. Wong: Proc. Phys. Soc. (London) 85, 723 (1965).

35. W. Heitler: The Quantum theory of radiation (Oxford University Press, London, 1953).

36. G.K. Wertheim: Phys. Today 20, 131 (1967).

37. M. Blume: Phys. Rev. Lett. 14, 96 (1965).

38. V.I. Gol'danskii, E.F.Makarov and V.V.Kharpov: Phys. Lett. 3, 344 (1966).

39. R.L.Walker, G.K.Wertheim and J.Vaccarino: Phys. Rev. Lett 6, 98 (1960).

40. E. Mathias, W.Schneider and R.M. Steffan: Phys. Rev. 125, 261 (1962).

41. L. Néel: Compt. Rend. 228, 664 (1949).

42. C .P.Bean and J.D.Livingston: J.Appl. Phys. (Suppl.) 30, 120S (1959).

43. I.S.Jacobs and C.P.Bean: Magnetism (Eds.G.T. Rado and H.Suhl, Academic Press, N.Y., 1963) Vol. III, p.271.

44. P.W. Selwood:Adsorption and Collective Paramagnetism (Academic Press, N.Y., 1962).

45. T.Nakamura, T. Shinjo, Y.Endoh, N. Yamatoto, M.Shiga and Y. Nakamura: Phys. Lett. 12, 178 (1964).

46. Y. Ishikawa: J. Appl. Phys. 35, 1054 (1964).

47. L. Néel : Ann. Geophys. 5, 99 (1949).

48. A. Aharoni: Phys. Rev. 135, A 447 (1964).

49. S.L.Ruby and G.Shirane: Phys. Rev. 123, 1239 (1961).

50. T. Shinjo: J. Phys. Soc. Jap. 21, 917 (1966).

51. A.M. Van der Kraan and J.J.Van Loef: Phys. Lett. 20,614(1966).

52. P. Roggwiller and W.Kundig: Solid St. Commn. 12, 901 (1973).

53. H. Topsøe, J.A.Dumesic and M.Boudart: J. Physique Colloq. 35, C6-411 (1974).

54. K.Krop, J. Korecki, J. Zukrowski and Karaś: Int. J. Magnetism 6, 19 (1974).

55. N.H. Gangas, A.Kostikas, A.Simopoulos and J.Vokotopoulou: Nature 229, 485 (1972).

56. R.M.Housley, R.W.Grant, A.H.Muir, M.Blander and M.Abdel-Gawad: Proc. 2nd Lunar Sci.Conf. Geochim. Cosmochim. acta Suppl. 2, 3, 2125 (1971).

57. A.K.Singh, B.K.Jain and K.Chandra: To appear in J. Phys. D: Appl. Phys. 11 (1978).

58. R.Bauminger, S.G.Cohen, A.Marinov, S.Ofer and E.Segal: Phys.Rev. 122, 1447 (1961).

59. O.C.Kistner and A.W.Sunyar: Phys.Rev. Lett. 4, 412 (1960).

60. M.DeCoster, H.Pollak and S.Amelinckx: Phys. Stat. Solidi 3, 283 (1963).

61. E.L.Sprenkel-Segel and S.S.Hanna: Geochim. Cosmochim. acta 28, 1913 (1964).

62. E.L.Sprenkel-Segel and S.S.Hanna: Mossbauer effect methodology (Ed. I.J. Gruverman, Plenum Press, N.Y.) 2, 113 (1966).

63. C.L.Herzenberg: Mossbauer effect methodology (Ed. I.J.Gruverman, Plenum Press, N.Y.) 5, 209 (1970).

64. A.G.Maddock: Panel on the Applications of Mossbauer Effect (IAEA, Vienna, 1972).

65. S.S.Hafner: Topics in Appl. Physics. Vol. 5 (Ed. U.Gonser, Springer-Verlag, Heidelberg 1975) p.167.

66. K. Nakamoto, M.Margoshes and R.E.Rundle: J.Am. Chem. Soc. 77, 6480 (1955).

67. K.A. Wickersheim and G.K.Korpi: J.Chem. Phys. 42, 579 (1965).

68. J.L.White and A.F.Burns: Science 141, 800 (1963).

69. H.H.Adler: Econ.Geol. 58, 558 (1963).

70. J.M. Hunt, P.Wisherd and L.C.Bonham: Analyt. Chem. 22, 1478 (1950).

71. R.E.Grim: Clay mineralogy (McGraw-Hill Book Co., N.Y.,1953).

72. H. Le Châtelier: Bull.Soc. Franc.mineral.10,204 (1887).

73. W.C. Roberts-Austin: Fifth report of alloy research Committee, Proc. Inst. Mech.Engrs. (London) 35,102 (1899).

74. C.N.Fenner: Am. J.Sci. 36, 331 (1913).

75. M.L.Keith and O.Tuttle: Am.J.Sci. Bowen Vol.,Part 1,203(1952).

76. R.W. Grimshaw and A.L.Roberts: Trans. Br. Ceram. Soc. 52, 50 (1953).

77. E.R.Schmidt and F.H.S. Vermaas: Am. Mineral. 40,422 (1955).

78. W.C.Kelley: Am.Mineral 41, 353 (1956).

79. W.Lodding and L. Hammel: Analyt. Chem. 32, 657 (1960).

80. R.C.Mackenzie: Scifax, d.t.a. data index,with mineral inorganic and organic sections (Clever Hume,London) 1962.

81. N. Benczer-Koller and R.H. Herber: Chemical applications of Mossbauer spectroscopy (Eds. V.I. Goldanskii and R.H. Herber, Academic Press, New York, 1968).

82. G.M. Kalvius and E.Kankeleit: Panel on the Applications of Mossbauer Effect (IAEA,Vienna, 1972).

83. S.S.Mitra and B.N.Singh: Phys.Rev. Lett. 16, 694 (1966).

84. S.B.Tomilov: Radickhimiya 6,377 (1964).

85. J.Bara, A.Z.Hrynkiewicz, and I.Stronski: Kernenergie 7, 317 (1964).

86. G.K.Wertheim, W.P.Kingston and R.H.Herber: J.Chem. Phys. 37, 687 (1962).

87. J. Stephen: Nucl.Instr. Methods 26, 269 (1964).

88. D.A.Shirley, M.Kaplan and P.Axel: Phys. Rev. 123, 816 (1961).

89. A.J.Bearden, M.G. Hauser and P.L.Mattern: Mossbauer Effect methodology (Ed. I.J. Gruverman,Plenum Press, N.Y.) 1, 67 (1965).

90. S.S.Hanna, J. Heberle, C.Littlejohn, G.J.Perlow, R.S.Preston and J.H. Vinscent: Phys. Rev. Lett. 4, 177 (1960).

91. R. Booth and C.E.Violet: Nucl. Instr. Methods 25, 1 (1963).

92. E. Kankeleit: Rev.Sci. Instrm. 35,194 (1964).

93. E. Kankeleit: Mossbauer Effect Methodology (Ed. I.J. Gruverman. Plenum Press,N.Y.) 1, 47 (1965).

94. B.K.Jain: Ph.D. Thesis, University of Roorkee,Roorkee,1977.

95. T.E. Cranshaw: Nucl. Instr. Methods 30, 101 (1964).

96. M. Michalski, J. Piekoszewski and A. Sawicki: Nucl. Instr. Methods 48, 349 (1967).

97. R.S.Preston, S.S.Hanna, and J.Heberle: Phys.Rev. 128,2207(1962)

98. F.Van der Woude and G. Boom: Rev. Sci. Instr. 36,800 (1965).

99. B.Sharon and D.Treves: Rev. Sci. Instr. 37,1252 (1966).

100. A.J.Nozik and M.Kaplan : Anal.Chem. 39, 854 (1967).

101. D.P.Johnson, G.A. Erickson and J.G.Dash: Rev. Sci. Instr. 39, 420 (1968).

102. G.M. Kalvius: Mossbauer Effect Methodology (Ed. I.J. Gruverman Plenum Press, N.Y.) 1, 163 (1965).

103. J.R. DeVoe, Ed.; NBS tech note no. 501, 7 (1969).

104. R.G.Barnes, R.L. Mossbauer, E.Kankeleit and J.M. Poindexter: Phys. Rev. 136A, 175 (1964).

105. P.P. Craig: Mossbauer Effect methodology (Ed. I.J. Gruverman, Plenum Press,N.Y.) 1, 135 (1965).

106. W.A. Steyert and M.D. Daybell: Mossbauer Effect Methodology (Ed. I.J. Gruverman, Plenum Press, N.Y.) 4, 3 (1968).

107. Industrial Minerals and rocks (American Inst. of mining and metallurgical Engrs.) 1949.

108. R.Bouchez, J.M.D. Coey, R. Coussement, K.P. Schmidt, M. Van Rossum, J. Aprahamian and J. Deshayes: J. de Physique Collq. 35, C6-541 (1974).

109. C. Janot and P. Delcroix: J.de Physique Colloq. 35,C6-557(1974)

110. B. Keisch : J. de Physique Colloq. 35,C6-151 (1974).

111. E.H. Kraus, W.F.Hunt and L.F. Ramsdell: Mineralogy (McGraw-Hill Book Co., Inc. USA, 1951).

112. H.H. Read: Elements of Mineralogy(Wood bridge Press, Guildford,1957).

113. J.L. Kulp and A.F.Trites: Am.Mineral. 36, 23 (1951).

114. W.A. Deer, R.A.Howie and J. Zussman: Rock-forming minerals Vol. 5, Non Silicates (Longmans, Green and Co. Ltd., London, 1963).

115. L. Pauling and S.B. Hendricks: Jour. Amer. Chem. Soc. 47, 781 (1925).

116. G.L. Taylor, A.P. Routsala, and R.O.Keeling,Jr.:Clays and Clay min. 16, 381 (1968).

117. A .I. Vogel: Quantitative inroganic analysis (Longmans, Green and Co. Pvt.Ltd., London, 1961).

118. E.R. Landa and R.G.Gast: Clays and Clay min. 21,121 (1973).

119. W. Smykatz-Klos : Differential thermal analysis, Applications and results in mineralogy (Springer-Verlag Berlin, 1974).

120. A.M. Van der Kraan: Phys. Stat. Solidi (a) 18, 215 (1973).

121. W. Kundig, H. Bommel, G. Constabaries and R.H. Lindquist: Phys.Rev. 142, 327 (1966).

122. N. Yamatoto: J. Phys. Soc. Ja p, 24,23 (1968).

123. J.K.Srivastava and R.P.Sharma: J.Physique Colloq. 35, C6-663 (1974).

124. A. Simopoulos, A.Kostikas, I. Sigalas, N.H.Gangas and A. Mourarika: Clays and Clay min. 23, 393 (1975).

125. D.Roy and R.Roy: Geochim.Cosmochim,acta 11, 72 (1957).

126. J.B.Forsyth, I.G. Hedley and C.E. Johnson: J.Phys. C 1, 179 (1968).

127. A .F. Wells: Structural inorganic Chemistry (Clarendon Press Oxford, 1975).

128. A.Z. Hrynkiewicz and D.S.Kulgawczuk: Acta Phys. Polon. 24, 689 (1963).

129. A.Z. Hrynkiewicz, D.S.Kulgawczuk and K. Tomala: Phys.Lett. 17, 93 (1965).

130. G.W.V. Oostterhout : Proc. Int. Conf. on Magnetism,Nottingham p.529 (1964).

131. M.J.Rossiter and A.E.M. Hodgson: J. Inorg.Nucl. Chem. 27, 63 (1965).

132. F.Van der Woude and A.J. Dekkar: Phys. Stat. Solidi: 13, 181 (1966).

133. I. Dezsi and M. Fodor : Phys. Stat. Solidi 15, 247 (1966).

134. A.Govaert, C.Dauwe, E. DeGrave and J.De Sitter: Solid St. Commn. 18, 389 (1976).

135. E.S. Dana and W.E.Ford: A Text book of Mineralogy (John Wiley and Sons, Inc., USA , 1955).

136. S. Goldsztaub: Compt. Rend. Acad. Sci. Paris 195,964 (1932).

137. E.C.Harder: U.S.Geol.Surv. Prof. Pap. 113 (1919).

138. R.L.Stanton : Ore Petrology (McGraw-Hill Book Co., Inc.,USA , 1972).

139. C. Janot and H. Gibert: Bull.Soc. fr. Mineral Cristallogr. 93, 213 (1970).

140. R.M. Housley, U. Gonser and R.W.Grant: Phys. Rev. Letters 20, 1279 (1968).

141. U. Gonser and R.W. Grant: Phys. Stat. Solidi. 21,381 (1967).

142. S.Krishnan: Iron Ores of India(Calcutta Press Ltd.Calcutta1955)

143. M. MarCadieu: Asiatic Soc. Bengal Jour. 24, 191 (1855).

144. R. Lydekker: Geol.Surv. Rec. 9, 155 (1876),
——— Ibid. 13, 26 (1880),
——— Ind. Geol.Surv. Mem. 22, 344 (1883).

145. H.H. Hayden: Mem.Geol, Surv. Ind. 36, 130 (1904).

146. C.S. Middlemiss: Ind. Geol.Surv. Rec. 48, 1 (1915),
——— Kashmir Mineral Survey Rept. 10 (1929).

147. H.H. LaTouche: Ind. Geol.Surv. 571 (1928).

148. S.K.Roy and A.N. Mukherjee: Ind. Geol.Min. Metall. Soc. Quart. J. 11, 49 (1939).

149. G.C.S.Gaur: Geology of magnesite deposits of Chamoli, Garhwal Himalayas, Unpublished Ph.D. Thesis,Roorkee University, India 1974.

150. H.B. Medlicott: Mem.Geol. Surv.Ind., III, Pt.2, 1 (1864).

151. D.N. Wadia: Ind. Geol. Surv. rec. 65, 189 (1931).

152. A. Heim and A. Gansser: Mem.Soc. Helv.Sci. Nat. 73,1 (1939).

153. K.S.Valdiya: Bhu-Vigyan 3, 37 (1971).

154. O'Rourke: Econ. Geol. 56, 331 (1962).

155. G. Kumar, S.H. Mehdi and G. Prakash: Himalaya Jour. Palaeont.Soc. Ind. 15, 86 (1972).

156. S.H. Mehdi, G.Kumar and G.Prakash: Him. Geol. 2, 481 (1972).

157.G.C.S.Gaur, V.K.S.Dave and R.S.Mithal: Him. Geol. (In press).

158. E.N.Cameron: Ore Microscopy (John Wiley and Sons, New York, 1961).

159. R.W.G. Wyckoff: Crystal Structure Vol.I (Inter Science Publishers, Inc.,U.S.A.,1965).

160. H. Pollak, M. Decoster and S.Amelinckx: Phys.Stat. Solidi 2, 1653 (1962).

161. B.J.Evans and S.S. Hafner: J.Appl.Phys. 40, 1411 (1969).

162. W. Meisel and G. Kreysa: Z.Anorg. Allg. Chem. 395, 31 (1972).

163. J.M.D. Coey : The Clay minerals, Use of Mossbauer effect to Characteristics them and study their transformation 1975.

164. W.T. Holser and C.J.Schneer: Geol.Soc.Ann. Bull. 72,369 (1961).

165. E. Banks, E.Kostiner and G.K.Wertheim: J.Chem. Phys. 45, 1189 (1966).

166. R.W. Grant, S.Geller, J.A.Cape , G.P.Espinosa: Phys. Rev. 175, 686 (1968).

167. H. Annersten, A.Lindh, T.Ericsson, L. Haggstrom, and R.Wappling: UUIP-796,(1973) (Uppsala University,Sweden).

168. W.A.Deer, R.A. Howie, J. Zussman: Rock forming minerals Sheet Silicates,(Wiley, N.Y., 1962).

169. L.I. Pauling: The nature of the chemical bond (Cornell Univ. Press, U.S.A., 1963).

170. C. Palache, H.Berman and C. Frondel: Dana's system of minerology, 7th Ed., (Wiley, New York, 1944).

171. R.E. Stevens: Am. Mineral.29, 1 (1944).

172. T.P. Thayer: Chromium, Am.Chem.Soc. Monograph (Ed.M.J.Udy) 132(i), 14 (1956).

173. E.D. Jackson: Min.Soc. Amer. Spec. Paper No.1,46 (1963).

174. T.N. Irvine: Can.J. Earth Sci. 2, 648 (1965).

175. G.L. Clark and A.Ally: Am. mineral.17, 66 (1932).

176. P.D.Malhotra and G.H.S.V. Prasada Rao: Am.Mineral. 41, 460 (1956).

177. K.L.Chakraborty: Econ. Geol. 60, 1660 (1965).

178. E.G. Da Silva, A.Abras and A.O.R. Sette Camara: J. Physique Colloq. 37,C6-783 (1976).

179. G.A.Patseas, J.L. Dormann and H.Blanchard: J.Physique Colloq. 37,C6- 787 (1976).

180. P.K. Banerjee: Mem. Geol. Surv. India 103,(1972).

181. S.Krishnaswamy: Description of economic mineral deposits (Oxford and IBH Publishing Co., New Delhi,1972).

182. S. Vardarajan, I.C. Pande and M.R.Srinivasa Rao: J. Geochem.Soc. of India 4, 44 (1969).

183. D.N. Wadia: Rec. Geol. Surv. India 72, 151 (1937).

184. H.J. Yearian, J.M. Kortright and R.H. Langenheim: J.Chem.Phys. 22, 1196 (1954).

185. M.H. Francomb: J. Phys.Chem.Solids 3, 37 (1957).

186. W.D. Derbyshire and H.J. Yearian: Phys. Rev. 112,1603 (1958).

187. M. Robbins, G.K. Wertheim, R.C.Sherwood and D.N.E. Buchanan: J.Phys.Chem.Solids 32, 717 (1971).

188. L.D. Muller: Physical Methods in determinative mineralogy (Ed. J. Zussman. Academic Press,London,1967) p.18.

189. A.P.Mall: J. Geochem.Soc.India 2, 111 (1967).

190. M. Tanaka, T.Tokoro and Y. Aiyama: J. Phys. Soc. Jap. 21, 262 (1966).

191. C.G. Shirane, D.E.Cox and S.L.Ruby: Phys. Rev. 125,1158(1962).

192. J. Sawicki : Czech J.Phys. B17, 371 (1967).

193. T. Mizoguchi and M.Tanaka: J. Phys. Soc.Jap. 18,1301 (1963).

194. H.B.Mathur, A.P.B.Sinha and C.M. Yagnik: Ind. J.Pure and Appl. Phys. 5, 155 (1967).

195. G.A. Sawatzky, F.Van der Woude and A.H. Morish: Phys. Rev. 183, 383 (1969).

196. F. Van der Woude, G.A.Sawatzky and A.H. Morish: Phys. Rev. 167, 533 (1968).

197. N.L. Bowen: The Evolution of igneous rocks (Dover publications, Inc., N.Y., 1956).

198. J. Hess and I. Perlman: Archaeometry 16, 137 (1974).

199. A. Kostikas, A. Simopoulos and N.H. Gangas: J.Physique Colloq. 35, C6-537 (1974).